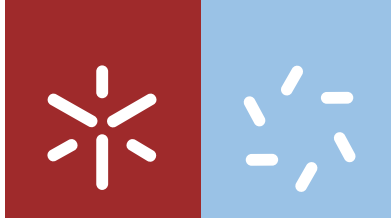


Universidade do Minho
Escola de Ciências

Inês Soares Ferreira

**Lipid based nanocarriers for the delivery of the
bioactive compound resveratrol**



Universidade do Minho
Escola de Ciências

Inês Soares Ferreira

Lipid based nanocarriers for the delivery of the bioactive compound resveratrol

Dissertação de Mestrado
Biofísica e Bionanossistemas

Trabalho efetuado sob a orientação da
**Professora Doutora Maria Elisabete Cunha Dias
Real Oliveira**
e do
Professor Doutor Hernâni Varanda Gerós

DECLARAÇÃO

Nome: Inês Soares Ferreira

Endereço eletrónico: ines.soares91@gmail.com Telefone: 917754229

Número do Bilhete de Identidade: 13998629

Título dissertação: “Lipid based nanocarriers for the delivery of the bioactive compound resveratrol”

Orientadores: Professora Doutora Maria Elisabete Cunha Dias Real Oliveira e Professor Doutor Hernâni Varanda Gerós

Ano de conclusão: 2015

Designação do Mestrado: Biofísica e Bionanossistemas

DE ACORDO COM A LEGISLAÇÃO EM VIGOR, NÃO É PERMITIDA A
REPRODUÇÃO DE QUALQUER PARTE DESTA DISSERTAÇÃO

Universidade do Minho, ____/____/____

Assinatura: _____

Acknowledgments

This dissertation benefited from the insights and direction of several people. First, I would like to express my gratitude to Professor Elisabete Oliveira, as head of the research group and my supervisor, for accepting me in her group and for giving me the necessary conditions for my work to be carried out and for all the knowledge she passed on to me. I would also like to express my deepest appreciation and gratitude to my co-supervisor, Professor Hernâni Gerós, for receiving me so well in his research group and for always being available. I will always be grateful for the education, guidance, mentorship and friendship he has provided me.

I would like to give my sincere gratitude to Doctor Marlene Lúcio for having accompanied me throughout my investigation. Her friendship, support, availability and the knowledge she shared with me, along with her useful suggestions, greatly improved this dissertation. I also want to show my thankfulness to Professor Manuela Côrte-Real for teaching me about the flow cytometry technique and to Cristina Ribeiro, for helping me during the flow cytometry experiments.

I want to acknowledge the contributions of my colleague Justine Demaître for the kindness in providing her results regarding the coefficient partition and the HSA binding assays. I also would like to thank my colleagues Jorge Rodrigues and Ana Garcia, which have accompanied me in the biology experiments, for their friendship and for helping me in any way they could. I also wish to extend my gratitude to all my laboratory colleagues for their help and advices whenever I needed. Besides, I want to thank them for their friendship and sympathy and for the relaxing moments, which made my work much more satisfying and amusing.

I want to show my gratefulness to all my caring friends and family. To my brother Pedro for his friendship and good mood which has helped me in the more stressful times. To my boyfriend for all the love and patience he has giving me throughout this year.

Last, but above all, to my loving parents for giving me the freedom to choose my path while teaching in me that freedom entails sense of responsibility. For all the opportunities they have offered me and for always encouraging me to follow my dreams. For their constant love, care and affection. In them I see my role model and I would be happy if my children were one day half as proud of me as I am of them. For all this and more, they will have my eternal gratitude.

Abstract

Resveratrol is a phenolic compound produced naturally by 72 different plant species, particularly grapevines, pines and legumes¹. This compound has powerful anti-oxidant, anti-inflammatory and anti-cancer effects^{2,3}. However, its fast metabolism and reduced solubility in biological fluids impairs its bioavailability. Therefore, it is essential to obtain a suitable carrier to achieve an effective therapy. Liposomes are great candidates as delivery systems since they present high biocompatibility, protection and controlled release of the drug.

In the present study, plain and resveratrol loaded DODAB:MO liposomes (1:2) were prepared and characterized over time for size, surface charge and polydispersity index to obtain information about the liposomes shelf stability. A thorough characterization of the system was carried out, namely regarding resveratrol biophysical effects in lipid membranes, encapsulation efficiency, controlled release and HSA binding assays. Furthermore, the effect of free and encapsulated resveratrol in the growth of a yeast culture was determined, along with its protective effect against hydrogen peroxide (H₂O₂) induced oxidative stress. Cell viability and reactive oxygen species production were also evaluated, as well as liposome internalization by yeast cells.

Results showed that resveratrol loaded liposomes produced by incubation were adequate for drug delivery purposes. Resveratrol proved to have a lipophilic character and being unevenly distributed in the lipid formulation, and its partition in the system proved to be spontaneous. Results evidenced the necessity to adapt the formulation to avoid release of the drug in storage conditions, as well as to avoid binding to HSA. Regarding the assays performed in yeast cells, resveratrol did not affect the growth of the yeast and protected the cells against the oxidative stress induced by H₂O₂. Moreover, neither free nor encapsulated resveratrol affected cell viability and both formulations promoted a decrease of the intracellular reactive oxygen species levels. Resveratrol loaded liposomes are successfully internalized by yeast cells.

Resumo

O resveratrol é um composto fenólico produzido naturalmente por 72 espécies de plantas, particularmente videiras, pinheiros e legumes¹. Este composto apresenta efeitos antioxidantes, anti-inflamatórios e anticancerígenos^{2,3}. No entanto, a sua rápida metabolização e a sua reduzida solubilidade em fluidos biológicos diminui a sua biodisponibilidade. Assim, a obtenção de um transportador adequado é essencial, de forma a alcançar uma terapia eficaz. Os lipossomas são ótimos candidatos como sistemas de entrega de fármacos, uma vez que apresentam alta biocompatibilidade, proteção e libertação controlada do fármaco.

No presente estudo, lipossomas compostos por DODAB:MO (1:2) com e sem resveratrol foram preparados e caracterizados ao longo do tempo em relação ao tamanho, carga de superfície e índice de polidispersividade, de forma a obter informação acerca da estabilidade dos lipossomas em condições de armazenamento. Uma caracterização minuciosa do sistema foi conduzida, nomeadamente em relação aos efeitos biofísicos do resveratrol em membranas lipídicas, bem como ensaios de eficiência de encapsulamento, libertação controlada e ligação à HSA. Além disso, foi determinado o efeito do resveratrol livre e encapsulado em culturas de leveduras, juntamente com o seu efeito protetor contra o stresse oxidativo induzido pelo peróxido de hidrogénio (H₂O₂). Foram também avaliadas a viabilidade celular e a produção de espécies reativas de oxigénio, bem como a internalização de lipossomas pelas células de levedura.

Os resultados obtidos mostram que lipossomas contendo resveratrol produzidos pelo método de incubação são adequados para fins de entrega de fármacos. O resveratrol provou ter um carácter lipofílico e estar distribuído de forma desigual na formulação lipídica, e a sua partição no sistema mostrou ser espontânea. Os resultados evidenciaram a necessidade de adaptar a formulação de forma a evitar a libertação de fármaco em condições de armazenamento, bem como a evitar a sua ligação à HSA. Relativamente aos ensaios conduzidos em células de levedura, o resveratrol não afetou o crescimento da cultura e protegeu as células contra o stresse oxidativo induzido pelo H₂O₂. Além disso, o resveratrol, quer livre quer encapsulado, não apresentou qualquer efeito na viabilidade celular e promoveu a diminuição dos níveis intracelulares de espécies reativas de oxigénio. Os lipossomas com resveratrol são internalizados com sucesso pelas células de levedura.

Table of Contents

Acknowledgments	iii
Abstract	v
Resumo	vii
Table of Contents	ix
Abbreviations	xiii
Figure Index	xv
Table Index	xxi
Equation Index	xxiii
Dissertation's Overall Plan and Objectives	xxv

CHAPTER 1

STATE OF THE ART	1
1.1. Phenolic compounds in chemoprevention	3
1.1.1. Cancer – a disease of the developed world	3
1.1.2. Phenolics in chemoprevention – the particular case of resveratrol	4
1.1.2.1. Chemical structure, sources and biosynthesis of resveratrol	6
1.1.2.2. Pharmacokinetics of resveratrol: absorption, metabolism, distribution and excretion	8
1.1.2.3. Toxicity of resveratrol	11
1.1.2.4. Anticarcinogenic activity of resveratrol	11
1.2. Liposomes as anti-cancer drug delivery systems	14
1.2.1. Lipid polymorphism	14
1.2.2. Liposome preparation and classification	17
1.2.3. Liposomes as drug-delivery systems	19
1.2.4. DODAB:MO (1:2) liposomes	23

CHAPTER 2

MATERIALS AND METHODS	27
2.1. Preparation of plain liposomes	29
2.2. Preparation of resveratrol loaded liposomes	30
2.2.1. Incubation method	30

2.2.2. Hydration method	31
2.2.3. Direct mixing method	31
2.3. Size and polydispersity index determination by dynamic light scattering (DLS)	32
2.4. Zeta potential determination by electrophoretic light scattering (ELS)	36
2.5. Shelf stability studies	38
2.6. Quantitative determination of resveratrol by spectroscopy	39
2.6.1. Construction of resveratrol calibration curves by UV/Visible Absorbance Spectroscopy	42
2.7. Encapsulation efficiency assays	43
2.8. Resveratrol biophysical effects in lipid membranes	45
2.8.1. Influence of resveratrol in the microviscosity and cooperativity of the liposomal formulation	45
2.8.2. Resveratrol partition coefficient (K_p) assays using a membrane-water system and derivative spectroscopy	48
2.8.2.1. Determination of the resveratrol partition coefficient (K_p) in liposomal systems in water	51
2.8.2.2. Determination of the resveratrol thermodynamic parameters of its membrane partition	51
2.8.2.3. Determination of the resveratrol partition coefficient (K_p) in liposomal systems at biologically relevant pH values	52
2.9. Controlled release assays	52
2.9.1. In storage conditions	52
2.9.2. In physiological conditions	53
2.10. HSA binding assays using dynamic light scattering (DLS) techniques	54
2.11. Preliminary assays with free and encapsulated resveratrol in a yeast model	56
2.11.1. Resveratrol effect in yeast cell growth under fermentative and respiratory conditions	56
2.11.2. Resveratrol effect in yeast growth under respiratory conditions in the presence of hydrogen peroxide	58
2.11.3. Effect of hydrogen peroxide in yeast cell death in respiratory conditions	59
2.11.4. Liposome internalization by yeast cells assessed by fluorescence microscopy	60
2.11.5. Cell viability and reactive oxygen species (ROS) quantification assays by flow cytometry	61

CHAPTER 3

RESULTS AND DISCUSSION	65
3.1. Liposomes present good characteristics for drug delivery purposes	67
3.2. Liposomes are stable for at least 4 weeks	70
3.3. Resveratrol can be quantified by UV/Vis absorbance spectroscopy	73
3.3.1. In ultrapure water (pH \approx 5.5)	74
3.3.2. In HEPES buffer (pH = 7.4)	75
3.3.3. In acetate buffer (pH = 5.0)	76
3.4. Incubation is the most efficient method to encapsulate resveratrol	77
3.5. Resveratrol promotes disorganization of the liposomal formulation and diminishes its microviscosity	81
3.6. Resveratrol has a lipophilic character and it is encapsulated in the liposomal formulation	83
3.7. Resveratrol partition in the liposomal formulation is spontaneous	89
3.8. Resveratrol is released from liposomes in water	92
3.9. Resveratrol loaded liposomes need PEGylation to avoid binding to HSA	95
3.10. Resveratrol does not affect the growth of yeast cells	98
3.11. Hydrogen peroxide inhibits yeast growth in a dose-dependent manner and resveratrol slightly counteracts this effect	100
3.12. Resveratrol loaded liposomes are efficiently internalized by yeast cells	104
3.13. Free and encapsulated resveratrol have no effect in cell viability	105
3.14. Free and encapsulated resveratrol decrease endogenous ROS levels	107

CHAPTER 4

CONCLUSIONS AND FUTURE PERSPECTIVES	111
References	113

Abbreviations

μ_{\max}	Maximum Specific Growth Rate
ADME	Absorption, Distribution, Metabolism and Excretion
AGEs	Advanced Glycation End Products
B	Phase Transition Cooperativity
COX	Cyclooxygenase
DDS	Drug Delivery Systems
DHE	Dihydroethidium
DLS	Dynamic Light Scattering
DNA	Deoxyribonucleic Acid
DODAB	Diocetyltrimethylammonium Bromide
DPH	1,6-diphenyl-1,3,5-hexatriene
EE	Encapsulation efficiency
ELS	Electrophoretic Light Scattering
EPR	Enhanced permeability and retention
FDA	Fluorescein Diacetate
GLCRSV	resveratrol-3-O- β -glucoside
GLURSV	resveratrol-3-O-glucuronide
H	Hexagonal Phase
HEPES	4-(2-hydroxyethyl)-1-piperazineethanesulfonic acid
HSA	Human Serum Albumin
IAPs	Inhibitor of Apoptosis Proteins family
IR	Infrared
k_i	Exponential Inhibition Constant
K_p	Partition Coefficient
LDV	Laser Doppler Velocimetry
LUVs	Large Unilamellar Vesicles
L	Lamellar Phase
L_{α}	Liquid-Crystalline Lamellar Phase
L_{β}	Solid-Crystalline or Gel Lamellar Phase
M	Micellar Phase
MLVs	Multilamellar Vesicles

MO	Monoolein (1-oleoyl-rac-glycerol)
mRNA	Messenger Ribonucleic Acid
MVVs	Multivesicular Vesicles
ODC	Ornithine Decarboxylase
PCS	Photon Correlation Spectroscopy
PdI	Polydispersity Index
PEG	Polyethylene Glycol
pK_a	Acid Dissociation Constant
Q	Cubic Phase
RAGE	Receptors for Advanced Glycation End Products
ROS	Reactive Oxygen Species
RR	Ribonucleic Reductase
RSV	Resveratrol
STS	Stilbene Synthase
SULRSV	resveratrol-3-sulfate
SUVs	Small Unilamellar Vesicles
T_m	Main Phase Transition Temperature
UV	Ultraviolet
X_{min}	Minimum Inhibitory Concentration
YPD	Yeast Extract Peptone Dextrose
ζ-Potential	Zeta Potential
λ_{max}	Wavelength of Maximum Absorption

Figure Index

Figure 1. Worldwide cancer incidence in both sexes (this statistic excludes all non-melanoma skin cancers) ¹⁰ .	3
Figure 2. Chemical structure of resveratrol (trans-3-5-4'-trihydroxystilbene).	7
Figure 3. Schematic representation of <i>trans</i> -resveratrol biosynthesis by stilbene synthase ⁵¹ .	7
Figure 4. Schematic representation of the pathways of resveratrol absorption, distribution, metabolism and excretion. GLCRSV, resveratrol-3-O- β -glucoside (piceid); SULRSV, resveratrol-3-sulfate; GLURSV, resveratrol-3-O- β -glucuronide (adapted from ¹⁸).	10
Figure 5. Impact of the packing parameter (γ) on lipid assemblies formed in aqueous solutions (adapted from ⁶⁶).	16
Figure 6. Enhanced permeability and retention (EPR) effect. Long-circulating drug carriers (1) penetrate through the leaky pathological vasculature (2) into the tumor interstitium (3) and degrade there, releasing a free drug (4) and creating its high local concentration ⁸⁶ .	22
Figure 7. Chemical structure (on the top) and molecular model (on the bottom) of the lipid dioctadecyldimethylammonium bromide (DODAB).	23
Figure 8. Chemical structure (on the top) and molecular model (on the bottom) of the lipid monoolein (MO).	24
Figure 9. Schematic representation of the preparation of plain DODAB:MO (1:2) liposomes by the lipid film hydration plus extrusion technique (adapted from ⁹⁶).	29
Figure 10. Schematic representation of the preparation of resveratrol loaded DODAB:MO (1:2) liposomes (2%) produced by the incubation method of encapsulation from previously formed liposomes by the lipid film hydration plus extrusion technique (adapted from ⁹⁶).	30
Figure 11. Schematic representation of the preparation of resveratrol loaded DODAB:MO (1:2) liposomes (2%) produced by the hydration of the lipid film method of encapsulation (adapted from ⁹⁶).	31
Figure 12. Schematic representation of the preparation of resveratrol loaded DODAB:MO (1:2) liposomes (2%) produced by the direct mixing method of encapsulation (adapted from ⁹⁹).	32
Figure 13. Schematic representation of a modern dynamic light scattering apparatus possessing both classic (90°) and backscatter (173°) configuration for detection of scattered light intensity ⁶⁵ .	33

Figure 14. Schematic representation of particles moving randomly in a liquid. Their motion speed results in different intensity fluctuations which are used to determine particle size (adapted from ¹⁰¹).	34
Figure 15. Schematic representation of the intensity <i>versus</i> the size distribution of two samples. The sample on the left presents particles with identical hydrodynamic radius, thus being a monodisperse population and having a small Pdl, while the sample on the right shows a heterogeneous population with the presence of aggregates which results in a higher Pdl, being this a polydisperse population (adapted from ⁹⁹).	35
Figure 16. Schematic representation of the electrical double layer surrounding a particle in suspension ¹⁰¹ .	37
Figure 17. Schematic representation of a dip cell (left) and the LDV technique (right) ¹⁰¹ .	38
Figure 18. Schematic representation of the components of a double beam spectrophotometer ¹⁰⁶ .	41
Figure 19. Example of a sigmoid profile curve representing the phase transition after the nonlinear fitting to equation 12, where the refined parameters are T_m and B .	47
Figure 20. Typical yeast population growth curve in a population grown in a culture flask.	57
Figure 21. Schematic representation of growth experiments to evaluate the effect of resveratrol on yeast growth in the presence of H_2O_2 .	58
Figure 22. Schematic representation of the dilution process carried out during the experiments to evaluate the effect of H_2O_2 on yeast cell death.	60
Figure 23. Mean liposome size and its standard deviation for placebo liposomes and 2% resveratrol loaded liposomes produced by incubation, hydration and direct mixing methods of encapsulation.	67
Figure 24. Mean Pdl and its standard deviation for placebo liposomes and 2% resveratrol loaded liposomes produced by incubation, hydration and direct mixing methods of encapsulation.	68
Figure 25. Mean ζ -potential and its standard deviation for placebo liposomes and 2% resveratrol loaded liposomes produced by incubation, hydration and direct mixing methods of encapsulation.	69
Figure 26. Mean liposome size and its standard deviation for placebo liposomes and 2% resveratrol loaded liposomes produced by incubation, hydration and direct mixing methods of encapsulation during the three months following liposome production.	70
Figure 27. Mean Pdl and its standard deviation for placebo liposomes and 2% resveratrol loaded liposomes produced by incubation, hydration and direct mixing	

methods of encapsulation during the three months following liposome production.	71
Figure 28. Mean ζ -potential and its standard deviation for placebo liposomes and 2% resveratrol loaded liposomes produced by incubation, hydration and direct mixing methods of encapsulation during the three months following liposome production.	72
Figure 29. pH values and its standard deviation for placebo liposomes and 2% resveratrol loaded liposomes produced by incubation, hydration and direct mixing methods of encapsulation during the three months following liposome production.	72
Figure 30. Absorbance spectra of resveratrol with growing concentrations solubilized in ultrapure water, HEPES buffer and acetate buffer.	74
Figure 31. Absorbance spectra of resveratrol standard solutions with increasing concentrations solubilized in ultrapure water.	74
Figure 32. Resveratrol calibration curve in ultrapure water at maximum wavelength of 305 nm.	75
Figure 33. Absorbance spectra of resveratrol standard solutions with increasing concentrations solubilized in HEPES buffer (pH = 7.4).	75
Figure 34. Resveratrol calibration curve in HEPES buffer (pH = 7.4) at maximum wavelength of 305 nm.	76
Figure 35. Absorbance spectra of resveratrol standard solutions with increasing concentrations solubilized in acetate buffer (pH = 5.0).	76
Figure 36. Resveratrol calibration curve in acetate buffer (pH = 5.0) at maximum wavelength of 305 nm.	77
Figure 37. First derivative of the absorbance spectra of twelve resveratrol standard solutions with growing concentrations ranging from 0.5 to 100 μ M solubilized in ultrapure water.	77
Figure 38. Resveratrol calibration curve in ultrapure water using the first derivative of the absorbance at maximum wavelength of 341 nm.	78
Figure 39. First derivative of the absorbance spectra of the placebo liposomes that remained in the filter after amicon ultracentrifugation (light red line) and of the resveratrol loaded liposomes produced by incubation that remained in the filter after amicon centrifugation (dark red line).	78
Figure 40. Graphic representation of the resveratrol (2%) encapsulation efficiency in resveratrol loaded DODAB:MO (1:2) liposomes produced by incubation, hydration and direct mixing methods.	79
Figure 41. Drug loading efficiency of increasing concentrations of resveratrol (0.5, 2, 4, 6, 10 and 20% (m/m)) to a 1 mM lipid concentration.	80

- Figure 42.** Representation of the mean count rate in percentage of DODAB:MO (1:2) liposomes with (white circles) and without (black circles) resveratrol versus temperature. Each point corresponds to the mean value of three measurements and the correspondent standard deviation is represented. The lines (black for plain liposomes and grey for resveratrol loaded liposomes) represent the best non-linear fitting according to the equation 12, where the refined parameters were T_m and B . 82
- Figure 43.** Absorbance spectra of three samples of resveratrol (43 μM) represented by RSV 1, RSV 2 and RSV 3, and of the samples of resveratrol loaded liposomes with increasing lipid concentrations and a fixed resveratrol concentration (S1-S9). The correspondent references prepared in the same manner as the samples but without the incorporation of the drug are presented in grey. 84
- Figure 44.** Representation of the first (A), second (B) and third (C) derivatives of three samples of resveratrol (43 μM) represented by RSV 1, RSV 2 and RSV 3, of the samples of resveratrol loaded liposomes with increasing lipid concentrations and a fixed resveratrol concentration (S1-S9), and of the reference samples presented in grey. The peaks used to calculate the resveratrol K_p are identified in the spectra. 85
- Figure 45.** Representation of the absorbance values of the first derivative at $\lambda = 341 \text{ nm}$ (A), of the second derivative at $\lambda = 351 \text{ nm}$, and of the third derivative at $\lambda = 343 \text{ nm}$ (C) and at $\lambda = 359 \text{ nm}$ (D), and respective nonlinear regressions fitted to equation 14. Below each graphic representation is presented the respective partition and correlation coefficients. The $\text{Log } K_p$ value is presented in mol.L^{-1} . 86
- Figure 46.** Representation of the second derivative of the absorbance values of three samples of resveratrol (43 μM), of the samples of resveratrol loaded liposomes with increasing lipid concentrations and a fixed resveratrol concentration, and of the reference samples. The bathochromic shift is also represented in the graphic. 88
- Figure 47.** Fiting of the third derivative spectrophotometric data collected at $\lambda = 311 \text{ nm}$ for resveratrol loaded DODAB:MO (1:2) liposomes at different temperatures calculated with derivative spectroscopy at different temperatures: 30°C (black), 37°C (red), 50°C (green), 55°C (dark blue), 60°C (light blue). 90
- Figure 48.** Van't Hoff regression for the resveratrol partition in DODAB:MO (1:2) LUVs. The pink square represents the L_α phase and the blue square represents the L_β phase. 90
- Figure 49.** Cumulative resveratrol release from DODAB:MO (1:2) liposomes in storage conditions (ultrapure water, $\text{pH} \approx 5.5$) and in acetate buffer ($\text{pH} = 5$). 93
- Figure 50.** Cumulative resveratrol release from DODAB:MO (1:2) liposomes in HEPES buffer ($\text{pH} = 7.4$) and in acetate buffer ($\text{pH} = 5$). 94
- Figure 51.** Size and ζ -potential changes upon binding to HSA of increasing concentrations of resveratrol in aqueous media. 95

- Figure 52.** Mean sizes (columns) and Pdl (dots) of resveratrol loaded liposomes in the presence (blue) and in the absence (red) of HSA, when the lipid concentration is increasing. 96
- Figure 53.** ζ -potential variation of plain and resveratrol loaded liposomes with increasing lipid concentrations in the presence of HSA. 97
- Figure 54.** Growth of *S. cerevisiae* W303 in YPD medium (fermentative conditions) (A) and in lactate/ethanol medium (respiratory conditions) (B) in the presence and absence of 100 μ M resveratrol. Resveratrol was prepared in ethanol 100% (v/v) before addition to the culture medium, so the final concentration of ethanol in the growth experiment was 2.2% (v/v). Control experiments with ethanol alone (final concentration: 2.2% (v/v)) and neither resveratrol nor ethanol are also shown. 98
- Figure 55.** Growth of *S. cerevisiae* W303 in lactate/ethanol medium (respiratory conditions) in the absence (A) and in the presence of 200 μ M resveratrol (+ EtOH 2.2% (v/v)) (B) and with ethanol 2.2% (v/v) (C) before and after the addition of H_2O_2 with growing concentrations (0, 0.5, 0.75, 1, 1.5 and 2 mM) to the culture media. 100
- Figure 56.** Protective effect of resveratrol on the inhibition of yeast cell growth mediated by 0.5 mM H_2O_2 . Growth of *S. cerevisiae* W303 occurred in lactate/ethanol medium (respiratory conditions) and 0.5 mM H_2O_2 in the absence and in the presence of 200 μ M resveratrol (+ EtOH 2.2% (v/v)) or ethanol alone. 101
- Figure 57.** Dependence of the specific growth rates of *S. cerevisiae* W303 grown in lactate/ethanol medium (respiratory conditions) on the extracellular H_2O_2 concentration in the absence (A) and in the presence of 200 μ M resveratrol (+ EtOH 2.2% (v/v)) (B) or ethanol alone (C), and the respective X_{min} . 102
- Figure 58.** Spot test analysis representing the growth of *S. cerevisiae* on YPD agar medium when cells were incubated with up to 5 mM H_2O_2 . 103
- Figure 59.** Bright-field (A), fluorescence (B) and overlay of both (C) micrographs of *S. cerevisiae* W303 yeast cells incubated with (1) 3 μ M DPH free fluorescent probe to study cell capacity to internalize it (control experiment) and with (2) resveratrol loaded DODAB:MO (1:2) liposomes labeled with 3 μ M DPH fluorescent probe. Scale bar = 7.5 μ m. 105
- Figure 60.** Flow cytometry analysis of *S. cerevisiae* W303 yeast cell populations to study cell viability with the FDA probe. Scattergram of a population of yeast cells in the absence of resveratrol (A); overlay histogram of autofluorescence (black line) and FDA induced fluorescence (green line) in the absence of resveratrol (B) and upon treatment of yeast cells with 200 μ M of free resveratrol (C) and resveratrol loaded liposomes (D). 106
- Figure 61.** Effect of free and encapsulated resveratrol on cell viability in *S. cerevisiae* W303 grown in lactate/ethanol medium. 107
- Figure 62.** Flow cytometry analysis of *S. cerevisiae* W303 yeast cell populations to study the effect of resveratrol against endogenous ROS with the DHE probe. Scattergram of a population of yeast cells in the absence of resveratrol (A); overlay

histogram of autofluorescence (black line) and DHE induced fluorescence (orange line) in the absence of resveratrol (B) and upon treatment of yeast cells with 200 μ M of free resveratrol (C) and resveratrol loaded liposomes (D). 108

Figure 63. Effect of free and encapsulated resveratrol on the percentage of cells producing intracellular ROS in yeast cells *S. cerevisiae* W303 grown in lactate/ethanol medium. 109

Table Index

Table 1. Biophysical parameters (B and T_m) of DODAB:MO (1:2) liposomes in the absence and presence of resveratrol.	83
Table 2. Coefficient partition (K_p) values of resveratrol in a LUV((DODAB:MO)(1:2))/H ₂ O system and the respective logarithms ($\text{Log } K_p$) and coefficient partition values of resveratrol in octanol:water systems ($\text{Log } P$).	87
Table 3. Coefficient partition (K_p) values of resveratrol at physiological relevant pH's in a LUV((DODAB:MO)(1:2))/H ₂ O system and the respective logarithms ($\text{Log } K_p$).	88
Table 4. Coefficient partition (K_p) values of resveratrol in a LUV((DODAB:MO)(1:2))/H ₂ O system and the respective logarithms ($\text{Log } K_p$) at different temperatures.	89
Table 5. Variation of the enthalpy (ΔH) \pm SD, entropy (ΔS) \pm SD and Gibbs free energy (ΔG) obtained for the resveratrol partition between the aqueous phase and DODAB:MO (1:2) liposomes at different temperatures.	91
Table 6. Maximum specific growth rate (μ_{max}) of <i>S. cerevisiae</i> W303 liquid cultures.	99
Table 7. Effect of H ₂ O ₂ on the growth of <i>S. cerevisiae</i> . Cells were cultivated in lactate/ethanol medium (respiratory conditions) in the absence and in the presence of 200 μ M resveratrol (+ EtOH 2.2% (v/v)) and with ethanol alone, in the presence of different H ₂ O ₂ concentrations.	103

Equation Index

Equation 1. Determination of the critical packing parameter (γ).	15
Equation 2. Stokes-Einstein equation for the diffusion coefficient (D) of the particle.	33
Equation 3. Henry's equation for electrophoretic mobility (μ_E) of a colloidal particle.	37
Equation 4. Determination of the intensity of transmitted light (I_λ).	40
Equation 5. Determination of the transmittance (T_λ).	40
Equation 6. Determination of the absorbance (A_λ).	40
Equation 7. Determination of the absorbance coefficient (α_λ).	40
Equation 8. Beer-Lambert equation.	40
Equation 9. Equation of a straight line.	43
Equation 10. Determination of the encapsulation efficiency (EE) in percentage.	44
Equation 11. Determination of the drug loading efficiency in percentage.	45
Equation 12. Modified Boltzmann equation.	47
Equation 13. Correlation between the absorbance and the partition coefficient (K_p).	49
Equation 14. Derivative of the partition coefficient (K_p).	50
Equation 15. Van't Hoff equation.	50
Equation 16. Gibbs free energy equation.	50
Equation 17. Determination of the dissociation constant (K_d).	54
Equation 18. Variation of the Langmuir isotherm.	55
Equation 19. Gibbs free energy (ΔG) equation of the binding.	55
Equation 20. Determination of the culture's specific growth rate (μ_{max}).	57
Equation 21. Determination of the growth inhibition constants (k_i, X_{min}).	59

Dissertation's Overall Plan and Objectives

In the past recent years, intensive research has been done in order to improve the therapeutic efficacy against several diseases, including cancer. It is known that conventional drug formulations present numerous limitations and thus new strategies have been developed to improve treatment performance. Liposomes are one of the most successful drug delivery systems that apply nanotechnology to potentiate the therapeutic effectiveness and reduce toxicities of conventional medicines. Numerous studies have reported the promising properties of resveratrol, including anti-inflammatory, antioxidant and anti-cancer roles.

With this in mind, this work aimed to develop and characterize a resveratrol loaded liposomal formulation with the purpose of trying to improve the therapeutic efficiency of this natural occurring polyphenol. After a thorough biophysical characterization of the resveratrol loaded liposomal formulation, some preliminary work was performed with the purpose of exploring the properties of free and encapsulated resveratrol in the yeast model *Saccharomyces cerevisiae*, one of the most intensively studied model organism in molecular and cell biology. Basic cellular mechanics of replication, recombination, cell division and metabolism are well conserved between yeast and larger eukaryotes, including mammals. Moreover, the complete sequence of its genome has proved to be extremely useful as a reference towards the sequences of human and other higher eukaryotic genes^{4,5}. Furthermore, this budding yeast grows well in culture, is stable as either a diploid or haploid cell type, and is amenable to both classical genetic as well as molecular genetic manipulations⁶.

This masters' dissertation is divided in four chapters, which are summarized below:

Chapter 1 – State of the Art

Presents an overview of the literature and of the previous research concerning this topic. This section includes an outline regarding the use of phenolic compounds, particularly resveratrol, in chemoprevention, as well as a review concerning liposomes and why these should be used as anti-cancer drug delivery systems.

Chapter 2 – Materials and Methods

Describes the experimental work carried out during this study. In each subchapter, the techniques employed, their theoretical basis, the instruments used and the protocols are described.

Chapter 3 – Results and Discussion

Presents the experimental results that arose from the laboratory work, as well as a discussion regarding these findings.

Chapter 4 – Conclusions and Future Perspectives

Depicts the main conclusions to be drawn from the experimental work, along with the suggestion of some new experiments to be performed in the near future in order to further comprehend the applications of the formulation at study.

CHAPTER 1

STATE OF THE ART

Contents

- 1.1. Phenolic compounds in chemoprevention
 - 1.1.1. Cancer – a disease of the developed world
 - 1.1.2. Phenolics in chemoprevention – the particular case of resveratrol
 - 1.1.2.1. Chemical structure, sources and biosynthesis of resveratrol
 - 1.1.2.2. Pharmacokinetics of resveratrol: absorption, metabolism, distribution and excretion
 - 1.1.2.3. Toxicity of resveratrol
 - 1.1.2.4. Anticarcinogenic activity of resveratrol
- 1.2. Liposomes as anti-cancer drug delivery systems
 - 1.2.1. Lipid polymorphism
 - 1.2.2. Liposome preparation and classification
 - 1.2.3. Liposomes as drug delivery systems
 - 1.2.4. DODAB:MO (1:2) liposomes

1.1. Phenolic compounds in chemoprevention

1.1.1. Cancer – a disease of the developed world

Cancer is one of the leading causes of morbidity and mortality worldwide (figure 1), with approximately 14 million new cases and 8.2 million cancer related deaths in 2012, numbers which are expected to rise by about 70% within the next two decades. Many different types of cancer are known, although breast, lung, liver, stomach, colorectal, oesophageal and prostate cancers account for over half of all new cases and are the most common causes of cancer death⁷. This complex biological disorder results from integrated effects of environmental, physical, metabolic and genetic factors³. Determining the real causes of cancer is a complex subject, but the well-known risk factors are alcohol and tobacco abuse, infections, radiation, obesity and lack of physical activity. Ageing is another important factor for the development of cancer since the overall risk accumulation is combined with the tendency for cellular repair mechanisms to be less effective as a person grows older².

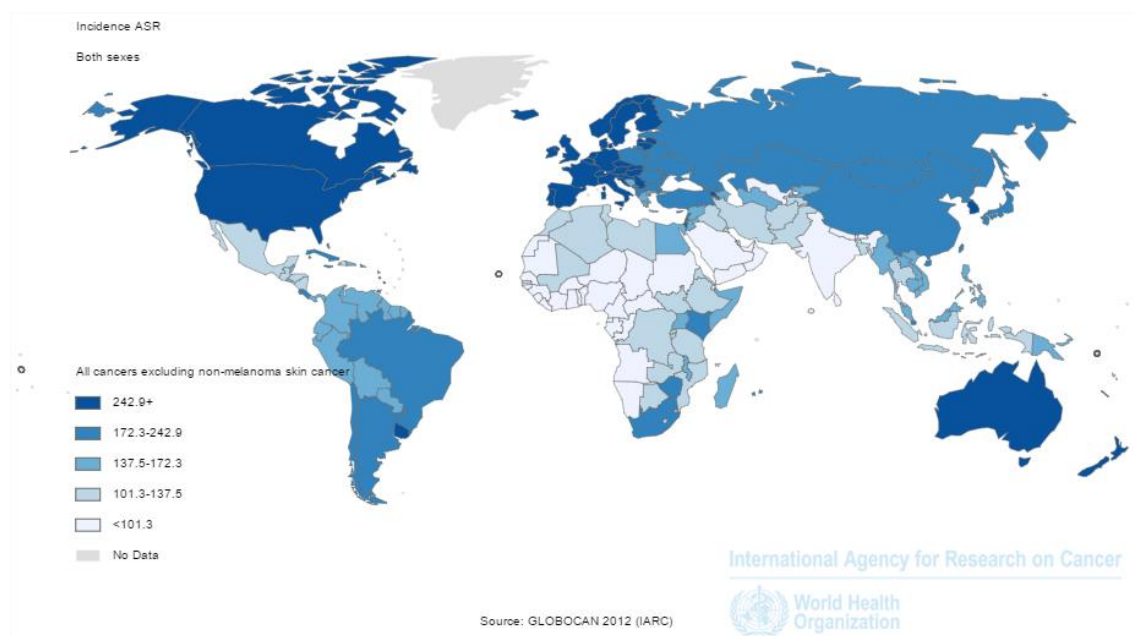


Figure 1. Worldwide cancer incidence in both sexes (this statistic excludes all non-melanoma skin cancers)¹⁰.

Cancer, also known as malignant neoplasia, refers to an extensive group of diseases that are associated with a disturbance in the control of cell growth and

metabolism. Indeed, the unbalanced control of cellular proliferation is one of the main characteristics of cancer cells¹¹. Since tumor formation is a multistep process, normal cells evolve progressively to the neoplastic stage. Along their way, these cells acquire particular abilities that enable them to become tumorigenic. These distinct hallmark capacities were proposed in 2000 by Hanahan and Weinberg¹¹ and are: (1) sustaining proliferative signaling through uncontrolled activation of oncogenes; (2) evading growth suppressors; (3) enabling replicative immortality through increased telomerase activity; (4) activating invasion and metastasis through the over activation of invasion-related proteases; (5) inducing angiogenesis, which consists in the building of an extensive network of blood vessels to maintain continuous supply of nutrients, and be able to sustain it; and (6) resisting cell death by evading apoptosis through the inhibition of proapoptotic signaling and through the stimulation of survival factor pathways. All these changes make cancer cells unresponsive to antigrowth signals, resulting in the loss of tumor suppressor gene activity⁸. Over the last decade, noteworthy progress was made in the field of cancer research which led to an improved understanding of these hallmark capabilities, but also led to modifications and, ultimately, expansions of the original concept¹².

Considering these concerns and knowing that chemoprevention aims to decrease the occurrence of cancer by the administration of natural or synthetic compounds¹³, the ideal chemopreventive agent would be one which could inhibit or reverse these processes in neoplastic cells while protecting normal cells⁹. In fact, the current treatments available are limited because they do not differentiate between normal and cancer cells, which causes side effects and early termination of therapy, ultimately harming the patient¹⁴.

1.1.2. Phenolics in chemoprevention – the particular case of resveratrol

Phenolic compounds, also known as phenols, represent the major group of phytochemicals found in plants, particularly in fruits, seeds and leaves¹⁵, and other types of foods and beverages such as chocolate, tea and wine¹⁶. These are a class of phenylalanine-derived chemical compounds that consist of a reactive hydroxyl group (-OH) bonded directly to an aromatic hydrocarbon ring, and they can be classified as simple phenols or polyphenols, based on the number of phenol units in

the molecule^{17,18}. Polyphenols comprise a large class of antioxidants, which are normally produced by plants for their antibiotic and antifungal properties¹⁹, and include flavonoids, anthocyanins, phenolic acids, lignans and stilbenes.

Dietary polyphenols have received tremendous attention among nutritionists due to their benefits on human health, since a high intake of fruits, vegetables and whole grains, which are rich in polyphenols, has been associated with lowered risks of various diseases, including cancer, chronic inflammation, cardiovascular and neurodegenerative diseases²⁰. Polyphenols reveal these health benefits through complementing and adding to the functions of antioxidant vitamins and enzymes as defense against oxidative stress, mainly caused by excess of reactive oxygen species (ROS)¹⁵. Polyphenols can decrease the oxidation rate either by preventing the free radicals formation or by deactivating the active species and the precursors of the free radicals, usually by donating an electron or a hydrogen atom¹⁶. More often, they act as chain breakers, this is, they act as direct radical scavengers of the lipid peroxidation chain reactions by donating an electron to the free radical, which neutralizes the radical and makes polyphenols to become less reactive radicals themselves, therefore stopping the chain reactions²¹⁻²³. In addition to this radical scavenging, polyphenols also act as transition metal chelators, which can prevent the oxidation caused by highly reactive hydroxyl radicals^{22,24}. So, while polyphenols are undeniably strong antioxidant molecules, most of the evidence of their antioxidant activity is based on *in vitro* studies, which are limited in terms of similarity to the mechanisms of antioxidant actions in a biological model. Nevertheless, these methods may portray well how polyphenols function as antioxidants, thus shedding light on the actual role of polyphenols in human health. However, caution must be taken since increasing evidence indicates that they may act in ways beyond the antioxidant functions *in vivo*¹⁶. For instance, once polyphenols have donated an electron or hydrogen atom, they become free radicals themselves, which can theoretically lead to pro-oxidant activities. Still, this is a question which needs to be further researched²⁵.

In recent times, natural substances isolated from food and developed as medicines have attracted substantial interest in the field of cancer, mainly because these compounds are part of the daily diet and can be consumed within a reasonable wide range of concentrations without major side effects¹⁴. With this in mind, the

connection between the potential health benefits of polyphenols and the biological routes associated with cancer has been widely investigated. The action of polyphenols has been studied in various cancers including breast, lung, skin, oral cavity, ovarian, esophagus, stomach, liver, pancreas, endometrial, thyroid, testicular bladder, small intestine, colon, urinary tract and prostate^{26,27}. It has been proved that polyphenols exhibit anti-cancer properties by interfering with molecular events involved in initiation, promotion, and progression stages²⁸.

Over the past 20 years, case-control studies have shown that a high intake of fruit and vegetables, and specific polyphenols found within these, helps to prevent the onset and progression of various types of cancer^{29,30}. At the cellular level, there is noteworthy evidence that some polyphenols influence carcinogenesis and tumor development³¹ by interacting with reactive intermediates³² and activated carcinogenic and mutagenic agents³³, by modulating the activity of key proteins involved in controlling cell cycle progression³⁴, by modulating cancer cell signaling^{13,35} and enzymatic activities³⁶, by promoting apoptosis³⁷⁻³⁹ and by influencing the expression of many cancer associated genes⁴⁰.

Another distinctive property of tumors is the increase in glucose uptake and the high rate of glycolysis which leads to the non-enzymatic glycation of proteins and the generation of advanced glycation end products (AGEs). The amount of some of these AGEs in several human tumors has been related to their involvement in cancer progression⁴¹. Interestingly, some polyphenols have been suggested to counteract AGEs formation both *in vivo* and *in vitro*, which indicates that these phenols may limit their impact on the carcinogenesis process⁴²⁻⁴⁵. Additionally, receptors for AGEs, such as RAGE, play a significant role in regulating cancer cell invasion and metastasis^{46,47} and some polyphenols can possibly inhibit cancer cell proliferation by blocking RAGE related signaling⁴⁸.

1.1.2.1. Chemical structure, sources and biosynthesis of resveratrol

Within the phenolic compounds subclass of stilbenes, resveratrol (RSV) (figure 2) is the common term for 3-5-4'-trihydroxystilbene which exists in both *trans* and *cis* isomeric forms. However, the *trans* isomer is widely studied and undoubtedly more abundant in plants¹⁸. This natural polyphenol and phytoalexin is

produced naturally by 72 different plant species, particularly grapevines, pines and legumes¹.

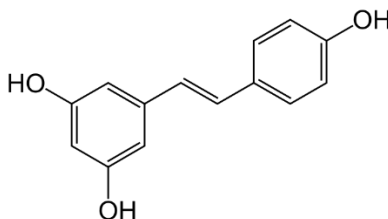


Figure 2. Chemical structure of resveratrol (trans-3-5-4'-trihydroxystilbene).

Grapes are the most abundant source of resveratrol for humans, particularly *Vitis vinifera*, *V. labrusca* and *V. muscadine* grapes, which are used in the production of several wines. This compound can be found in roots, seeds and stems of vines, but the concentration is higher in grape's skin, which contains from 50 to 100µg/g⁴⁹. The production of resveratrol is induced in response to multiple stress conditions, such as injury, chemical signals from pathogen fungi attack, exposure to ozone, sunlight, heavy metals⁵⁰, among others, and this process is carried out by the stilbene synthase (STS) enzyme, as shown in figure 3.

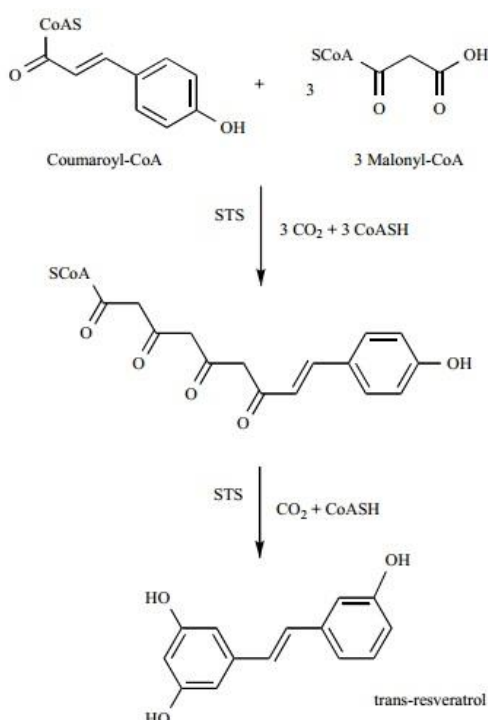


Figure 3. Schematic representation of *trans*-resveratrol biosynthesis by stilbene synthase⁵¹.

STS catalyzes three condensation reactions between coumaroyl-coenzyme A and three molecules of malonyl-coenzyme A via cleavage of three carbon dioxide molecules. Moreover, STS also catalyzes the loss of the terminal carboxyl group, leading to the production of the C14 molecule resveratrol⁵¹.

1.1.2.2. Pharmacokinetics of resveratrol: absorption, metabolism, distribution and excretion

To understand the potential beneficial properties of a given compound, it is necessary to study its absorption, distribution, metabolism and excretion (ADME). Several studies concerning the resveratrol bioavailability have been conducted both in rodents and humans.

Resveratrol consumed orally tends to be oxidized in the human digestive tract, and this process can be avoided when these molecules undergo glycosylation. Therefore, glycosylated resveratrol will not be oxidized, which will preserve its biological activity and increase its stability and bioavailability. However, several studies show that resveratrol is absorbed in the small intestine, particularly at the jejunum and the ileum, and the intestinal epithelial cells (enterocytes) are unable to absorb glycosylated resveratrol, and so this absorption process requires glycosidases. Once in the enterocytes, resveratrol is extensively metabolized resulting mainly in sulfatide and glucuronide conjugates¹⁸, suggesting that resveratrol is released from the intestinal epithelial cells in these conjugated soluble forms into the blood stream⁵². This biochemical changes that occur almost immediately after ingestion can also occur in the liver⁵¹. Although modifications such as glucuronidation and sulphation typically reduce the resveratrol cell permeability and aid in its excretion, which will diminish its bioavailability, resveratrol administered *in vivo* showed high efficiency. This combined with the fact that *in vivo* concentrations of individual metabolites can be more than ten times higher than those of the native compound, has led to speculation that resveratrol metabolites could themselves be active in promoting many of the health benefits attributed to resveratrol⁵³. However, several studies show less pharmaceutical impact of these metabolites⁵¹.

Numerous studies performed in humans show that about 70% of orally administered resveratrol (25 mg) is absorbed and metabolized in less than 30 minutes with a peak plasma level of approximately 2 μ M of resveratrol metabolites and a half-life of 9 to 10 hours. However, the resveratrol absorption and metabolization can vary between individuals depending on factors such as the hepatic function and the metabolic and enzymatic activity of the local intestinal microflora⁵¹, and also depending on the relative amounts of resveratrol and its conjugates present in the food source or dietary complement¹⁸.

One of the factors that impair resveratrol bioavailability is its poor water solubility, which hinders its ability to be solubilized in the blood. However, resveratrol is able to bind itself to plasma proteins and thus assure its body distribution and bioavailability⁵¹. Resveratrol can be bound to serum proteins such as hemoglobin and human serum albumin (HSA) by taking advantage of the electrostatic interactions which result, among other factors, from positively charged residues that are close to the binding compound. Both complexes formed are spontaneous and exothermic⁵⁴. The conversion of resveratrol into hydrophilic conjugates also facilitates its entry into the blood stream and its diffusion throughout the body. Although resveratrol can be found in the colon shortly after oral intake, its distribution in tissues requires a few hours. The liver and the gallbladder filter resveratrol and its metabolites from the circulation and transport them back into the intestine through the bile for a delayed absorption and this process is called recirculation. Figure 4 shows a schematic representation of the pathways of resveratrol ADME. Studies regarding the uptake and metabolism of resveratrol by human liver have shown that human hepatocytes exhibit an initial increasing rate of uptake (minutes), followed by a stable rate in the next few hours⁵⁵. Even though treatment with high doses of resveratrol results in great accumulation of the drug in the liver, no toxicity or hepatocyte lysis is observed, which suggests that resveratrol has an important role in the prevention of liver diseases⁵¹.

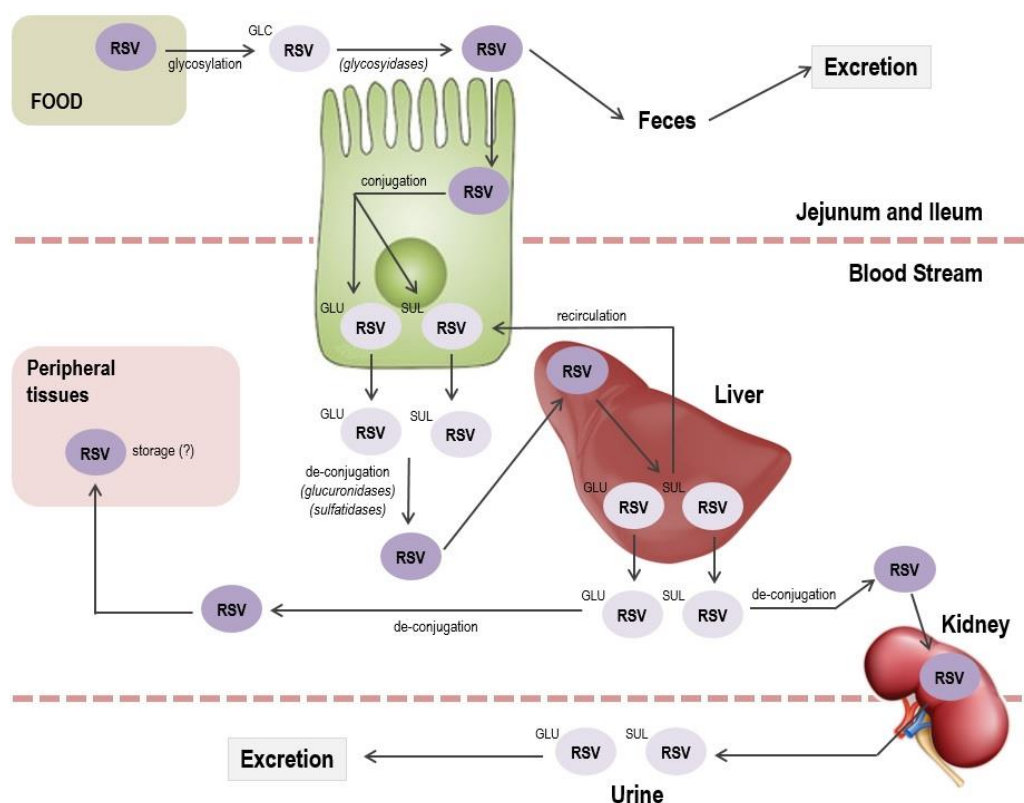


Figure 4. Schematic representation of the pathways of resveratrol absorption, distribution, metabolism and excretion. GLCRSV, resveratrol-3-O- β -glucoside (piceid); SULRSV, resveratrol-3-sulfate; GLURSV, resveratrol-3-O- β -glucuronide (adapted from ¹⁸).

In the last step of pharmacokinetics, resveratrol metabolites are eliminated from the organism and excretion is almost equally distributed between urine and feces⁵¹. However, the excretion time depends strongly on the resveratrol concentration present in plasma – small amounts of resveratrol are rapidly metabolized and eliminated whereas a higher dose of intake results in retention and accumulation of the compound in tissues, thus becoming available for cellular uptake and intracellular signaling¹⁸. Resveratrol and its metabolites are almost completely eliminated from tissues 72 hours after a single dose. In humans, the two major metabolites identified in urine were glucuronide- and sulfate-conjugates of resveratrol and of dihydro-resveratrol. The total recovery of glucuronic and sulfate conjugations in urine and feces was about 71-98% after oral doses and 54-91% after intravenous doses, while the native form of resveratrol presented a near to zero retrieval, which suggests that the circulating form of resveratrol is primarily the modified metabolites rather than its native form⁵¹.

1.1.2.3. Toxicity of resveratrol

Toxicity assessments are an important part of new drug safety profiling, since bioactive drugs may have adverse effects on the organism and on its metabolism.

Resveratrol, when administered to rodents and dogs for 13 weeks at doses up to 1000 and 1200 mg/kg/day respectively, resulted in dose-related increases in plasma levels of free and conjugated resveratrol. However, clinical observations failed to recognize any proof of resveratrol toxicity⁵⁶. Moreover, human clinical studies have been performed with single doses of 5 g of resveratrol and no adverse side effects were observed⁵¹. These observations indicate that 450 mg/day of resveratrol represent a safe dose for a 70 kg individual. Therefore, in humans, resveratrol seems to be well tolerated and to have weak toxicity, indicating that this bioactive compound can be used as a pharmacological drug in human medicine⁵⁷.

1.1.2.4. Anticarcinogenic activity of resveratrol

Antitumor agents are compounds that inhibit cancer development by blocking tumor cell transformation and proliferation, and by inducing tumor cell death¹⁸. Thus, chemoprevention and chemotherapy consist in using natural, synthetic or biologic substances to reverse, suppress or prevent the development of cancer. Amongst the food-derived molecules that can be used as antitumor agents, resveratrol is particularly interesting since it has been shown to modulate a wide range of different intracellular mediators involved in multi-stage carcinogenesis, inflammation, cell cycle and apoptosis. Evidence also supports its association with antioxidant and anti-inflammatory activities⁵¹.

Antioxidant effects

Electron acceptors react easily with free radicals, originating ROS. These chemically reactive molecules are continuously generated in cells exposed to aerobic environments, and have been associated with the initiation and progression of cancer⁵⁸, through directly damaging deoxyribonucleic acid (DNA) and other macromolecules⁵³. Resveratrol has an intrinsic antioxidant capacity that is related

to its chemopreventive effects, since it is an excellent radical scavenger that can protect cell membranes against lipid peroxidation and avoid DNA damage caused by the generation of ROS. These protective effects result from the activation of antioxidant enzymes, such as superoxide dismutase, catalase, glutathione reductase, glutathione peroxidase, glutathione transferase and oxidoreductases⁵¹. *In vivo*, resveratrol has been shown to increase plasma antioxidant capacity and decrease lipid peroxidation⁵³.

Anti-promotion effects

Cyclooxygenases (COX) produce prostaglandins from arachidonic acid and these compounds are able to stimulate tumor growth by acting on cell proliferation, angiogenesis and immunosuppression. Therefore, COX inhibitors are considered valuable therapeutic agents against several cancers⁵⁹. Resveratrol decreases the total COX activity of tumors and normal tissues *in vivo* through selective inhibition of COX-1 activity and/or reduction of COX-2 at the messenger RNA (mRNA) level. *In vitro* studies have shown that the transcriptional inhibition of COX-2, as well as another important player in carcinogenesis, ornithine decarboxylase (ODC), could be accomplished through inhibition of protein kinase C. Resveratrol does not directly inhibit ODC activity, but reduces its expression *in vivo* and prevents its induction by carcinogens⁵³.

Moreover, inflammation mediators such as COX-2, inducible nitric oxide synthase, interferon- γ , pro-inflammatory cytokines and tumor necrosis factor- α , are also involved in carcinogenesis, particularly in the promotion and progression stages. Resveratrol is able to block the expression of these various components of pro-inflammatory signaling through the suppression of the nuclear factor- κ B and of the activator protein-1. Also, resveratrol promotes a reduction of the intracellular levels of Ca^{2+} which act as a secondary messenger during cell inflammatory activation. Resveratrol also downregulates the Akt/CREB activation, a pathway that responds to various signals that drive the cell proliferation, differentiation and adaptive responses⁵¹. All functions mentioned above imply that resveratrol could slow tumor development through multiple complementary mechanisms⁵³.

Inhibition of angiogenesis

Angiogenesis is the physiological process through which new blood vessels form from pre-existing vessels and it is necessary to maintain the growth of most solid tumors with a diameter beyond 3 mm. Resveratrol, when delivered systemically at a 2.5-100 mg/kg dose, has shown to prevent tumor-induced neovascularization and to promote wound healing. Moreover the suppression of COX and ODC by resveratrol could have a role in the inhibition of angiogenesis since these enzymes promote vascularization and tumor growth.

Alterations in cell cycle and apoptosis

Resveratrol can also combat tumor formation and development by inducing cell cycle arrest and apoptosis. *In vivo* tumor models indicate that resveratrol has anti-proliferative and pro-apoptotic effects by downregulating cell cycle proteins and increasing apoptosis⁵³. Resveratrol is an effective inhibitor of ribonucleotide reductase (RR), and this inhibition leads to the arrest of the cell cycle in the G1 phase. Resveratrol also inhibits the oncogenic and oxidative stress activated tyrosine kinase Src and therefore blocks the activation of the signal transducer and activator of transcription Stat3 in malignant cells, also resulting in cell cycle arrest and loss of viability. Furthermore, resveratrol leads to accumulation, phosphorylation and acetylation of p53, a tumor suppressor protein that activates the cyclin inhibitor p21 and results in the G1/S arrest. Moreover, resveratrol also downregulates the cyclin D1 enzyme which is overexpressed in cancers and is required for cell cycle G1/S transition⁵¹.

The capacity of resveratrol to induce cell cycle arrest leads to subsequent cell apoptosis⁵⁹. Resveratrol has also been suggested to downregulate surviving, which belongs to the inhibitor of apoptosis proteins family (IAPs). Moreover, in acute lymphoblastic leukemia cells, resveratrol has been shown to induce mitochondria-mediated apoptosis through the depolarization of mitochondrial membranes by inhibiting the F1 complex of the F0/F1 ATPase proton pump⁵¹. Interestingly, resveratrol exerts its pro-apoptotic effect on tumor cells alone, while normal cells remain unharmed⁵⁹. For instance, resveratrol has been shown to sensitize several

tumor lines, but not normal human fibroblasts, to TRAIL (tumor necrosis factor-related apoptosis-inducing ligand)-induced apoptosis⁵³.

1.2. Liposomes as anti-cancer drug delivery systems

1.2.1. Lipid polymorphism

Amphiphilic lipids are those consisting of molecules with a polar water-soluble headgroup covalently linked to a water-insoluble hydrocarbon chain, also referred to as tails⁶⁰. Thus, amphiphilic lipids tend to lower the contact surface tension between the two media, acting as surfactants or tensioactive agents⁶¹.

Lipids have the ability to self-assemble in dynamic macrostructures in water, which is driven by its amphiphilic nature. Amphiphilic lipids tend to aggregate so that its hydrophobic portions are well apart from the water and its hydrophilic portions are in contact with the solvent, and the aggregation process is held by the hydrophobic effect⁶¹. Lipid molecules assemblies tend to form polymorphic structures or phases⁶² upon hydration. These different phases result from an optimization of the hydrophobic effect with a variety of intra- and intermolecular interactions, in combination with a number of geometric packing constraints. The lipid arrangement of major importance in cell biology is the lipid bilayer that constitutes the biological membranes. Such an aggregate possesses lipids in lamellar fluid phase (L_α) and is comprised of a periodic arrangement of lipid bilayers alternating with water layers to define a one-dimensional liquid crystal. Other common lipid arrangements are the micelles. Lipid molecules that are dispersed in an aqueous solution tend to form aggregates with the hydrophilic portions in contact with the surrounding solvent, being the hydrophobic portions entrapped in the micelle center. These are considered normal micellar phases (M_I). When the lipid molecules are exposed to a non-polar solvent, the hydrophilic groups are entrapped in the micelle center and the hydrophobic groups are exposed to the surrounding solvent, resulting in inverted micellar phases (M_{II}). Micellar phases can polymerize in two types of hexagonal phases corresponding to two-dimensional arrays of hexagonally coordinated cylinders in which the lipid acyl chains are oriented inside (H_I) and outside (H_{II}) the cylinders⁶³. Cubic phases (Q) are also lipid arrangements that show

a particular interest. These phases have interesting thermodynamically stable structures that consist of curved bicontinuous lipid bilayers in three dimensions, separating two congruent networks of water channels. It is suggested that the cubic phase is an intermediate of a phase transition between the H_{II} and the L_{α} phases, and that it is stabilized at a particular temperature⁶⁴.

All the lipid phases described above are considered disordered (liquid-crystalline) lipid phases. However, there are other lipid phases that are known as ordered (gel) lipid phases, which are an evidence of the structural characteristics and dynamics of lipid membranes. Amphiphilic lipids possess a specific temperature at which they undergo a transition from a two-dimensional constrained plane (gel phase) to a more freely dispersed state (liquid-crystalline phase) referred to as main phase transition temperature (T_m). The gel-to-liquid-crystalline phase transition increases the fluidity of the lipid membranes and has important consequences in lipids behavior⁶⁵.

The abovementioned lipid phases are also known as lyotropic phase structures, because the structural arrangement of lipid aggregates depends on several factors such as the temperature, the amount of water, the system's pH, the concentration of the amphiphilic molecule and the critical packing parameter (γ). The critical packing parameter is the relation between the size of the polar headgroups and the size of the nonpolar tails and is determined by equation 1, as follows:

$$\gamma = \frac{v}{\alpha_0 \cdot l_c} \quad (1)$$

where γ is the critical packing parameter, v is the volume of the hydrophobic tail, l_c is the effective length of the hydrophobic tail and α_0 is the mean surface area occupied by the hydrophilic head. The values of the packing parameter are associated with different lipid aggregates that are entropic driven and favored by the geometry of the monomers (figure 5).

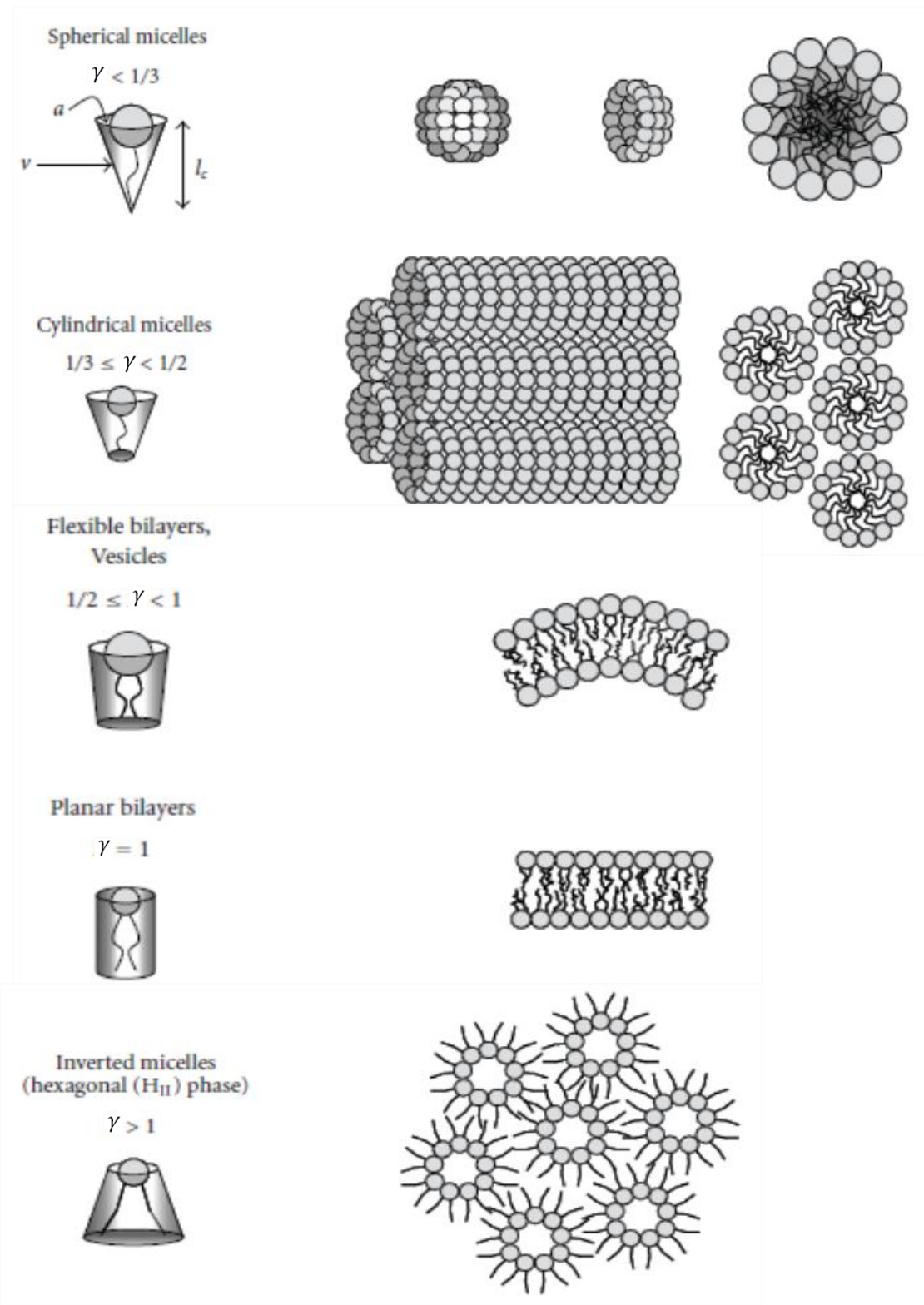


Figure 5. Impact of the packing parameter (γ) on lipid assemblies formed in aqueous solutions (adapted from ⁶⁶).

When $\gamma < 1/3$, the molecules preferentially adopt a conic shape, since they possess a large polar headgroup area and a single nonpolar tail, and tend to form

spherical micelles (M). When $\frac{1}{3} < \gamma < \frac{1}{2}$, the area of the polar headgroup diminishes until 0.33 when compared with the nonpolar tail, and the molecules adopt a geometry resembling a truncated cone, forming non-spherical micelles which can polymerize originating type one hexagonal phases (H_I). When $\frac{1}{2} < \gamma \leq 1$, the molecules adopt a nearly cylindrical shape and only planar bilayers are formed that bend to form closed vesicles that are entropically able to exist (L). When $\gamma = 1$, the molecules adopt the form of a cylinder and only planar bilayers are formed. Finally, when $\gamma > 1$, the area of the nonpolar tails is larger than the area of the polar headgroups, leading to the formation of inverted structures with negative spontaneous curvature, such as inverted micelles (M_I) which can polymerize originating type two hexagonal phases (H_{II})^{66,67}.

1.2.2. Liposome preparation and classification

Currently, liposomes are the most clinically established nanocarrier systems for drug delivery⁶⁸. Because liposomes are composed by amphiphilic lipids, in aqueous media, their thermodynamic phase properties and self-assembling characteristics influence entropically focused confiscation of their hydrophobic sections into spherical bilayers⁶⁹. Therefore, liposomes are artificial and spherical lipid bilayer vesicles that are formed by the self-assembly of amphiphilic lipids in aqueous solutions, resulting in one or several concentric lipid bilayers, with an aqueous phase in their lumen and in-between their bilayers⁷⁰. Liposome size can vary from 50 nm to several micrometers⁶⁸.

There are different subclasses of liposomes that can be produced by a wide variety of techniques. Small Unilamellar Vesicles (SUVs) are liposomes with a diameter comprised between 25 and 100 nm and can be produced by techniques such as sonication, French press and through several extrusion cycles. Large Unilamellar Vesicles (LUVs) are composed by a single lipid bilayer and have diameters between 100 and 500 nm. These vesicles can be prepared via dilution from organic solvents, detergent dialysis or extrusion of Multilamellar Vesicles (MLVs). MLVs are liposomes that can have diameters ranging from 500 up to 1000 nm and are composed of concentric layers. These can be produced by techniques involving organic solvents, freeze-thaw procedures, lipid film hydration and ethanol

injection. However, the MLVs should be produced in absence of organic solvents or detergents since these are very difficult to remove subsequently. Lastly, Multivesicular Vesicles (MVs) are liposomes which have similar sizes to those obtained in MLVs but present bilayers with distinct centers that are delimited by a wider external lipid membrane. These vesicles can also be produced by methods such as lipid film hydration and ethanol injection. All of these different types of liposomes present some advantages and disadvantages and it is sometimes difficult to define the optimal procedure for a specific application^{65,71}. The choice of the liposome preparation method depends on parameters such as the physicochemical characteristics of the lipid molecules and of the drug to be incorporated, the nature of the medium in which the lipid vesicles will be dispersed, the optimum size, polydispersity and shelf life of the vesicles for the intended application, the batch-to-batch reproducibility and the possibility of large-scale production of safe and efficient liposomal systems, among others⁷². The more commonly used techniques to produce liposomes are lipid film hydration, extrusion, sonication and solvent dispersion methods, mainly ethanol injection, which will be described subsequently.

The lipid film hydration method usually results in the formation of MLVs and consists in dissolving the lipids and mixing them in an organic solvent, usually chloroform, to assure a homogeneous lipid mixture. After obtaining a clear lipid solution, the solvent is removed to yield a lipid film. This can be achieved by evaporating the solvent using a nitrogen or argon stream or by using a rotary evaporator. Once this process is complete, the hydration of the dry lipid film is accomplished by adding an aqueous medium to the dry lipid film container and agitating. The hydrating medium temperature should be above the gel-to-liquid crystalline phase transition T_m of the lipid. The hydration time may vary according to the lipid species and structure, but a hydration time of approximately one hour with vigorous stirring and above the T_m is recommended⁷². Even though this liposome preparation method consists in a simple technique, there are some disadvantages associated with it, namely the heterogeneous population and the poor encapsulation efficiency of hydrophilic drugs. However, this experimental method can be coupled with other techniques such as sonication or extrusion⁷³.

Sonication is one of the most extensively used methods for preparation of SUVs. In this method, MLVs are submitted to a sonication bath or to a sonication

probe under a passive atmosphere. The disruption of the lipid vesicles is promoted by ultrasounds and leads to the formation of a relatively homogeneous population of SUVs. The main drawbacks of this technique are the low encapsulation efficiency, the possible degradation of the lipids and compounds to be encapsulated and the presence of MLVs along with SUVs^{65,69}.

Extrusion consists in forcing a dispersion of MLVs through polycarbonate membrane filters with well-defined pore sizes and under pressures of 300/400 psi. This process leads to the formation of SUVs and LUVs with sizes ranging from 25-100 nm and 100-500 nm respectively^{65,71}. This technique has several advantages when compared to other techniques, namely the possibility to produce liposomes of strictly calibrated size. However, it presents several disadvantages such as the difficulty in maintaining a high temperature throughout the whole experiment and the prolonged duration of the extrusion cycles⁷⁴.

The preparation of liposomes by ethanol injection consists in slowly injecting a lipid solution dissolved in ethanol into a pre-heated vast excess of aqueous media with continuous stirring, resulting in the formation of MLVs. This method also has some drawbacks, such as the heterogeneity of the population since the liposomes are formed in an uncontrolled manner, the difficult removal of the ethanol due to the azeotropic nature of the ethanol/water mixture, and the high probability of inactivation of several biologically active molecules due to the presence of even low amounts of ethanol⁶⁹.

1.2.3. Liposomes as drug-delivery systems

The introduction of drugs into the human body can be accomplished by several anatomic routes, such as gastrointestinal, parenteral, transdermal and pulmonary routes⁷⁵. In order to attain the therapeutic purpose, it is of extreme importance to choose the most suitable administration route. For that reason, several factors must be taken into consideration when administering a drug, specifically its intrinsic properties, the disease to be treated and the desired duration of the therapeutic effect⁷⁶. However, conventional drug formulations through systemic delivery have many shortcomings, namely nonspecific toxicity, side effects in non-targeted cells and tissues, and inability to precisely control the dosage⁷⁷. In fact,

with the conventional drug formulations, the drug dose maintenance in the organism is accomplished by repeated administrations, which means the existence of dose peaks at administration times alternated with sub-therapeutic drug levels⁷⁶. Hence, it is verified an impossibility of controlling the drug level over a long period of time, which constitutes a significant disadvantage of the conventional drug formulations. With that in mind, new strategies have been developed to improve treatment performance by controlling various parameters such as the rate, period of time and drugs' delivery to the target tissues, thus leading to the appearance of the so called drug delivery systems (DDS)⁷⁸. The goal of any DDS is to direct the biologically active compound towards a specific organ or tissue – targeted drug delivery⁷⁹ – and to deliver the drug in a controlled manner – time period and releasing rate –, but also to maintain the drug level in the body within therapeutic window⁸⁰. Moreover, a less frequent and more efficacious dosing regimen will most likely increase patient comfort, safety and compliance. Such systems may also result in improved efficacy with smaller amounts of the drug⁸¹.

In spite of the obvious advantages of the DDS, such as the extension of the duration of action and bioavailability of the drug, the minimization of drug degradation and loss, the prevention of the adverse side effects, the reduction of the dosing frequency, among others, these systems also present some disadvantages. These disadvantages comprise the possible toxicity of the materials, the harmful degradation of products, the patient's discomfort with device usage, the possible necessity of surgical intervention either on systems application or removal, and the high cost of the final product⁷⁶.

Recent reports have suggested that cancer cells drug uptake is particle-size dependent and that the maximum uptake by cells occurs at sizes at the nanoscale, which inflated the relevancy of nanotechnology in this field. Therefore, nanoscale structures are possibly the most appropriate candidates to serve as drug carriers for studies in biological applications⁸². Among these nanoscale structures are liposomes, which, in recent years, have gained attention as carrier systems for therapeutically active agents due to their unique characteristics. Improving the therapeutic potential of liposomes has focused mainly on developing strategies for actively targeting the liposomes to a tumor site and by triggering release of therapeutic payloads using pathological differences in the tumor's

microenvironment⁷⁰. Next, some of the major advantages of liposomes on cancer therapy will be presented. One of the major benefits of liposomes lies in the amphiphilic nature of these systems. The presence of hydrophilic and hydrophobic regions in the structure allows the encapsulation of lipophilic drugs, in the lipid bilayer, of hydrophilic drugs, in the aqueous internal core, and of amphiphilic drugs, which would locate their lipophilic regions in the lipid bilayer and their hydrophilic regions in the aqueous media⁷². Despite being synthetic structures, liposomes are easy to produce and are composed of physiological components, making them biocompatible and biodegradable. This fact makes liposomes interesting DDS since the immune system is not activated upon their release in the organism and is also associated with a decreased risk of severe toxicity^{70,83}. However, some optimizations are required so that liposomes can avoid the cells from the reticuloendothelial system, for example by surface modification with polyethylene glycol (PEG) and by size tuning to avoid sizes bigger than 250 nm. The liposome size manipulation is also of extreme importance in tumor targeting since the biodistribution of the formulation is very different from that of low molecular weight drugs. As the size of the liposomes is above the kidney clearance threshold (≈ 5 nm), they tend to circulate for prolonged periods of time. Tumor blood vessels are present at a larger extent than in normal cells (due to tumor induced angiogenesis) and are leakier than healthy blood vessels. Furthermore, tumor blood vessels present poor lymphatic drainage. The combination of these factors results in passive, progressive and relatively selective accumulation of nanoparticles in malignant tissue over time. This phenomenon is known as the enhanced permeability and retention (EPR) effect^{84,85} (figure 6). Prolonged systemic circulation allows longer interaction of liposomes with the target because the higher number of passages of blood through the target enhances the EPR effect⁸⁶. The superficial charge of liposomes can also be manipulated by selecting positively or negatively charged lipids to compose the liposomal formulation. The chosen lipids can also present a neutral charge but neutral liposomes have a more unstable character and tend to form aggregates. The superficial charge manipulation is very important since this parameter strongly affects cellular adhesion and the subsequent delivery of the drug. Liposomes composed by cationic lipids have high affinity to cells since the cell membrane is slightly negatively charged⁸⁷. Another

advantage of liposomal systems is the fact that they possess many similarities with cellular membranes, such as a fluid nature, a lipid bilayer with a lamellar structure and an amphiphilic nature. All of these factors coupled with its reduced size make them able to cross cell membranes by endocytosis, fusion, adsorption or lipid exchange processes, thus being able to deliver the drug to the targeted cell.

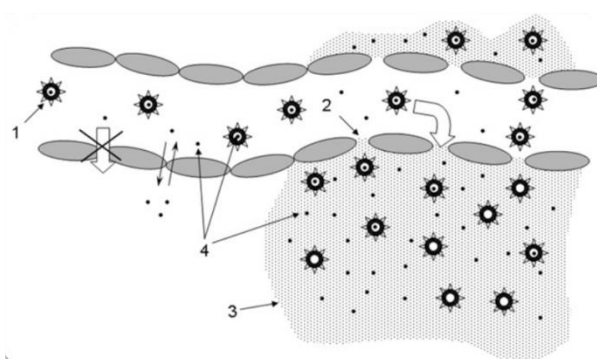


Figure 6. Enhanced permeability and retention (EPR) effect. Long-circulating drug carriers (1) penetrate through the leaky pathological vasculature (2) into the tumor interstitium (3) and degrade there, releasing a free drug (4) and creating its high local concentration⁸⁶.

The size and superficial charge manipulation are examples of passive targeting strategies since they are based simply on taking advantage of unique physiological and pathophysiological characteristics. However, targeting efficiency can be improved by using active targeting strategies. The active targeting consists in the functionalization of the surface of liposomes with affinity ligands by several conjugation chemistries. These ligands can be antibodies, peptides, aptamers or small molecules that will only bind to specific receptors on the cell surface. The liposomes will then recognize and bind to target cells through ligand-receptor interactions by the expression of receptors or epitopes on the cell surface. So that the specificity can be as high as possible, those receptors should be highly expressed on tumor cells, but not on normal cells⁶⁸. The surface modification of liposomes can also be addressed to provide them with other functionalities, including long systemic circulation, increased cellular internalization and organelle-specific drug delivery⁸⁸.

Besides this type of specific targeting, liposomes also have the advantage of releasing the encapsulated drug in response to certain stimuli, such as pH or temperature variations. The response to stimuli such as pH by these systems is very interesting since tumors develop unique microenvironments that are generally

more acidic (pH 5.7 to 7.2)⁸⁹ due to the increased glycolysis and plasma membrane proton-pump activity of tumor cells, leading to a more accentuated production of lactic acid than that of normal cells⁹⁰.

1.2.4. DODAB:MO (1:2) liposomes

Cationic liposomes are spherical vesicles that include both cationic and neutral surfactants in their composition and can differ in size, lamellarity or charge⁹¹. The cationic liposomal formulation investigated during the course of this study was composed of dioctadecyldimethylammonium bromide (DODAB), a monovalent cationic lipid, and monoolein (MO), a neutral helper lipid, in a one to two molar ratio (1:2).

DODAB (figure 7) is a cationic surfactant first synthesized by Kunitake and Okajata⁹². This lipid is commonly used in liposomes and consists of a double saturated acyl chain (C18:0) attached to a quaternary ammonium group. This quaternary ammonium headgroup is the hydrophilic portion of the lipid and grants it its positive charge, which promotes internalization by the cellular membranes. DODAB is a bilayer-forming lipid that tends to form LUVs in excess water⁹³, and has a relatively high gel-to-liquid crystalline T_m (45°C)⁹⁴.

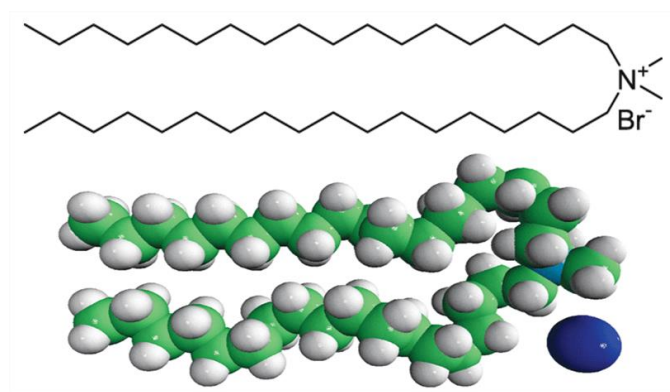


Figure 7. Chemical structure (on the top) and molecular model (on the bottom) of the lipid dioctadecyldimethylammonium bromide (DODAB).

Since the T_m of DODAB is superior to the human physiological temperature, DODAB's bilayers will display a strong rigidity at normal body temperature. On one hand, this characteristic has the advantage of producing extremely stable liposomes

that can circulate into the human body during a large period of time without the release of the encapsulated drug. On the other hand, this increased rigidity of the liposomes may have the disadvantage of diminishing the encapsulation efficiency. This major limitation of DODAB can be overcome by the addition of a helper lipid with a lower T_m to the formulation, which in this case was MO⁹⁵.

MO (figure 8) is a natural-occurring neutral surfactant presented in 1984 as a biocompatible encapsulating material with control-releasing properties. This lipid has also been proposed as a helper lipid for non-viral transfection in a new liposomal formulation that also includes the synthetic surfactant DODAB⁹⁶. Moreover, MO has interesting characteristics including its non-toxicity, biocompatibility and biodegradability caused by the esterase activity in many biological tissues⁹⁷. MO possesses a single unsaturated acyl chain (C18:1) attached to a glycerol head group, with a *cis* double bond at the 9,10 position. The glycerol molecule is attached to the hydrocarbon chain with an ester bond and has two free hydroxyls left which creates the hydrophilic region of the molecule. MO has the particularity of forming two inverted bicontinuous cubic phases (Q_{II}^D and Q_{II}^G) that create non-lamellar structures with negative curvature in excess water⁹⁸, which decreases the structural rigidity of DODAB vesicles. Moreover, the use of MO in liposomal formulation brings other advantages apart from the fluidization of DODAB's membranes, namely it causes an increase in lateral mobility of the lipid chain which in turn causes an improvement in the fusion of the liposomes with the cell membrane⁹⁵. Also, the inverted non-lamellar structure facilitates the release of the vesicular content⁹⁶.

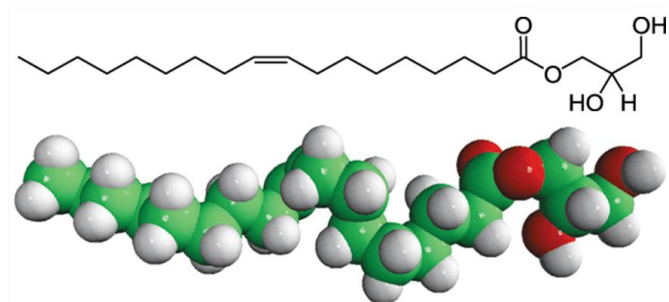


Figure 8. Chemical structure (on the top) and molecular model (on the bottom) of the lipid monoolein (MO).

The molar ratio of DODAB:MO (1:2) studied through this project promotes the formation of lamellar phases of DODAB containing inverted non-lamellar phases of MO. This leads to the formation of a vesicle that has structural rigidity caused DODAB, which is required for the retention of the encapsulated compound, and that has a fluid content as consequence of the MO inverted non-lamellar phases, which is interesting for encapsulation purposes.

CHAPTER 2

MATERIALS AND METHODS

Contents

- 2.1. Preparation of plain liposomes
- 2.2. Preparation of resveratrol loaded liposomes
- 2.3. Size and polydispersity index determination by dynamic light scattering (DLS)
- 2.4. Zeta potential determination by electrophoretic light scattering (ELS)
- 2.5. Shelf stability studies
- 2.6. Quantitative determination of resveratrol by spectroscopy
- 2.7. Encapsulation efficiency assays
- 2.8. Resveratrol biophysical effects in lipid membranes
 - 2.8.1. Influence of resveratrol in the microviscosity and cooperativity of the liposomal formulation
 - 2.8.2. Resveratrol partition coefficient (K_p) assays using a membrane-water system and derivative spectroscopy
- 2.9. Controlled release assays
- 2.10. HSA binding assays using fluorescence quenching and DLS techniques
- 2.11. Preliminary assays with free and encapsulated resveratrol in a yeast model
 - 2.11.1. Resveratrol effect in yeast cell growth under fermentative and respiratory conditions
 - 2.11.2. Resveratrol effect in yeast growth under respiratory conditions in the presence of hydrogen peroxide
 - 2.11.3. Effect of hydrogen peroxide in yeast cell death in respiratory conditions
 - 2.11.4. Liposome internalization by yeast cells assessed by fluorescence microscopy
 - 2.11.5. Cell viability and reactive oxygen species (ROS) quantification assays by flow cytometry

2.1. Preparation of plain liposomes

Before the preparation of liposomes, two lipid stock solutions – 20 mM DODAB and 20 mM MO – in ethanol *pro analysis* were prepared. Three batches of plain liposomes (placebo) were prepared by adding 167 μL of the DODAB solution and 334 μL of the MO solution to a glass tube. Approximately 1.5 mL of chloroform were added to each glass tube to better solubilize the lipids and to help evaporation. The solution was maintained under a constant stream of nitrogen until all the liquid was evaporated, leaving the lipid film adsorbed to the glass tube walls. The lipid film was hydrated with 10 mL of ultrapure water and the suspension was incubated above the lipids T_m (60°C), alternating with vigorous vortex stirring, in order to remove all the lipid film adsorbed to the glass tube walls. This process lasted for approximately 30 min and resulted in a suspension of MLVs of DODAB:MO (1:2) with a 1 mM final concentration. The MLVs suspension was then repeatedly passed through a *Lipex* extruder heated to a 60°C temperature and under pressures of 6 bar. The suspension was passed through *Nuclepore Track-Etched* polycarbonate membrane filters with different pore diameters to obtain small and homogeneous LUVs – two times through a 400 nm filter, two times through a 200 nm filter and ten times through a 100 nm filter. The triplicate samples of placebo liposomes obtained were then stored at 4°C for further shelf stability test. The schematic representation of this procedure is presented in figure 9.

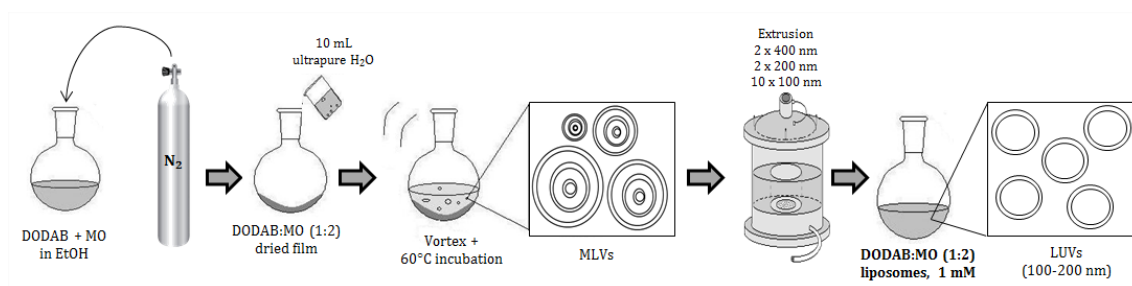


Figure 9. Schematic representation of the preparation of plain DODAB:MO (1:2) liposomes by the lipid film hydration plus extrusion technique (adapted from ⁹⁶).

2.2. Preparation of resveratrol loaded liposomes

In order to assess which is the most efficient way to encapsulate the phenolic compound resveratrol into DODAB:MO (1:2) liposomes, three different encapsulation methods were tested – incubation, hydration, and direct mixing.

2.2.1. Incubation method

The DODAB:MO lipid films were prepared as described in chapter 2.1. Lipid films were hydrated with 5 mL of ultrapure water and incubated above the lipids T_m (60°C), alternating with vigorous stirring resorting to a vortex. This process lasted approximately 30 min and led to the formation of 2 mM DODAB:MO (1:2) MLVs. The suspensions were then extruded as described in the chapter 2.1., resulting in 2 mM plain liposomes. Next, 4 mL of a 40 μ M resveratrol solution in ultrapure water were added to 4 mL of the liposomal suspension and incubated at 60°C during 60 min, resulting in resveratrol loaded liposomes, where the lipid concentration was 1mM and the resveratrol concentration was 20 μ M (2%). The samples were stored at 4°C until further analysis. When testing higher resveratrol concentrations, and since resveratrol is poorly soluble in water, a given amount of the resveratrol solution in ethanol was dried in the bottom of the tube with a stream of nitrogen and the liposome suspension with a 1 mM concentration was added to the resveratrol film and incubated as described above. The schematic representation of this procedure is presented in figure 10.

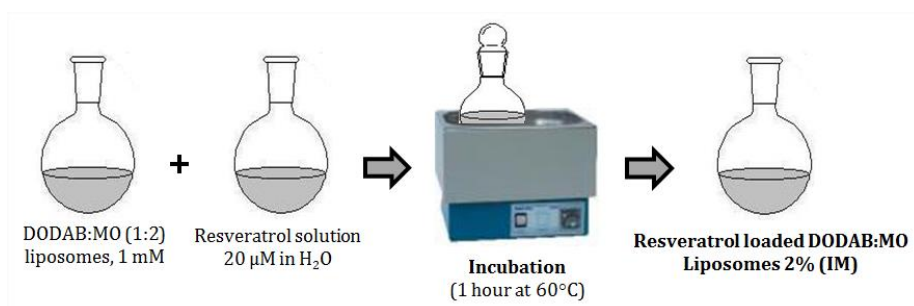


Figure 10. Schematic representation of the preparation of resveratrol loaded DODAB:MO (1:2) liposomes (2%) produced by the incubation method of encapsulation from previously formed liposomes by the lipid film hydration plus extrusion technique (adapted from ⁹⁶).

2.2.2. Hydration method

The DODAB:MO lipid films were prepared as described in the chapter 2.1. Lipid films were hydrated with 10 mL of a 20 μ M resveratrol solution in ultrapure water. The suspensions were incubated above the lipids T_m (60°C), alternating with vigorous stirring recurring to a vortex, followed by a 60 min incubation at 60°C. The resulting suspensions were then extruded as described in chapter 2.1., resulting in resveratrol loaded liposomes, where the lipid concentration was 1 mM and the resveratrol concentration was 20 μ M (2%). The samples were stored at 4°C for further shelf stability test. The schematic representation of this procedure is presented in figure 11.

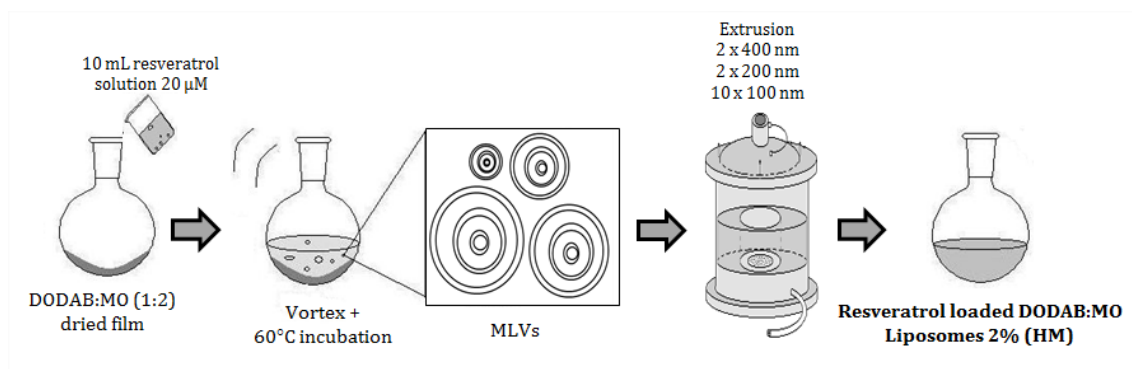


Figure 11. Schematic representation of the preparation of resveratrol loaded DODAB:MO (1:2) liposomes (2%) produced by the hydration of the lipid film method of encapsulation (adapted from ⁹⁶).

2.2.3. Direct mixing method

Resveratrol loaded liposomes were prepared by adding 167 μ L of the DODAB stock solution, 334 μ L of the MO stock solution and 3617 μ L of a 55.29 μ M resveratrol solution in ethanol to a glass tube. Approximately 1.5 mL of chloroform were added to each glass tube and the solution was maintained under a constant stream of nitrogen until a dried film was obtained. The film was hydrated with 10 mL of ultrapure water and the suspension was incubated above the lipids T_m (60°C), alternating with vigorous stirring resorting to a vortex. This process lasted approximately 30 min. The MLVs suspension containing resveratrol was then extruded as described in chapter 2.1. Once more, resveratrol loaded liposomes were

obtained, where the lipid concentration was 1mM and the resveratrol concentration was 20 μ M (2%). Samples were stored at 4°C until further analysis. The schematic representation of this procedure is presented in figure 12.

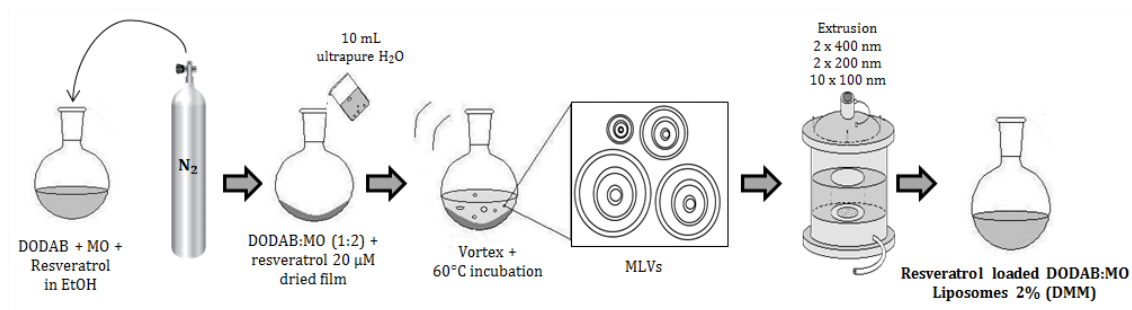


Figure 12. Schematic representation of the preparation of resveratrol loaded DODAB:MO (1:2) liposomes (2%) produced by the direct mixing method of encapsulation (adapted from ⁹⁹).

2.3. Size and polydispersity index determination by dynamic light scattering (DLS)

In order to evaluate the mean size and the polydispersity index (Pdl) of the liposomes with and without resveratrol, the dynamic light scattering (DLS) technique was used, and a brief description of this technique will be presented below.

The DLS technique, also known as photon correlation spectroscopy (PCS), is an important and powerful light-scattering technique for studying the properties of suspensions and solutions of colloids, biological solutions, macromolecules and polymers that is absolute, non-invasive and non-destructive¹⁰⁰. Figure 13 represents a diagram of an advanced dynamic light scattering apparatus capable of measuring the intensity of scattered light for solutions with low particle concentration/low particle dimensions (173° backscatter detection), as well as for solutions with high particle concentration/high particle dimensions (90° classic detection)⁶⁵.

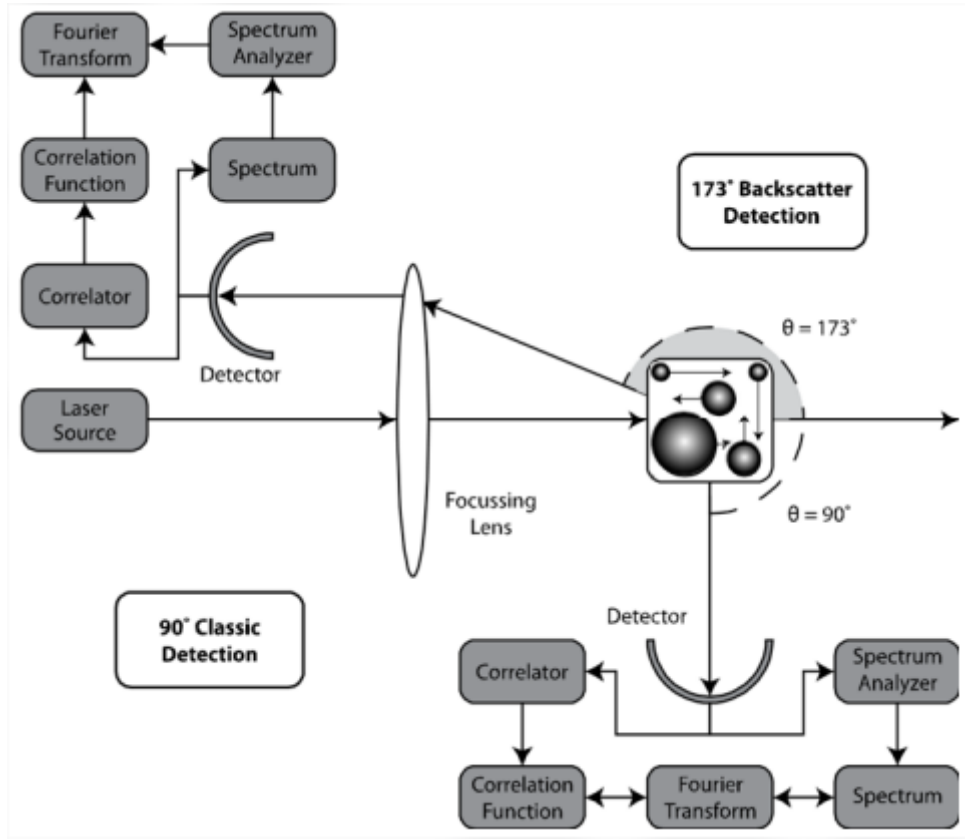


Figure 13. Schematic representation of a modern dynamic light scattering apparatus possessing both classic (90°) and backscatter (173°) configuration for detection of scattered light intensity⁶⁵.

The DLS technique consists in illuminating a given sample with a laser beam and measuring time-dependent intensity fluctuations of the scattered light arising from particles undergoing random Brownian motion¹⁰⁰. When present in a liquid medium, particles undergo this movement due to the collision of the surrounding molecules. An important feature of Brownian motion for DLS is that small particles move faster, leading to faster intensity fluctuations due to their high diffusion coefficient, and large particles move more slowly, resulting in slower intensity fluctuations. The relationship between the size of a particle and its speed due to Brownian motion is defined in the Stokes-Einstein equation (equation 2) and is simply illustrated in figure 14.

$$D = \frac{k_B T}{6\pi\eta R_H} \quad (2)$$

where D is the diffusion coefficient of the particle, k_B is the Boltzman constant ($1.38 \times 10^{-23} \text{ m}^2 \text{ kg s}^{-2} \text{ K}^{-1}$), T is the temperature, η is the dynamic viscosity of the dispersion medium and R_H is the hydrodynamic radius of the particle. As the detector measures all scattered light intensities originated by the particles, the correlator compares all the signals at successive time intervals to calculate the rate at which the intensity is varying, making possible to estimate the size of the particles due to the intensity fluctuations observed, by using specific algorithms that associate the decay rates of the autocorrelation function with a number of size classes, producing a size distribution^{65,101}.

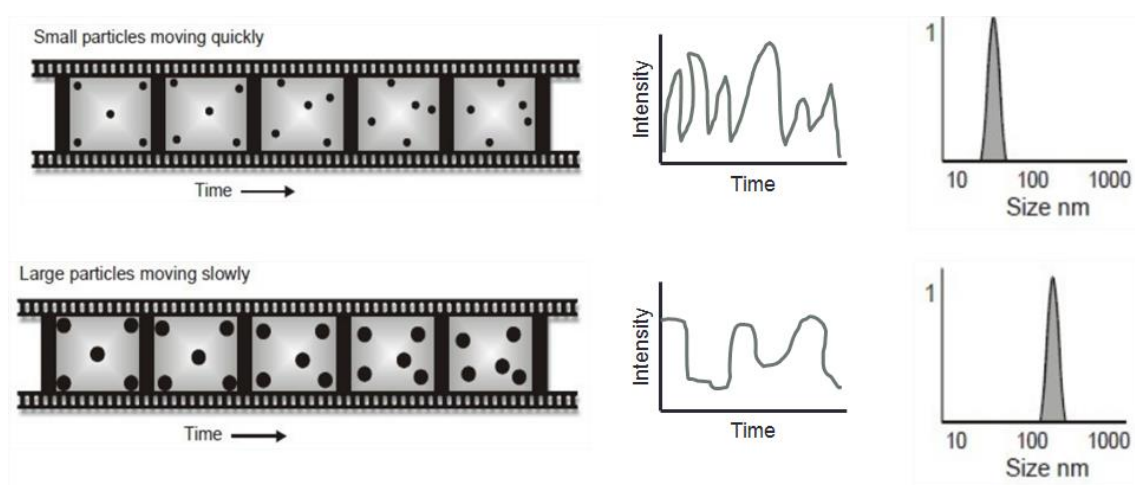


Figure 14. Schematic representation of particles moving randomly in a liquid. Their motion speed results in different intensity fluctuations which are used to determine particle size (adapted from ¹⁰¹).

The DLS technique also provides information regarding the sample's PDI, which is a number calculated from a simple two parameter fit to the correlation data – the cumulants analysis. In this analysis, a single particle size mode is assumed and a single exponential fit is applied to the autocorrelation function and the polydispersity describes the width of the assumed Gaussian distribution. The PDI is dimensionless and, according to the Zetasizer manufacturer, should be smaller than 0.6-0.7 in order to obtain a reliable measurement. However, the PDI is an indicator of the particle aggregation – a high PDI shows a polydisperse system and if the PDI is closer to zero it denotes a monodisperse system (figure 15). The reason why a system is polydisperse can be due to aggregation/agglomeration but it can also

simply be due to different primary size. That being said, it is advisable to have a small Pdl in order to obtain a monodisperse suspension and a reliable measurement.

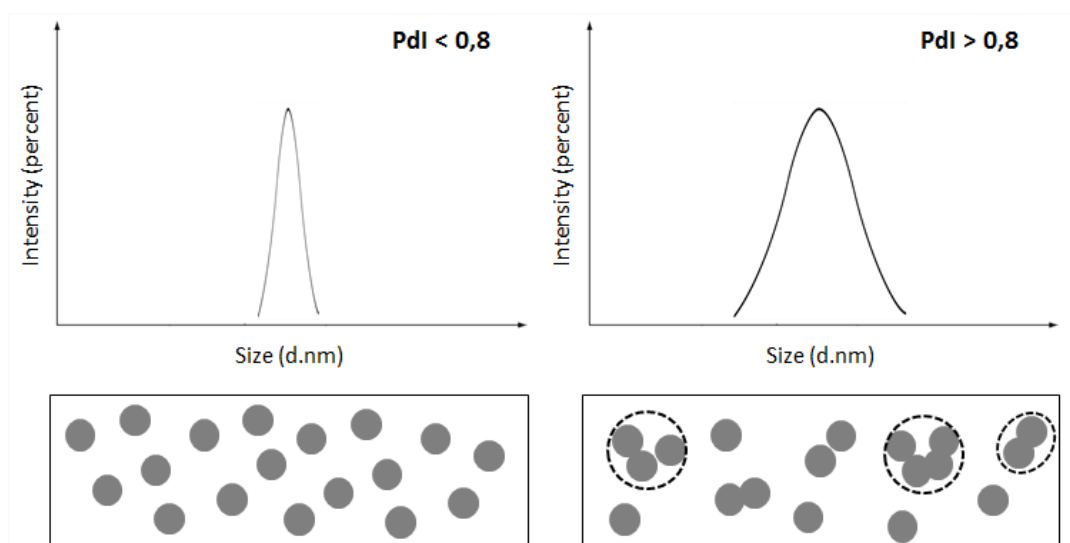


Figure 15. Schematic representation of the intensity *versus* the size distribution of two samples. The sample on the left presents particles with identical hydrodynamic radius, thus being a monodisperse population and having a small Pdl, while the sample on the right shows a heterogeneous population with the presence of aggregates which results in a higher Pdl, being this a polydisperse population (adapted from ⁹⁹).

When rigid nanoparticles are measured, it is said that a Pdl above 0.08 denotes a polydisperse system. However, the liposomes are more soft and shapeable and, in this particular case, with liposomes containing two different lipid molecules plus an encapsulated drug it becomes challenging to obtain such low values of Pdl. For this reason, Pdl values lower than 0.2 were considered acceptable for a monodisperse system.

In order to determine the mean size of liposomes with and without the encapsulated drug and their Pdl, 1 mL aliquots of DODAB:MO (1:2) plain liposomes and DODAB:MO (1:2) resveratrol loaded liposomes (2%) produced by incubation, hydration and direct mixing encapsulation methods were placed in disposable polystyrene cuvettes for DLS measurements driven by the Zetasizer Nano ZS (Malvern Instruments). The measurements were performed at 25°C in water using the *Malvern Dispersion Technology Software* (DTS). Equilibration time was defined to 60 sec and each reading consisted in five independent measurements with eleven runs each. The particle mean size (nm) and its Pdl were then determined, and the error values were taken into account.

2.4. Zeta potential determination by electrophoretic light scattering (ELS)

Particles in suspension, i.e. particles that are in contact with a liquid, tend to acquire an electrical superficial charge. This charge at the particle surface affects the distribution of ions in the surrounding interfacial region, which results in an increased concentration of counter ions (ions of opposite charge to that of the particle) close to the surface. Therefore, an electrical double layer is present around each particle. The liquid layer contiguous to the particle is composed by two parts – an inner region, called the Stern layer, where the ions are strongly bound to the particle, and an outer, diffuse region where the ions are less firmly attached (figure 16). Within the diffuse layer there is a notional boundary in which the ions and particles form a stable entity. When a particle moves, the ions within this boundary move with it, but any ions beyond the boundary do not travel with the particle. This boundary is known as the surface of hydrodynamic shear or slipping plane and the potential that exists at this boundary is called the zeta potential (ζ -potential). The determination of this ζ -potential is essential since its magnitude gives an indication of the surface charge of the particle and of the potential stability of the system. If all the particles in suspension have a large negative or positive zeta potential then they will tend to repel each other and there is no tendency to flocculate. However, if the particles have low ζ -potential values then there is no force to prevent the particles coming together and flocculating. The general dividing line between stable and unstable suspensions is generally taken at either +30 mV or -30 mV. Particles with ζ -potential values more positive than +30 mV or more negative than -30 mV are normally considered stable¹⁰¹.

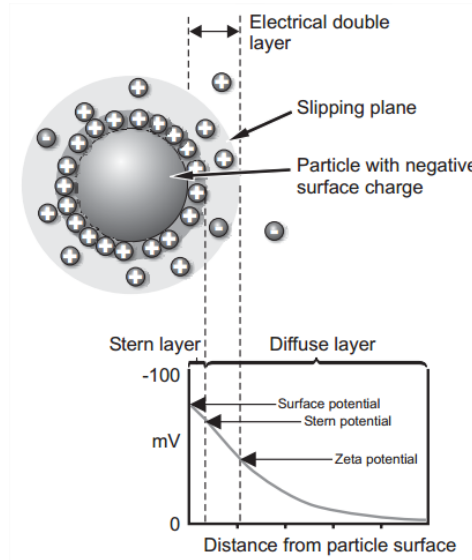


Figure 16. Schematic representation of the electrical double layer surrounding a particle in suspension¹⁰¹.

Electrophoretic light scattering (ELS), sometimes called ζ -potential, is a quasi-elastic light scattering technique used to measure the surface charge of colloidal particles in liquid media¹⁰². The Malvern Zetasizer Nano ZS calculates the ζ -potential by determining the electrophoretic mobility, which is obtained by performing an electrophoresis experiment on the sample and measuring the velocity of the particles using Laser Doppler Velocimetry (LDV), and then applying the Henry equation (equation 3), as follows:

$$\mu_E = \frac{2\varepsilon \zeta f(ka)}{3\eta} \quad (3)$$

where μ_E stands for the electrophoretic mobility, ε is the dielectric constant, ζ is the zeta potential, $f(ka)$ is Henrys function (which can be either 1.5 or 1.0 depending on particle size and dielectric constant of the medium) and η is the viscosity of the medium.

The electrophoretic mobility is assessed with resource to a cell with electrodes at either end to which a potential is applied. This will lead to the movement of particles from one electrode towards the electrode of opposite charge and so their velocity can be measured and expressed in unit field strength as their mobility. The technique used to measure this velocity is LDV which combines the light scattered at a 17° angle with the reference beam. This will then produce a fluctuating intensity signal where the rate of fluctuation is proportional to the speed of the particles

(figure 17). At that point, a digital signal processor is used to extract the characteristic frequencies in the scattered light¹⁰¹.

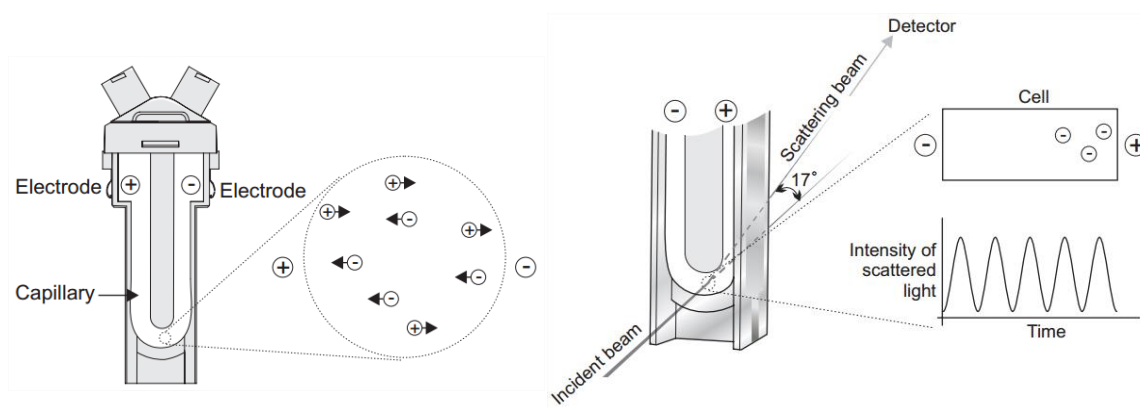


Figure 17. Schematic representation of a dip cell (left) and the LDV technique (right)¹⁰¹.

In order to determine the ζ -potential of the liposomes at study, 0.8 mL aliquots of each sample (the same samples as those evaluated in terms of size and Pdl) were placed in 0.7 mL universal dip cells for ζ -potential measurements. The dip cell was then placed in a Malvern Zetasizer Nano ZS particle analyzer and the Malvern DTS was run with a monomodal mode data processing at 25°C in water. The equilibration time was defined to 60 sec and each reading consisted in five independent measurements with ten runs in each measurement. The particles' ζ -potential (mV) was determined and the error values were taken into account.

2.5. Shelf stability studies

Since liposomes have been considered for their use as drug delivery systems, they must meet strict stability criteria over time. Hence, industrial application of liposomes requires extensive shelf stability studies. The expiration date period or shelf-life of a product is defined as the time at which the average product characteristic remains within the approved specification after manufacture.

The long term stability of a drug product containing lipids can be highly affected by the lipid species used in the formulation. In a general way, the more unsaturated a compound, the easier the product is oxidized, and thus the shorter the shelf life of the product. On the other hand, saturated lipids, such as DODAB, and monounsaturated lipids, such as MO, offer the greatest stability in terms oxidation.

However, they also have much higher phase transition temperatures and thus present other formulation shortcomings¹⁰³. Stability issues due to hydrolytic degradation are also a problem with lipid derived products. Aqueous formulations of drug products tend to be less stable since the presence of water in excess can lead to rapid hydrolytic degradation in lipid preparations. This hydrolysis depends on a variety of factors including pH, temperature, buffer species, ionic strength, acyl chain length and the state of aggregation. On the plus side, cationic liposomes, such as DODAB:MO liposomes, can be stable at 4°C for a relatively long period of time if they are properly sterilized¹⁰⁴.

With the purpose of assessing the different liposomal formulations in terms of shelf stability, parameters such as mean liposomal size, PDI, superficial charge and pH were measured throughout time. The time points tested were days 0, 7, 14, 28, 56 and 84. These measurements were performed mainly to assess if the lipid nanoparticles were suffering from membrane rupture, aggregation or sedimentation, and how the three different resveratrol encapsulation methods were influencing the stability of the liposomal formulation.

Mean size and PDI measurements were performed as described in chapter 2.3.. The superficial charge of the liposomes was assessed by ζ -potential measurements as mentioned in chapter 2.4.. Regarding the pH evaluation, this parameter was assessed resorting to a pH selective electrode connected to a decimilivoltmeter.

2.6. Quantitative determination of resveratrol by spectroscopy

During the course of this work it will be necessary to determine the resveratrol concentration in certain samples, which was done resorting to spectroscopy techniques, namely UV/Vis absorbance spectroscopy.

Molecular absorption spectroscopy in the ultraviolet and visible spectral regions is a widely used technique for the quantitative determination of a large number of inorganic, organic and biological species.

When a light beam passes through an absorbing medium, and if the energy provided by the light beam is enough to promote an energetic level transition of the electrons from a ground state to an excited state, the photons in the light beam will be absorbed. The absorption capability of a given compound can be used to quantify

that same compound, by measuring the intensity of the light beam, on a specific wavelength, before and after its interaction with the sample. These parameters can be correlated by equation 4, as follows:

$$I_{\lambda} = I_0 e^{-\alpha_{\lambda} l} \quad (4)$$

where I_{λ} is the intensity of the transmitted light, I_0 is the intensity of the incident light, α_{λ} is the absorption coefficient and l is the thickness of the sample. When absorption occurs, the intensity of the transmitted light (I_{λ}) that is captured by the detector will be inferior to the intensity of the incident light (I_0). The ratio of light that passes through the sample at a specific wavelength is referred to as transmittance (T_{λ}) and is given by equation 5:

$$T_{\lambda} = \frac{I_{\lambda}}{I_0} \quad (5)$$

The transmittance (T_{λ}) is directly related to the absorbance (A_{λ}) by applying equation 6:

$$A_{\lambda} = -\log T_{\lambda} \quad (6)$$

The higher the concentration of a given sample, the higher the absorbance will be, since the concentration is related to the absorption coefficient by equation 7:

$$\alpha_{\lambda} = 2.303 \varepsilon_{\lambda} c \quad (7)$$

where α_{λ} is the absorption coefficient, ε_{λ} is the molar absorption coefficient and c is the concentration of the sample. Also, the greater the distance covered by the light beam, the higher the absorbance will be. All this previous relations can be put together by the Lambert-Beer law (equation 8), as follows:

$$A_{\lambda} = \varepsilon_{\lambda} c l \quad (8)$$

Therefore, the Lambert-Beer law provides a direct proportionality between the light absorbance and the concentration of a compound at a given wavelength (λ). However, this law can only be applied for monochromatic radiation (for each wavelength radiation there is a corresponding absorption coefficient) and for

samples that present a unique absorbent species. If there is more than one absorbent species in the same sample, the absorbance corresponds to the sum of the absorbance of both species¹⁰⁵.

In the present study, a scanning spectrophotometer Shimadzu UV-3101PC UV-Vis-NIR was used to analyze the samples. This spectrophotometer emits electromagnetic radiation from the ultraviolet (UV) to the infrared (IR) regions, using deuterium lamps for the UV region (190-350 nm) and tungsten lamps for the visible-IR region (350-2500 nm). The radiation emitted by the lamps will pass through a slit, which was defined to have a 1 nm width, and will then pass through a diffraction grating and through a monochromator. The light beam will then pass through a beam splitter that will divide the beam in two beams, one being aimed to the sample cell, and the other being aimed to the reference cell. The light that passes through both samples will then be transferred to the photodiodes, which are photodetectors that generate a current proportional to the incident light intensity. This photodiodes are connected to a computer that will process the data and produce an absorbance spectrum that represents the absorbance variation *versus* the wavelength of the incident radiation (figure 18).

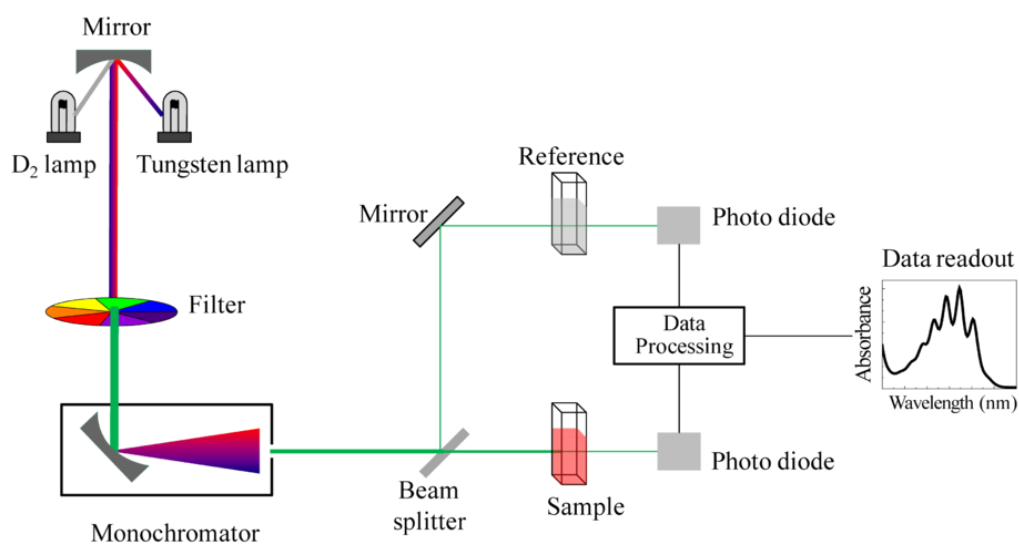


Figure 18. Schematic representation of the components of a double beam spectrophotometer¹⁰⁶.

In order to obtain more accurate results, a baseline was done to remove the “background noise” from the sample. This background noise consists in unnecessary

and undesirable peaks caused by oxygen, carbon dioxide, impurities in the air and in the liquid sample itself, among others. Therefore, when a baseline is performed, only the desired sample will be measured, and the results will be more reliable. In order to do this, a first reading was made with two cells containing the solvent placed in the equipment. The first one was used as a control and remained in the equipment throughout the whole experiment (reference), and the second one was only used to do the baseline, since it contained only the solvent in which the compound to be studied was dissolved in. The latter sample is called a blank and it will be subtracted from the actual data by the equipment software.

The absorbance of all the samples assessed throughout this study was measured using the *UV-PC software* and the wavelength ranged from 220 to 400 nm. In order to ensure that the background noise is the minimum possible, the scan speed was defined to low and the sampling interval was defined to 1 nm.

2.6.1. Construction of resveratrol calibration curves by UV/Visible Absorbance Spectroscopy

The simpler way to determine the resveratrol concentration in a given sample is to construct a resveratrol calibration curve that correlates the absorbance of a sample with the resveratrol concentration in that sample. Since, during this study, three different solvents were used, three calibration curves had to be made, one for each solvent. The first solvent used was ultrapure water – a 100 μM resveratrol solution in ultrapure water was prepared and then eleven other solutions were prepared by successively diluting the 100 μM initial solution, resulting in twelve final standard solutions with resveratrol concentrations of 100, 80, 60, 40, 20, 10, 5, 4, 3, 2, 1 and 0.5 μM . The next solvent consisted in HEPES buffer (0.01 M; pH = 7.4) and ultrapure water in a 1:1 ratio – a 100 μM resveratrol solution was prepared and was successively diluted, resulting in eight final standard solutions with resveratrol concentrations of 100, 80, 60, 40, 20, 10, 5, 1 μM . Lastly, a 100 μM resveratrol solution in a solvent that consisted in acetate buffer (0.2 M; pH = 5) and ultrapure water in a 1:1 ratio was prepared and was also successively diluted, resulting in eight final standard solutions with resveratrol concentrations of 100, 80, 60, 40, 20,

10, 5, 1 μM . The absorbance spectra of all the standards were measured at 200-400 nm using, for each case, water, HEPES buffer or acetate buffer as reference.

The appropriate wavelength to construct the calibration curve is the wavelength corresponding to the peak with higher absorbance intensity. Resveratrol presents two satisfactory absorption peaks, but only one was chosen to construct the calibration curve. In the calibration curve, each resveratrol concentration corresponds to the maximum intensity in the corresponding spectrum at the selected wavelength.

After obtaining the scatter plot that correlates the samples absorbance to the resveratrol concentration, a linear trend line was adjusted to the data that can be expressed by a mathematical equation (equation 9):

$$y = mx + b, \quad R^2 \approx 1 \quad (9)$$

where y corresponds to the absorbance intensity, m corresponds to the slope of the linear plot and also to the molar absorption coefficient (ϵ_λ), x corresponds to the resveratrol concentration, b corresponds to the y intercept and R^2 corresponds to the determination coefficient. The y intercept value (b) should not be statistically different from zero, since it is expected that an absorbance intensity of 0 corresponds to a 0 μM resveratrol concentration. Regarding the determination coefficient (R^2), this should be as close to the unity as possible, indication that the data fits well the linear regression.

2.7. Encapsulation efficiency assays

Ideally, the total amount of resveratrol added to each liposomal formulation would be effectively encapsulated in the system. However, resveratrol may not be entirely encapsulated in the system and some of it may remain free in the aqueous solution. Moreover, in encapsulation methods such as the hydration and direct mixing methods, resveratrol is added prior to the liposomes extrusion, which can lead to the accumulation of some resveratrol in the polycarbonate membrane filters. Therefore, in order to determine if the resveratrol encapsulation into the liposomal system was effective and which of the studied encapsulation methods is more

efficient, an amicon centrifugation followed by a derivative spectroscopy analysis was performed. The samples were prepared as described in chapter 2.2., resulting in resveratrol loaded liposomes with 2% resveratrol produced by incubation, hydration and direct mixing method.

Prior to the beginning of the assay, the amicon centrifugal filter units were washed with 3 mL of a water:ethanol mixture (1:1) and centrifuged at 4000 rpm during 15 min. This process was repeated two more times to ensure that the filters were thoroughly cleaned. One last centrifugation was performed with ultrapure water, after which the amicon tubes were carefully dried with paper and the amicon filters were dried by inverting and shaking until there was no water remaining.

Resveratrol encapsulation efficiency was then assessed by placing 1.5 mL of each sample in the amicon centrifugal filter units (100 kDa) and then submitting the amicon filters to centrifugation at 3000 rpm during 10 min. This will cause the non-encapsulated resveratrol to pass through the filter and get deposited in the falcon tube, while the resveratrol present in the liposomes remains in the filter, since the liposomes are not able to pass through the filters. Next, the content of the amicon filters and the content of the falcon tube were transferred to 1.5 mL *Eppendorf* tubes and ultrapure water was added to each *Eppendorf* tube in order to make up the solution to a total volume of 1500 μ L. Each sample was then analyzed by spectrophotometry as described in chapter 2.6.1. and a derivative of the spectra was performed in order to nullify the liposome's light scattering effect in the resveratrol spectra, which will be explained later on. This way, it is possible to know the resveratrol concentration present in the tube (i.e. non-encapsulated resveratrol), the resveratrol concentration present in the filter (i.e. encapsulated resveratrol) and the total resveratrol concentration (i.e. sum of the tube and filter concentrations). The resveratrol encapsulation efficiency was then determined by applying equation 10, as follows:

$$EE (\%) = \frac{[Resveratrol]_{filter}}{[Resveratrol]_{total}} \times 100 \quad (10)$$

where *EE* corresponds to the resveratrol encapsulation efficiency in percentage, $[Resveratrol]_{filter}$ represents the resveratrol concentration in the amicon filter, and

$[Resveratrol]_{total}$ corresponds to the sum of the filter and the tube resveratrol concentrations.

After analyzing the results and selecting the method by which the highest encapsulation efficiencies are obtained, a new experiment was conducted in which different resveratrol concentrations were added to the liposomes, namely 5, 40, 60 and 100 μ M, which resulted in resveratrol loaded liposomes with a resveratrol content of 0.5, 4, 6 and 10% respectively. The drug loading efficiency of these new resveratrol loaded liposomes was assessed as previously described in this chapter and by employing equation 11, as follows:

$$Drug\ loading\ (\%) = \frac{(mass\ of\ the\ total\ drug - mass\ of\ free\ drug)}{mass\ of\ total\ lipid} \times 100 \quad (11)$$

2.8. Resveratrol biophysical effects in lipid membranes

2.8.1. Influence of resveratrol in the microviscosity and cooperativity of the liposomal formulation

In the past recent years, pharmacological research has largely focused on the use of surfactant-derived organized systems, such as liposomes, to carry and release drugs. Therefore, determination of the T_m of surfactant molecules is of fundamental importance since the colloidal drug carrier system's properties strongly depend upon their phases. Liposomes' phase transitions in biological media are associated with abnormalities in its macroscopic physical properties such as the stability, fluidity or permeability of membranes which are closely dependent on their T_m . For instance, a liposome becomes highly permeable near the gel to crystalline T_m of its membrane¹⁰⁷. Furthermore, the study of the drug-membrane interaction is of great importance since it allows to predict what happens in the pharmacokinetic and pharmacodynamics phases and in which way the drug influences the membrane dynamics. In liposomes, the membrane dynamics is of extreme importance since it determines, among other things, if the formulation releases more or less easily the encapsulated drug. Moreover, drugs interacting with membrane and liposomal

lipids can modify the membrane dynamics due to the drug influence on several parameters that determine the fluidity of the system, such as: the order and/or packaging of the lipid membrane constituents, as well as the microviscosity and cooperativity of the phase transition.

In the present study, the DLS technique was employed to determine the T_m of the liposomal formulation since the phase transition induces variations in the optical properties of the system, which leads to a correlation with its refraction and absorption coefficients. At critical temperatures (pre-transition or main transition temperature), conformational modifications of the amphiphilic compounds such as lateral diffusion, lateral expansibility, bilayer thickness, bending, permeability, among others, occur. This can involve size variations, specified by the hydrodynamic radius measurements. However, surface modifications of aggregates are not always correlated with the diffusion coefficient which enters into the calculation of the hydrodynamic radius. On the other hand, the mean count rate (average number of photons detected per second) appears to be much more reliable because of its raw sight, simplicity and reproducibility. The changes in the measured scattering intensity reflect changes in the optical properties of the material but are not directly size dependent. Therefore, discontinuity in the mean count rate as the temperature is altered, corresponds to a change in optical properties of the material studied, i.e. transition from initial state to another state. Therefore, each phase transition of the liposomal system produced by a variation of the temperature can be easily characterized with this technique¹⁰⁸.

With the purpose of understanding how resveratrol impacts membrane biophysical properties such as T_m and phase transition cooperativity (B), a plain liposomal formulation of DODAB:MO (1:2) with a 6 mM concentration was prepared as described in chapter 2.1.. Also, a 6mM DODAB:MO (1:2) formulation containing resveratrol (0.7%) was prepared according to the protocol described in chapter 2.2.1.. The assay was conducted in the presence and in the absence of the drug within the liposomal system. An 1 mL aliquot of the DODAB:MO (1:2) liposomes with and without resveratrol was placed in a disposable polystyrene cell and the measurements were performed in a Zetasizer Nano ZS (Malvern Instruments) employing the DLS technique. The position of the detector was at 173° relative to the laser source (backscatter detection). A first optimization stage was performed,

where cell position and attenuator settings for the cell, sample, and measurement type were determined by the default software that adjusts these values based on the sample optical properties such as turbidity, etc. This step was repeated five times in order to achieve accurate reproducibility in the intensity of the scattered light. These parameters were then introduced and locked manually for the second stage of the experiment. The attenuator was defined to 6 and the cell position was defined to 4.65 nm. In this second stage, software was used in trend mode which allows multiple measurements to be made over a range of temperatures, being the initial temperature defined to 25°C and the final temperature defined to 60°C, since the phase transition temperature of both lipids composing the formulation are contained within this range of temperatures. The temperature interval was defined to 1°C and the number of measurements made at each step after equilibration time was 3. Data were collected as “mean count rate *versus* temperature” as showed in figure 19 and treated with a modified Boltzmann regression curve (equation 12), presented below:

$$CR = b_{L1} + m_{L1}T + \frac{b_{L2} - b_{L1} + m_{L2}T - m_{L1}T}{1 + 10^{B(\frac{1}{T} - \frac{1}{Tm})}} \quad (12)$$

where CR represents the average count rate, b_{L1} and b_{L2} represent the y intercept of the straight lines before (b_{L1}) and after (b_{L2}) the phase transition, m_{L1} and m_{L2} represent the slope of the straight lines before (m_{L1}) and after (m_{L2}) the phase transition, T represents the absolute temperature within the cell, B represents the phase transition cooperativity of the system and Tm represents the main phase transition temperature of the system (transition from the gel phase to the liquid-crystalline phase).

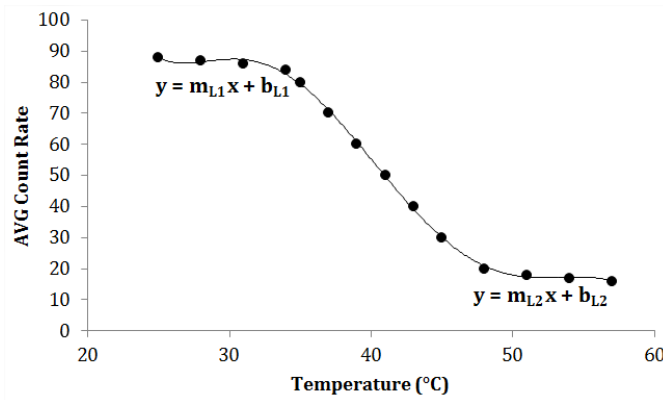


Figure 19. Example of a sigmoid profile curve representing the phase transition after the nonlinear fitting to equation 12, where the refined parameters are Tm and B .

2.8.2. Resveratrol partition coefficient (K_p) assays using a membrane-water system and derivative spectroscopy

The action of a given drug in the organism has three distinct phases:

(i) The pharmaceutical phase consists in the dissolution of the active ingredient from the formulation so that the drug is ready to be absorbed into the body. This phase is determined by the drug's physicochemical properties and the administration route;

(ii) The pharmacokinetic phase consists in the drug's route throughout the body until it reaches the site of action and includes processes such as absorption, distribution, metabolism, excretion and toxicity (ADME/Tox), which will influence the drug concentration;

(iii) The pharmacodynamic phase consists in the drug interaction with the site of action (drug-receptor, drug-enzyme or nonspecific drug interaction), which leads to the pharmacological effect¹⁰⁹.

Therefore, the existence of *in vitro* studies for drug characterization and profiling of these phases is essential, not only to avoid the high costs of *in vivo* cell studies, but also to select beforehand the most promising drugs with high pharmacological activity and low side effects¹¹⁰. A common approach to these *in vitro* studies is to use simple and controllable membrane models, such as liposomes in order to define and characterize the drug's clinical profile.

The lipophilicity of a compound is a very important characteristic for the pharmacological study of that compound and refers to its ability to be dissolved in fats, oils, lipids and non-polar solvents. The lipophilicity of a drug is a key feature since it is strongly related to ADME/Tox processes. For instance, the passive transport of drugs across membranes implies the existence of an equilibrium between the liposolubility (solubility in membranes) and hydrosolubility (solubility in aqueous media like blood and cytosol). The drug should be liposoluble enough to be able to cross membranes and be available in biological tissues (bioavailability) but not so much that would lead to bioaccumulation and toxicity. The partition coefficient (K_p) of a drug is the ratio of concentrations of a compound in a mixture of two immiscible phases at equilibrium and it is used to determine the lipophilicity of the drug. For example, liposomes can carry hydrophilic, hydrophobic and

amphiphilic molecules due to their biphasic properties. Molecules with distinct Kp will be located in different parts of the liposomes – hydrophilic molecules will be either trapped in the inside aqueous phase or attached to the polar surface of the liposomes, where they are in contact with the external aqueous surroundings; on the other hand, lipophilic molecules will be completely encapsulated within the lipid bilayer.

The Kp determination through UV/Vis spectrophotometry is based on the compound spectral variations that arise from the compound being located in environments with different polarity¹¹¹. Given the definition of Kp and the conditions under which the law of Lambert-Beer is applied, the absorbance of a solution containing a given drug concentration (Abs), which is shared between the membrane (m) and water (w) phases can be related with Kp according to equation 13¹¹².

$$Abs_T = \frac{Abs_w + (Abs_m - Abs_w)Kp [L]V\phi}{1 + Kp[L]V\phi} \quad (13)$$

where Abs_T corresponds to the total absorbance of the compound, Abs_m corresponds to the compound absorbance in the lipid phase, Abs_w corresponds to the compound absorbance in the water phase, Kp corresponds to the adimensional partition coefficient, $[L]$ corresponds to the lipid concentration (mol.L^{-1}) and $V\phi$ corresponds to the lipid molar volume (L.mol^{-1}). The application of this equation, however, is inadequate to systems that cause light scattering, as is the case of liposomes. In order to eliminate the spectroscopic interference of light scattering, the absorption spectra of the liposomal suspension with the same lipid concentration as the samples will also be measured. These spectra will then be subtracted from the correspondent sample spectra. Still, this subtraction is not enough to totally eliminate the liposome's background interference. Therefore, the derivative spectrophotometry should be employed by using the Savitzky-Golay algorithm, which uses a second order polynomial convolution of thirteen points and a wavelength interval of 1 nm. These sub-routines are provided by the spreadsheet Kp calculator 3.1, a tool developed by the research group. The Kp determination by derivative spectrophotometry is calculated by adjusting equation 14 to the

experimental data (D versus $[L]$) through a non-linear regression method where the adjustable parameters are Dm and Kp , using *OriginPro 9.0*.

$$D = Dw + \frac{(Dm - Dw)Kp [L]V \phi}{1 + Kp [L]V \phi} \text{ where, } D = \frac{\partial^n Abs}{\partial^n \lambda} \quad (14)$$

where D corresponds to the derivative of the compound total absorbance, Dw corresponds to the derivative of the compound absorbance in water and Dm corresponds to the derivative of the compound absorbance in the membrane.

In medicinal chemistry, the thermodynamics of the transfer of drug components from one medium into another are useful parameters and they can be calculated when the Kp is measured as a function of different temperatures. The retrieved information can be used to predict the absorption, membrane permeability and the *in vivo* distribution of the drug. That being said, the thermodynamic parameters of the system can be calculated using the Kp values of the system at different temperatures and the Van't Hoff equation (equation 15), as follows:

$$\ln(Kp) = -\frac{\Delta H}{RT} + \frac{\Delta S}{R} \quad (15)$$

where ΔH (kJ.mol⁻¹) is the enthalpy change between the membrane and the water phase, which corresponds to the energy released from the system when it remains under constant pressure; R is the ideal gas constant (8.314 Jmol⁻¹K⁻¹); T is the temperature in Kelvin; and ΔS (kJ.mol⁻¹) is the entropy change of the liposome/water system, which is a measure for the disorder of the system.

Finally, knowing the enthalpy and the entropy of the system and using equation 16, it is possible to calculate the Gibbs free energy (ΔG) in kJ.mol⁻¹.K⁻¹, which will provide information regarding the spontaneity of the changes that occur in the system.

$$\Delta G = \Delta H - T\Delta S \quad (16)$$

2.8.2.1. Determination of the resveratrol partition coefficient (K_p) in liposomal systems in water

In order to determine the resveratrol K_p in the liposomal system, nine suspensions with a final volume of 1500 μL were prepared in *Eppendorf* tubes, containing a fixed resveratrol concentration (43 μM), increasing concentrations of the DODAB:MO (1:2) liposomal system (51, 10, 200, 301, 400, 600, 800, 1000 and 2000 μM) and ultrapure water to act as a solvent. Nine other suspensions were prepared in another set of *Eppendorf* tubes containing blanks or references. The references presented the same increasing concentrations of lipid as the ones stated above but did not contain resveratrol. Furthermore, three other references were prepared containing only resveratrol with a 43 μM concentration, also with ultrapure water as a solvent. Samples were then incubated in a 60°C bath for 60 min. After incubation, the samples were analyzed by UV/Vis spectrophotometry with a wavelength range from 220 to 400 nm, at slow scanning speed and with a sampling interval of 1 nm.

2.8.2.2. Determination of the resveratrol thermodynamic parameters of its membrane partition

A K_p assay at different temperatures was carried out with the intention of determining the thermodynamic parameters of resveratrol membrane partition. Samples were prepared as described in chapter 2.8.2.1. and incubated in a 60°C bath for 30 min. Next, samples were analyzed by UV/Vis spectrophotometry at temperatures of 30, 37, 50, 55 and 60°C. The TCC Controller 260 was used to regulate temperature. The readings were carried out five minutes after the insertion of the cell in the spectrophotometer so that the temperature within the cell was undoubtedly stable.

2.8.2.3. Determination of the resveratrol partition coefficient (K_p) in liposomal systems at biologically relevant pH values

Lastly, a *K_p* assay at different relevant physiological pH, namely the blood pH (mimicked by HEPES buffer with a pH = 7.4) and the tumor microenvironment pH (more acidic, in this case mimicked by Trizma buffer (0.1 M) with a pH = 5), was carried out. After the preparation of liposomes with double lipid concentration (2 mM), the same amount of the liposomal suspension and of the respective buffer was added to a falcon to obtain buffered liposomes (1 mM). Once again, the samples were prepared as described in chapter 2.8.2.1.. However, instead of the volume of the *Eppendorf* tubes being made up with ultrapure water, it was completed with a mixture of buffer:ultrapure water (1:1). The samples were then incubated in a 60°C bath for 30 min and analyzed by UV/Vis spectrophotometry.

2.9. Controlled release assays

Liposomes are one of the most extensively used nanocarriers in medicine and there are several approaches to target liposomes to a specific site. However, this targeting of the liposomal system is useless if the encapsulated drug is not released at the intended site. Therefore, the *in vitro* kinetics of drug release from liposomes must be determined since this is an essential feature of the liposome's design and will define the quality of the formulation and its performance *in vivo*¹¹³. Ideally, when liposomes are yet to arrive to the action site, the drug release should be as slow as possible in order to avoid significant drug loss in the organism and hence reducing its toxicity¹¹⁴. On the other hand, after the liposome accumulation at the target site, the drug must be released at a controlled rate, which can be achieved by formulation features and/or imposed chemical or physical means¹¹⁵.

2.9.1. In storage conditions

To assess the resveratrol release from the DODAB:MO (1:2) liposomes in storage conditions, resveratrol loaded liposomes (20%) were prepared as described in chapter 2.2.1.. The assay was carried out in liposomes with a resveratrol

concentration of 200 μ M since these liposomes were the ones used in the biological experiments. The liposomes were maintained in a large falcon tube, with ultrapure water as solvent, at 25°C. The time points selected to assess the drug release were 0, 1, 2, 3, 4, 5, 22, 24, 28, 45 and 46 h. The time point 0 h corresponds to the first time point taken after the liposomes cooled down after their production. At each time point 1.5 mL of the samples was placed in an amicon centrifugal filter unit (100 kDa) and the protocol followed was the same as the one described in chapter 2.7.. In this case, the resveratrol release from the liposomes corresponds to the concentration found in the amicon tube, since the resveratrol that passes through the filter is the resveratrol that was already released from the liposomes. The samples were then analyzed by spectrophotometry as described in chapter 2.6.1.. Resveratrol concentration was calculated using resveratrol calibration curve in ultrapure water and the cumulative values of this concentration were plotted against the time to obtain a release profile of the encapsulated drug.

2.9.2. In physiological conditions

The protocol followed to assess the resveratrol release from the DODAB:MO (1:2) liposomes in physiological conditions was the same as the one described in chapter 2.9.1.. To mimic the physiological conditions in the blood, HEPES buffer with a pH of 7.4 was used. The liposomes were produced with a lipid concentration of 2 mM and then diluted in buffer in a 1:1 ratio. The time points selected to perform the measurements were 0, 1, 2, 3, 4, 5, 22, 24, 28, 45 and 46 h. In this case, the resveratrol concentration in the samples was determined through a resveratrol calibration curve performed in ultrapure water:HEPES buffer (1:1). In order to simulate the tumor microenvironment, acetate buffer with a pH of 5 was used. Once again, liposomes were produced with a lipid concentration of 2 mM and then diluted in buffer in a 1:1 ratio. The time points selected to perform the measurements were 0, 1, 2, 3, 4, 22, 23, 25, 26, 45 and 46 h. The resveratrol calibration curve used to determine its concentration in the samples was performed in ultrapure water:acetate buffer (1:1).

2.10. HSA binding assays using dynamic light scattering (DLS) techniques

Most drugs are able to bind to plasma proteins when they enter the body and are absorbed to the blood plasma system and so drug-protein interactions are a very important object of study, particularly the interaction of drugs with the human serum albumin (HSA), since this is the most abundant protein in blood plasma and serves as a depot and transport protein for numerous endogenous and exogenous compounds¹¹⁶. HSA is a soluble and monomeric protein produced in the liver and it is responsible not only for the transport of endogenous drugs but also for the transport of hormones and fatty acids, for the maintenance of the osmotic pressure, among other functions. It has been shown that HSA binds to a large number of different compounds in a reversible manner and different ligand binding sites have been identified for HSA, two of which are major drug binding sites¹¹⁷. The drug-HSA complex can be regarded as a form of drug in the biology temporary storage that can effectively avoid drug elimination and thus maintain the total and effective concentrations of the drug in plasma. Moreover, the binding of drugs to HSA controls their free and active concentrations and provides a reservoir for a longer action. Therefore, the interaction of drugs and its competition for the binding sites of HSA might strongly affect its bioavailability, distribution, elimination, pharmacodynamics and toxic properties¹¹⁸.

Under any specific set of solution conditions, an equilibrium will be established between the free and bound forms of the enzyme. The position of this equilibrium is commonly quantified in terms of the dissociation constant (K_d), for the binary complex at equilibrium (equation 17). The relative affinity or binding strength of the different enzyme-ligand complexes is inversely proportional to the value of K_d – the tighter the ligand binds, the lower the value of K_d . The K_d can be determined by fluorescence quenching of the intrinsic fluorescence, according to the following equation¹¹⁹:

$$k_d = \frac{[enzyme]_f [ligand]_f}{[enzyme - ligand]} \quad (17)$$

where K_d represents the dissociation constant, $[enzyme]_f$ and $[ligand]_f$ represent the free concentrations of the two molecules and $[enzyme-ligand]$ represents the concentration of the binary enzyme-ligand complex.

In terms of the fluorescence signal, a variation of the Langmuir isotherm (equation 18) can be written as follows:

$$\%Quenching = \frac{y_{max}}{1 + \frac{k_d}{[ligand]}} \quad (18)$$

Moreover, the K_d can be related to the Gibbs free energy of the binding (equation 19) for the receptor-ligand complex as follows¹¹⁹:

$$\Delta G_{binding} = RT \ln(K_d) \quad (19)$$

A fresh stock solution of HAS 18 μM was prepared at each day of use. After preparation of liposomes as described in chapters 2.1. and 2.2.1., different sets of *Eppendorf* tubes were prepared:

- (i) 9 μM HSA (without liposomes) + increasing resveratrol concentrations (0, 20, 25, 50, 75, 100, 125, 150, 175, 200 and 225 μM) ;
- (ii) 20 μM resveratrol loaded liposomes with increasing lipid concentrations (10, 50, 100, 500, 1000 and 1500 μM) without HSA;
- (iii) 20 μM resveratrol loaded liposomes with increasing lipid concentrations (10, 50, 100, 500, 1000 and 1500 μM) with 9 μM HSA;
- (iv) Plain liposomes with increasing lipid concentrations (10, 50, 100, 500, 1000 and 1500 μM) with 9 μM HSA.

To determine the binding of resveratrol to HSA, DLS techniques were used. The size of the particles was measured with the Zetasizer Nano ZS at 37°C, performing 5 measurements with an equilibration time of 120 seconds per sample. To measure the surface charge of the particles, the Zetasizer Nano ZS was also used but only one measurement per sample was made, also at 37°C with an equilibration time of 60 seconds. The data were treated using the *Zetasizer software*, *Excel 2007* and *OriginPro 9.0*.

2.11. Preliminary assays with free and encapsulated resveratrol in a yeast model

As reported before, in the present study, *S. cerevisiae* was used as a eukaryotic model system to test the influence of free and encapsulated resveratrol, since very few studies regarding this problem have been reported. The *S. cerevisiae* strain W303-1A was used in these experiments, which possesses an *ybp1-1* mutation which abolishes Ybp1p function, increasing the yeast sensitivity to oxidative stress.

2.11.1. Resveratrol effect in yeast cell growth under fermentative and respiratory conditions

Monitoring the growth rate of a microorganism in a liquid media is a standard lab technique achieved from the plot of the number of cells versus time, which generates a growth curve (figure 20). As the number of cells in culture increases, the turbidity or optical density (*OD*) of the culture increases. The turbidity of a cell culture is the scattered light resultant from the cells suspended in the liquid media and it can be measured by spectrophotometry. Initially, in the lag phase the population size remains constant since the cells are only synthesizing the enzymes and factors needed for cell division and population growth. The exponential growth phase is a pattern of balanced growth wherein all the cells are dividing regularly at a constant rate. The stationary phase is the phase where the population growth is limited by factors such as exhaustion of nutrients, accumulation of inhibitory metabolites or end products, or exhaustion of space, and so the population of cells simply stops growing and dividing. The death phase occurs if the incubation continues after the population reaches the stationary phase, in which the viable cell population declines (the death phase is generally not detectable by the *OD*). It is noteworthy that the addition of fresh culture medium to the flask results in a new exponential growth phase until a new higher plateau is reached.

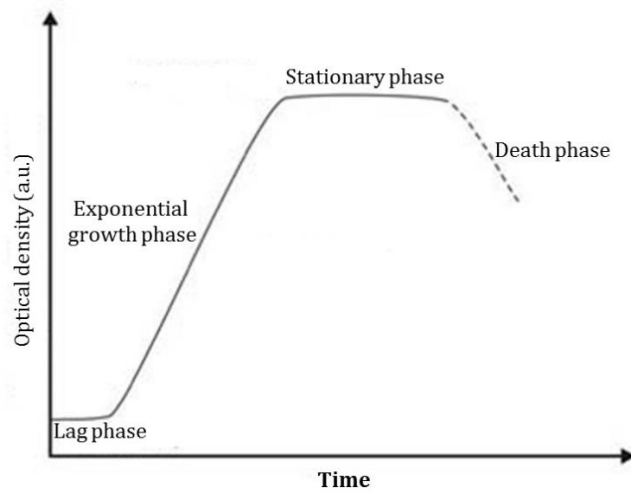


Figure 20. Typical yeast population growth curve in a population grown in a culture flask.

In order to determine whether the phenolic compound resveratrol has any influence in the growth of yeast cells, *S. cerevisiae* W303-1A cells were grown in YPD (1% yeast extract, 1% peptone and 2% glucose; fermentative conditions) and in lactate/ethanol medium (1% yeast extract, 1% peptone, 0.5% lactate, 0.5% ethanol; respiratory conditions). The cultures were incubated at 30°C with agitation (200 rpm) and good aeration in the presence and absence of 100 μ M resveratrol prepared in 100% ethanol (final concentration: 2.2%). Appropriate control experiments with ethanol alone were also carried out.

The culture's growth was monitored by measuring the *OD* at 640 nm with a Thermo Spectronic Genesys 20 Visible Spectrophotometer. The specific growth rate (μ_{max}) of the cultures was estimated from the slope of the linear part of the curve obtained after plotting the logarithm of the *OD* values against time (*t*), as follows (equation 20):

$$\mu_{max} = \frac{\ln OD_{t_2} - \ln OD_{t_1}}{t_2 - t_1} \quad (20)$$

where μ_{max} corresponds to the specific growth rate of the culture, $\ln OD$ corresponds to the natural logarithm of the *OD*, and t_1 and t_2 correspond to the aliquotation time points. In total, three growth curves were constructed for each condition, as follows:

- (i) Growth under fermentative conditions (control 1);

- (ii) Growth under fermentative conditions + 2.2% ethanol (control 2);
- (iii) Growth under fermentative conditions + 100 μ M resveratrol + 2.2% ethanol;
- (iv) Growth under respiratory conditions (control 1);
- (v) Growth under respiratory conditions + 2.2% ethanol (control 2);
- (vi) Growth under respiratory conditions + 100 μ M resveratrol + 2.2% ethanol.

2.11.2. Resveratrol effect in yeast growth under respiratory conditions in the presence of hydrogen peroxide

Oxidative stress occurs when the production of oxidizing agents, free radicals and reactive oxygen species (ROS), surpasses the antioxidant capacity of cellular antioxidants in a biological system. This imbalance between oxidants and antioxidants often leads to tissue injuries and to the progression of degenerative diseases in humans³⁰. Hydrogen peroxide (H_2O_2) is a byproduct of mitochondrial oxidative metabolism³¹ that leads to oxidative stress, and so it was used as oxidative stress inducer in this study.

Yeast cells were cultivated in lactate/ethanol medium, lactate/ethanol medium supplemented with 200 μ M resveratrol (final ethanol concentration: 2.2%) and in lactate/ethanol medium supplemented with ethanol alone (2.2%). The methodology used was very similar to the one reported above.

When cultures reached mid-exponential phase, 5 mL aliquots were transferred to glass tubes with growing concentrations of H_2O_2 (0, 0.5, 0.75, 1, 1.5 and 2 mM) (figure 21).

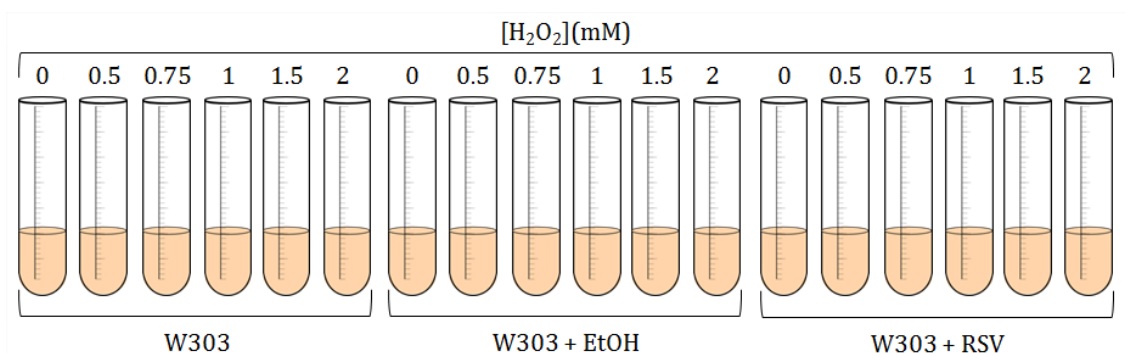


Figure 21. Schematic representation of growth experiments to evaluate the effect of resveratrol on yeast growth in the presence of H_2O_2 .

The glass tubes were maintained at 30°C under agitation (200 rpm) with good aeration, and the addition of H₂O₂ was done 4 h after. Samples were taken at 0, 1, 2, 3 and 4 h after the addition of H₂O₂. Growth was measured by spectrophotometry at *OD*₆₄₀ as reported above to determine growth inhibition parameters.

The growth inhibition constants were calculated according to the following equation:

$$\ln \mu^x = \ln \mu^0 - k_i(X - X_{min}) \quad (21)$$

where μ^0 is the specific growth rate in the absence of H₂O₂, μ^x is the specific growth rate in the presence of H₂O₂, X is the H₂O₂ concentration, X_{min} is the minimum ethanol concentration above which the toxic effect is measurable, and k_i is the exponential inhibition constant.

2.11.3. Effect of hydrogen peroxide in yeast cell death in respiratory conditions

Besides the study described in the previous chapter, which allowed the visualization of the H₂O₂ effect on yeast cell growth, a study regarding the H₂O₂ effect on yeast cell death was also carried out. In this assay, the yeast cell's capacity to grow in a solid medium when subjected to different concentrations of H₂O₂ at different time points was evaluated.

Cells grown in lactate/ethanol media were treated with different concentrations of H₂O₂ (0, 0.5, 1, 2 and 5 mM) and maintained at 30°C with agitation (200 rpm) and good aeration. Aliquots of the samples were taken at 0, 1, 2 and 3 h of incubation. Each sample was diluted (figure 22) to obtain 4 different dilutions, as follows: 10⁻¹, 10⁻², 10⁻³ and 10⁻⁴. Five µL of each sample were dropped in a petri dish with YPD medium. The petri dishes were then incubated at 30°C during approximately 48 h and then placed in the ChemiDoc-It®^{TS2} Imaging System to obtain the photos of the grown cultures.

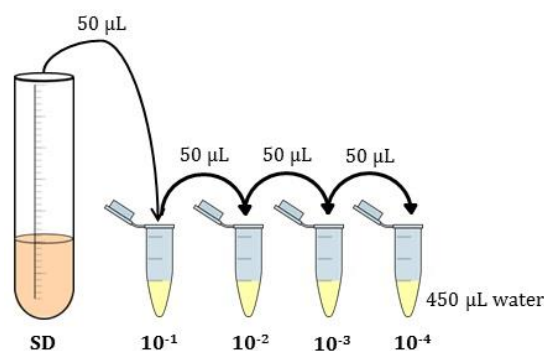


Figure 22. Schematic representation of the dilution process carried out during the experiments to evaluate the effect of H_2O_2 in yeast cell death.

2.11.4. Liposome internalization by yeast cells assessed by fluorescence microscopy

Fluorescence microscopy is an essential technique in biology that allows the observation of biological species, fixed or alive, in great detail when compared with other microscopy techniques²⁷. This microscopy technique relies on the principle that a specimen is illuminated with a light of a specific wavelength that will be absorbed by the fluorophores, which in turn will cause them to emit light of longer wavelengths³⁴. The basic fluorescence microscope possesses critical modifications in the illumination and imaging beam pathways, namely a specific light source (mercury lamp), a multipurpose mirror (dichroic mirror that is highly reflective below the cut-off wavelength and highly transmissive above it), a system of filters (one in front of the condenser and one behind the objective), and a more powerful electronic detection system³⁵. The use of this technique made possible to identify cells and submicroscopic cellular components and entities with a high degree of specificity amid non-fluorescing material. In the same sample, through the use of multiple staining, different probes can simultaneously identify several target molecules³⁰. Moreover, the incorporation of fluorescent probes lipids in the liposomal formulation allows the visualization and tracking of the liposomes during their extracellular and intracellular route^{37,38}.

The fluorescent probe 1,6-diphenyl-1,3,5-hexatriene (DPH), used in the present study, is widely used for the structural and dynamic studies of hydrophobic regions in biological membranes. Several studies have shown that DPH permeates

into the membrane and that this probe, besides being located in the center of the lipid bilayer, is also capable of entering the cell and of being incorporated into the membranes of the cellular organelles and into the intracellular lipid droplets³⁹. Moreover, the intercalation of DPH into membranes is accompanied by strong enhancement of its fluorescence, since its fluorescence is practically negligible in water⁴⁰.

Liposomes (2 mM) were prepared as described in the section 2.2.1. with the difference that the fluorescent probe DPH (3 μ M) was incorporated during liposome formation and the suspension was protected from light exposure. When the *S. cerevisiae* cell culture reached the mid-exponential growth phase, liposomes were added at a 1:1 cell suspension/liposome suspension ratio. The resulting mixture was incubated at 30°C with agitation (200 rpm) and good aeration for 4 h. A control was made with the cells containing the DPH probe at the same concentration, only without the liposomes. Both cultures were protected from light exposure to avoid losing the probe's fluorescence.

Fluorescence microscopy analysis of the samples was performed with a Leica Microsystems DM-5000B epifluorescence microscope with appropriate filter settings. Images were acquired with a Leica DCF350FX digital camera and processed with *LAS AF Leica Microsystems software*.

2.11.5. Cell viability and reactive oxygen species (ROS) quantification assays by flow cytometry

Flow cytometry is a laser-based and biophysical technology that simultaneously measures and analyzes multiple characteristics of single particles, typically cells, as they flow in a fluid stream through a beam of light. This technique allows simultaneous multiparametric analysis of the physical and chemical characteristics of up to thousands of particles per second. These characteristics are determined using an optical-to-electronic coupling system that records how the cell or particle scatters incident laser light and emits fluorescence and include particle's relative size, relative granularity or internal complexity, and relative fluorescence intensity. A flow cytometer can be compared to a microscope, except that instead of

producing an image of the cell, flow cytometry provides an automated quantification of set parameters for a large number of cells.

A flow cytometer is composed of three main systems – fluidics, optics and electronics. The fluidics system is a liquid stream that transports and aligns the cells so that they can pass in a single line through the laser beam for sensing; the optics system is composed of lasers to illuminate the particles in the sample stream and of optical filters to direct the resulting light signals to the appropriate detectors; the electronic system will then transform the generated forward-scattered light (FSC) and side-scattered light (SSC) as well as fluorescence signals from light signals into electronic signals that can be processed by the computer.

In the flow cytometer, any suspended particle or cell from 0.2 to 150 μM in size is suitable for analysis and cells from solid tissues must be disaggregated before analysis. In the flow chamber, the particle suspension is collected by a needle and immersed in a specific fluid – sheath fluid. This fluid creates a pressure which forces the particles to move in a single line, one by one, at the center of the fluid, in a process called hydrodynamic focusing. The particles moving in the fluid will then be intercepted by a laser beam and the interaction of the particles with the laser will be captured by proper detectors, for instance a FSC detector, a SSC detector and one or more fluorescence detectors (FL-1, FL-2, FL-3, FL-4, etc.). The information captured by these detectors can be generated by the forward or side scattering of the light beam and by the fluorescence emitted by fluorochromes after excitation of the light beam⁴¹.

In the present study, flow cytometry analysis of W303 yeast cells was performed in an Epics XL Beckman Coulter flow cytometer equipped with an argon-ion laser with a beam emitting at 488 nm at 15 mW. Green, orange and red fluorescence were collected through a 525 nm band-pass filter, a 620 nm band-pass filter and a 675 nm band-pass filter, respectively. For each sample, 20000 events were analyzed at a low flow rate. Data were analyzed with *Flowing Software 2.5.1*.

2.11.5.1. Cell viability assays

3,6-Diacetoxyfluoran, commonly known as fluorescein diacetate (FDA), is an acetoxymethyl ester derivative that has been used extensively as a cell viability and activity stain. This cell-permeant esterase substrate is a non-polar compound that is taken up by cells by an active transport phenomenon and, once within the cell, is hydrolyzed by non-specific esterases. Fluorescein, a polar compound and a product of FDA hydrolysis, is not eliminated from the cell as quickly as its parent compound, which results in intracellular fluorescein accumulation, and so the viable cells appear fluorescent⁴². Therefore, this viability probe measures both enzymatic activity, which is required to activate its fluorescence, and cell-membrane integrity, which is required for intracellular retention of the fluorescent product.

In order to evaluate the cell viability of yeast cells by flow cytometry, the following mixtures were prepared in Eppendorf tubes:

- (i) Yeast cells + 200 μ M resveratrol loaded 1mM liposomes;
- (ii) Yeast cells + 200 μ M resveratrol;
- (iii) Yeast cells alone.

After incubation at 30°C during 12-16 h, samples were centrifuged at 5000 rpm during 2 min and the resulting pellet was resuspended in 1 mL of PBS buffer (pH 7.4, NaCl 137 mM, KCl 2.7mM, phosphate 10 mM) containing 4 μ g/mL of the cell viability probe FDA. Flow cytometry analysis of each sample was performed 20 min after incubation with the probe.

2.11.5.2. ROS production assays

Dihydroethidium (DHE) is a reduced form of the commonly used DNA dye ethidium bromide. DHE itself exhibits blue fluorescence in the cell cytoplasm and it has been widely used to evaluate ROS production, since it has the ability to freely permeate cell membranes⁴³ and, upon reaction with superoxide anions, forms a red fluorescent product (2-hydroxyethidium) that intercalates with DNA. This fluorescent probe is probably the most specific and least problematic dye since it

detects essentially superoxide radicals, is retained well by cells, and may even tolerate mild fixation⁴⁴.

In order to evaluate the ROS production by yeast cells by flow cytometry, the following mixtures were prepared in Eppendorf tubes:

- (i) Yeast cells + 200 μ M resveratrol loaded 1mM liposomes;
- (ii) Yeast cells + 200 μ M resveratrol;
- (iii) Yeast cells alone.

After incubation at 30°C during 12-16 h, samples were centrifuged at 5000 rpm during 2 min and the resulting pellet was resuspended in 1 mL of PBS buffer (pH 7.4, NaCl 137 mM, KCl 2.7mM, phosphate 10 mM) containing 5 μ g/mL of the ROS-sensitive probe DHE. Flow cytometry analysis of each sample was performed 30 min after incubation with the probe.

CHAPTER 3

RESULTS AND DISCUSSION

Contents

- 3.1. Liposomes present good characteristics for drug delivery purposes
- 3.2. Liposomes are stable for at least 4 weeks
- 3.3. Resveratrol can be quantified by UV/Vis absorbance spectroscopy
 - 3.3.1. In ultrapure water (pH \approx 5.5)
 - 3.3.2. In HEPES buffer (pH = 7.4)
 - 3.3.3. In acetate buffer (pH = 5.0)
- 3.4. Incubation is the most efficient method to encapsulate resveratrol
- 3.5. Resveratrol promotes disorganization of the liposomal formulation and diminishes its microviscosity
- 3.6. Resveratrol has a lipophilic character and is encapsulated in the liposomal formulation
- 3.7. Resveratrol partition in the liposomal formulation is spontaneous
- 3.8. Resveratrol is released from liposomes in water
- 3.9. Resveratrol loaded liposomes need PEGylation to avoid binding to HSA
- 3.10. Resveratrol does not affect the growth of yeast cells
- 3.11. Hydrogen peroxide inhibits yeast growth in a dose-dependent manner and resveratrol slightly counteracts this effect
- 3.13. Resveratrol loaded liposomes are efficiently internalized by yeast cells
- 3.14. Free and encapsulated resveratrol have no effect in cell viability
- 3.15. Free and encapsulated resveratrol decrease the intracellular ROS levels

3.1. Liposomes present good characteristics for drug delivery purposes

The first objective of this study was to develop a plain DODAB:MO (1:2) liposomal formulation (placebo), prepared by the lipid film hydration method. Subsequently, resveratrol loaded liposomes (2%) were prepared by three different encapsulation methods in order to perceive which method was the most efficient for resveratrol encapsulation. The samples were analyzed by DLS and ELS to understand the influence of resveratrol in parameters such as mean liposome size, Pdl, and surface charge. All the samples were produced in triplicate and the results presented correspond to the mean values and standard deviations of the measurements. The mean size of the plain and resveratrol loaded DODAB:MO (1:2) liposomes produced by incubation, hydration and direct mixing methods are presented in figure 23.

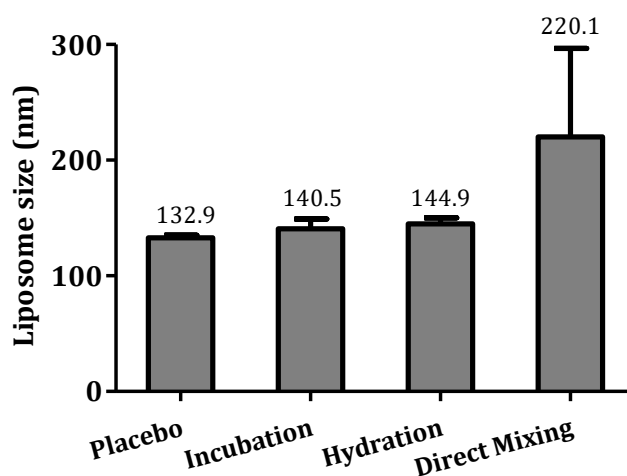


Figure 23. Mean liposome size and its standard deviation for placebo liposomes and 2% resveratrol loaded liposomes produced by incubation, hydration and direct mixing methods of encapsulation.

The DODAB:MO (1:1) placebo liposomes present diameters of around 130 nm. Resveratrol loaded liposomes produced by incubation and hydration methods are only slightly larger (≈ 140 nm) than the plain liposomes, which means that the introduction of the drug into the liposomal system does not significantly increase liposome size. Therefore, all of these liposomes are suitable for drug

delivery purposes, since the optimal size of a nano-sized agent that induces the most efficient therapeutic effect is reportedly between 100 and 200 nm in diameter¹³³. This efficient therapeutic effect is due to the fact that the particle size is above the kidney clearance threshold, which allows the particles to circulate for prolonged periods of time, and due to the fact that the particle size results in passive, progressive and relatively selective accumulation of these particles in the malignant tissues over time⁸⁵. However, the resveratrol loaded liposomes produced by direct mixing present mean sizes above 200 nm, meaning that this method is not appropriate to produce liposomes for drug delivery.

The mean Pdl of the plain and resveratrol loaded liposomes is presented in figure 24.

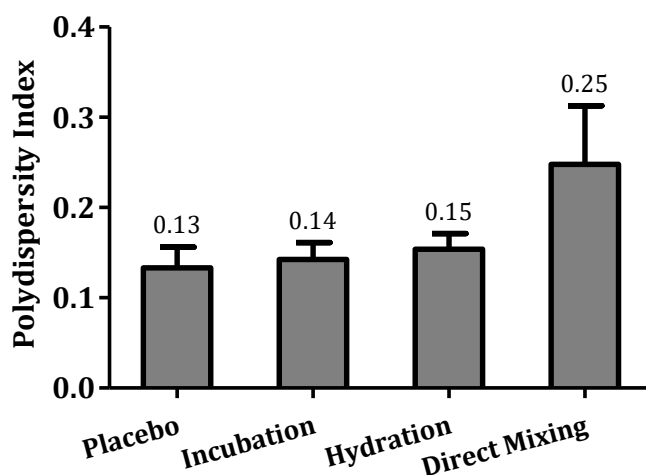


Figure 24. Mean Pdl and its standard deviation for placebo liposomes and 2% resveratrol loaded liposomes produced by incubation, hydration and direct mixing methods of encapsulation.

Once more, the resveratrol encapsulation does not seem to have great influence in the liposomal system, since plain liposomes and resveratrol loaded liposomes produced by incubation and hydration methods present similar Pdl values. Also, the Pdl is lower than 0.2, which is an acceptable value and denotes a monodisperse system. Once again, liposomes produced by direct mixing method present unacceptable values, above the desired 0.2.

The surface charge of liposomes is a very important physicochemical property, since this parameter strongly affects the stability of the particles, the cellular

adhesion and the subsequent delivery of the encapsulated drug. Liposomes composed by cationic lipids, such as the DODAB:MO (1:2) liposomes at study, tend to have higher affinity to cells since cell membranes are slightly negatively charged⁸⁷. Figure 25 presents the ζ -potential of the plain and resveratrol loaded liposomes produced by the three encapsulation methods studied.

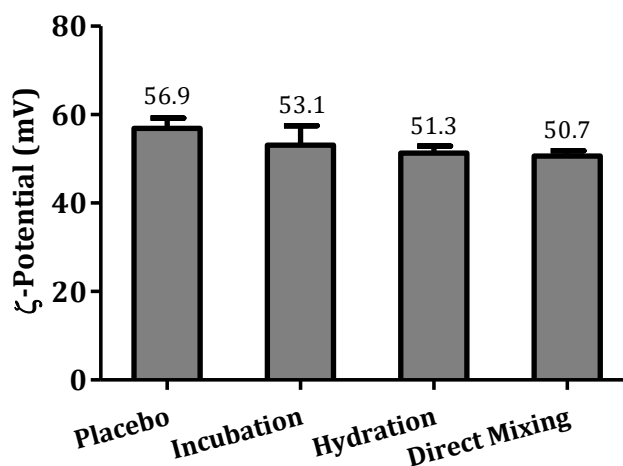


Figure 25. Mean ζ -potential and its standard deviation for placebo liposomes and 2% resveratrol loaded liposomes produced by incubation, hydration and direct mixing methods of encapsulation.

Z-potential values are not quantitatively identical to the surface charge values of the particle but are very helpful in the qualitative prediction of the particle surface charge. Therefore, for simplification comparisons and results analysis, the term surface charge will be employed.

As anticipated, all liposomes present a highly positive surface charge owing to the presence of the positively charged lipid DODAB. The placebo liposomes present a ζ -potential value of approximately $+ 56.9 \pm 2.3$ mV which is consistent with the previously obtained values for the same system¹³⁴. All particles in suspension with a large negative or positive surface charge tend to repel each other and there is no tendency to form aggregates. On the other hand, when particles present low surface charge then there is no force to prevent the particles of coming together and aggregating. The common dividing line between stable and unstable particles is usually taken at either +30 mV or -30 mV¹⁰¹, so it is possible to conclude that all liposomes are stable and have no tendency to form aggregates. Resveratrol loaded

liposomes present lower ζ -potential values than plain liposomes, which can be due to the fact that the neutral molecule resveratrol is located near the positive DODAB polar headgroups, which will diminish the density of positive charges, thus diminishing the surface charge.

Although positively charged liposomes can have the advantage of a higher affinity to cell membranes, these particles also have some shortcomings, such as the associated cytotoxicity. Also, these particles are easily cleared in *in vivo* systems since they may trigger the immune system¹³⁵. However, the high charges of liposomes are a very good starting point to subsequent addition of PEG moieties that will reduce the highly positive charge density, while protecting liposomes from adsorbing to HSA.

3.2. Liposomes are stable for at least 4 weeks

The stability of plain and resveratrol loaded liposomes was assessed by evaluating parameters such as liposome size (figure 26), Pdl (figure 27), ζ -potential (figure 28) and pH (figure 29) throughout time, namely the three months following their production. These measurements will also help to evaluate how the three different resveratrol encapsulation methods were influencing the stability of the liposomal formulation.

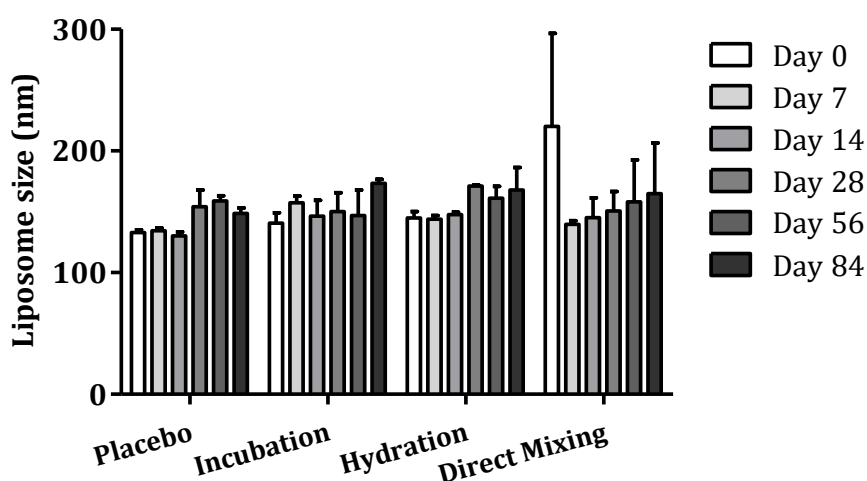


Figure 26. Mean liposome size and its standard deviation for placebo liposomes and 2% resveratrol loaded liposomes produced by incubation, hydration and direct mixing methods of encapsulation during the three months following liposome production.

Results presented in figure 26 show that liposome size increases over time although their size never reaches above the undesired 200 nm. These results are consistent with the results presented in figure 27 where it is possible to observe that the PDI of the liposomes also increases throughout time. The liposomal suspensions present an increase in the heterogeneity as time passes, probably due to particle aggregation and liposomal fusion, which results in liposomes with a higher mean size.

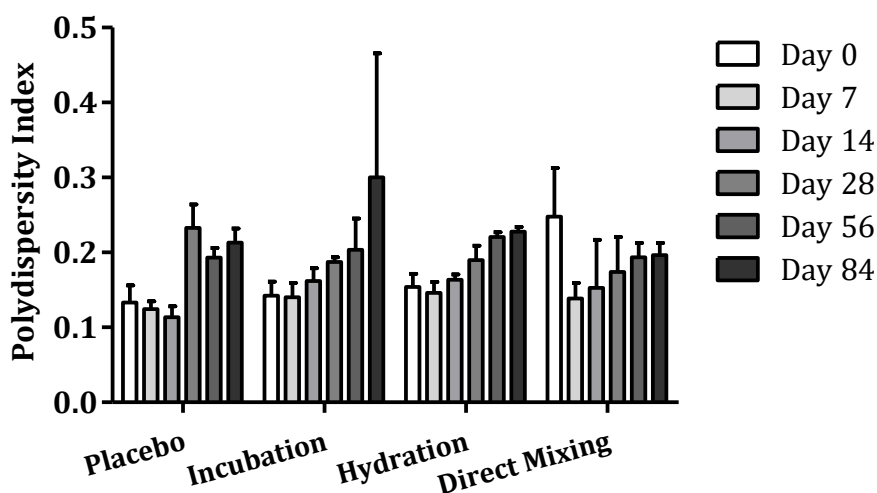


Figure 27. Mean PDI and its standard deviation for placebo liposomes and 2% resveratrol loaded liposomes produced by incubation, hydration and direct mixing methods of encapsulation during the three months following liposome production.

Interestingly, resveratrol loaded liposomes produced by direct mixing, that showed high mean size and PDI at the time of their production, seem to have reduced its size and heterogeneity over time to values close to the ones obtain for the other liposome batches. This is probably owed to the fact that the resveratrol molecules were added directly to the lipid mixture, previous to the vesicle formation. When the lipid film was hydrated, the lipid molecules probably had difficulty to form stable aggregates in the presence of the resveratrol molecules. However, after some time, the lipid vesicles seem to have reached a more stable conformation.

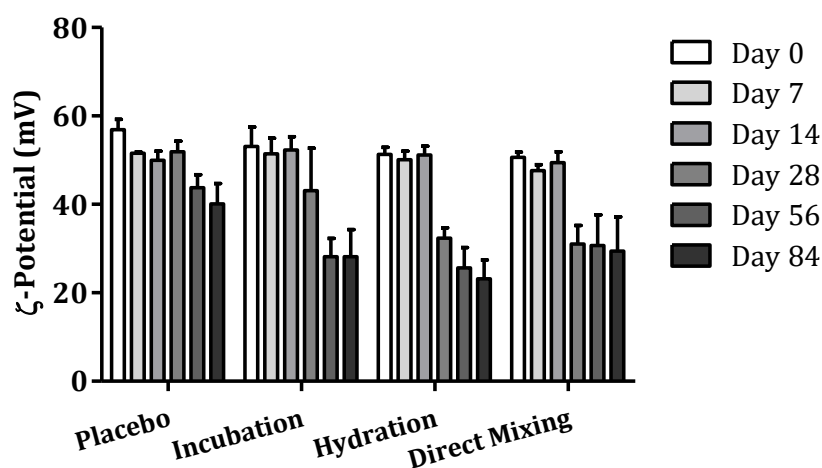


Figure 28. Mean ζ -potential and its standard deviation for placebo liposomes and 2% resveratrol loaded liposomes produced by incubation, hydration and direct mixing methods of encapsulation during the three months following liposome production.

Regarding the liposomes surface charge, after the first month of storage the ζ -potential decreases to values below the desired +30 mV. This might be due to the monoolein migration from the liposome core to its surface where it will be embedded in the DODAB double layer. Resveratrol that was initially located in the liposome core can also migrate to the liposome surface. The accumulation of these neutral molecules near the DODAB polar headgroups will cause a lower density of the positive charge, which in turn will reduce the system's ζ -potential. The decrease of the liposome's surface charge will lead to a greater tendency for aggregation and fusion to occur, which explains the increase in the samples Pdl and mean size.

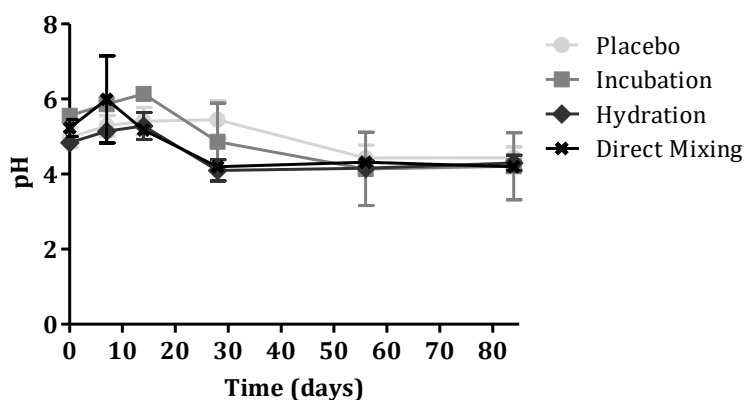


Figure 29. pH values and its standard deviation for placebo liposomes and 2% resveratrol loaded liposomes produced by incubation, hydration and direct mixing methods of encapsulation during the three months following liposome production.

At the time of its production, all batches of liposomes presented a pH of approximately 5, which is consistent with the pH of the solvent they were produced in, since ultrapure water with dissolved CO₂ has a pH of around 5.5. During the first week, in some cases during the first two weeks, the pH of the liposomal formulations increases. After that the suspensions tend to increase their acidity. Since resveratrol is an antioxidant compound, one would expect that it would prevent or attenuate the lipid hydrolysis. However, that is not verified since the media gets more and more acidic as time passes, probably due to the fatty acids liberation from the formulation. This fact, by itself, does not mean that the resveratrol is not protecting against oxidation, but its presence in the formulation probably leads to a higher destabilization than the antioxidant capacity of the compound, especially in such low concentrations. The presence of resveratrol in the liposomal formulation can destabilize the system since the lipids will be more permeable and susceptible to peroxidation. One month after liposome production, liposomes produced by incubation method seem to be the most stable, since these present the less acidic pH values. However, when two and three months have passed, all liposomal suspensions present roughly the same pH values, of around 4.3.

In a general manner, incubation seems to be the best method to encapsulate resveratrol in a DODAB:MO (1:2) system since it leads to the formation of smaller liposomes with higher homogeneity. Moreover, it seems to result in a stable system which is less susceptible to lipid peroxidation. This method also presents the advantage of the resveratrol being added subsequently to the extrusion cycles, which ensures that no resveratrol is being allocated in the polystyrene filters.

3.3. Resveratrol can be quantified by UV/Vis absorbance spectroscopy

In the present study there was the need to quantify resveratrol present in three different media – ultrapure water, HEPES buffer:water (1:1) and acetate buffer:water (1:1). In figure 30 is possible to observe that the same resveratrol concentration in different media results in spectra with different absorbance values. Therefore, three different calibration curves had to be constructed, one for each solvent used.

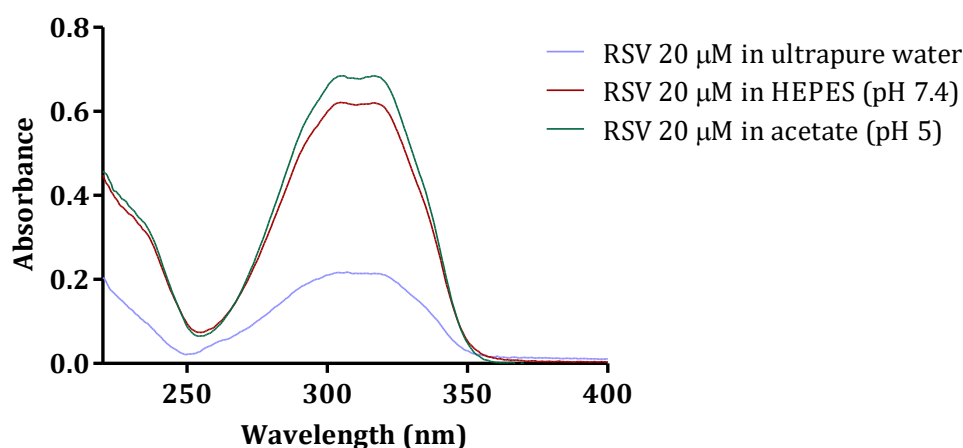


Figure 30. Absorbance spectra of resveratrol with growing concentrations solubilized in ultrapure water, HEPES buffer and acetate buffer.

3.3.1. In ultrapure water (pH \approx 5.5)

Figure 31 represents the absorbance spectra of twelve resveratrol standard solutions in ultrapure water with increasing concentrations from 0.5 to 100 μ M.

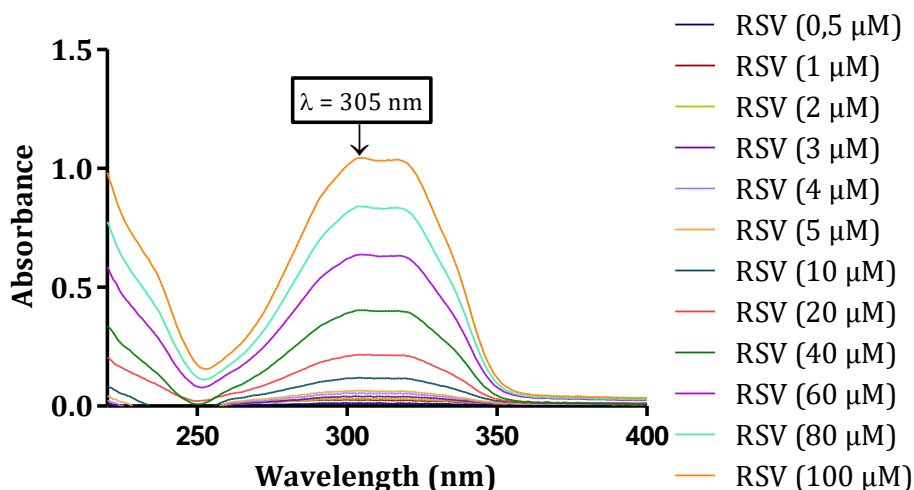


Figure 31. Absorbance spectra of resveratrol standard solutions with increasing concentrations solubilized in ultrapure water.

To quantify resveratrol it is crucial to obtain a direct correlation between resveratrol absorbance and resveratrol concentration. The analysis of the resveratrol absorbance spectra presented in figure 31 shows that resveratrol has its maximum absorbance at the wavelength of 305 nm. Therefore, the calibration curve

is plotted by displaying the absorbance of each standard solution at the wavelength of 305 nm against the resveratrol concentration, as it is shown in figure 32.

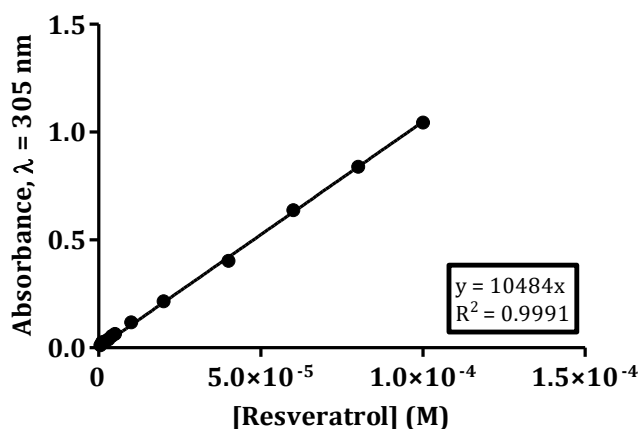


Figure 32. Resveratrol calibration curve in ultrapure water at maximum wavelength of 305 nm.

3.3.2. In HEPES buffer (pH = 7.4)

Figure 33 represents the absorbance spectra of eight resveratrol standard solutions in HEPES buffer (pH = 7.4) with increasing concentrations from 1 to 100 μ M.

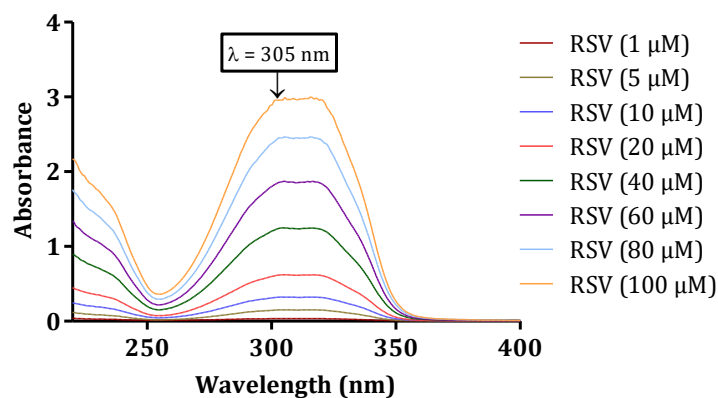


Figure 33. Absorbance spectra of resveratrol standard solutions with increasing concentrations solubilized in HEPES buffer (pH = 7.4).

The calibration curve is plotted by displaying the absorbance of each standard solution at the maximum wavelength of 305 nm against the resveratrol concentration, as it is shown in figure 34.

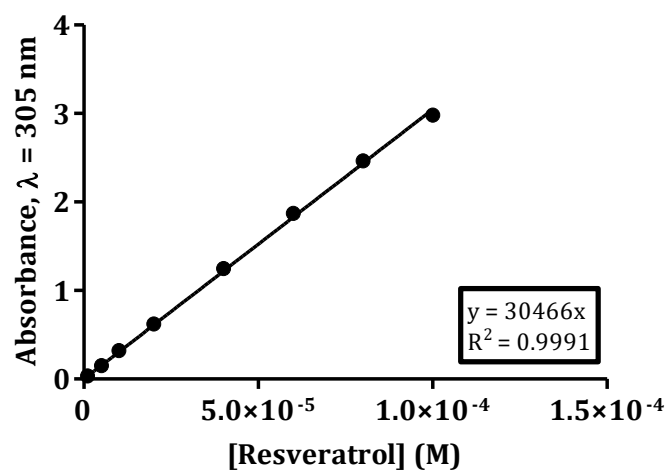


Figure 34. Resveratrol calibration curve in HEPES buffer (pH = 7.4) at maximum wavelength of 305 nm.

3.3.3. In acetate buffer (pH = 5.0)

Figure 35 represents the absorbance spectra of eight resveratrol standard solutions acetate buffer (pH = 5.0) with increasing concentrations from 1 to 100 μM .

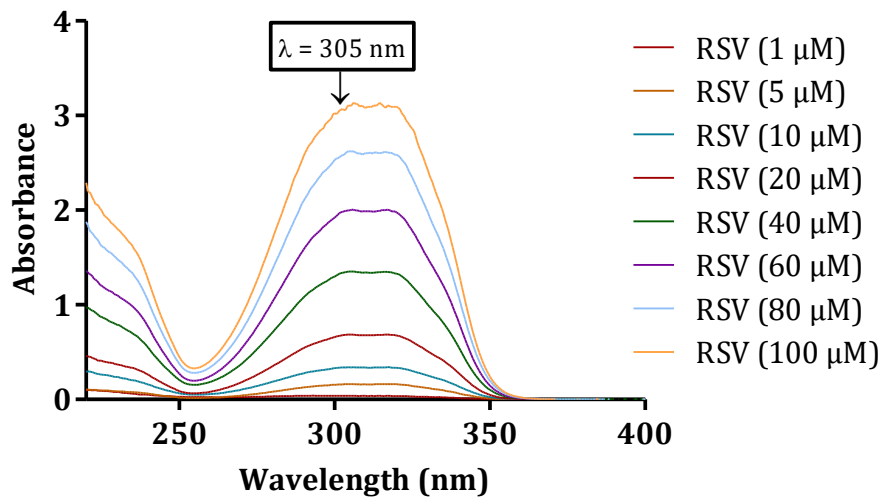


Figure 35. Absorbance spectra of resveratrol standard solutions with increasing concentrations solubilized in acetate buffer (pH = 5.0).

The calibration curve is plotted by displaying the absorbance of each standard solution at the maximum wavelength of 305 nm against the resveratrol concentration, as it is shown in figure 36.

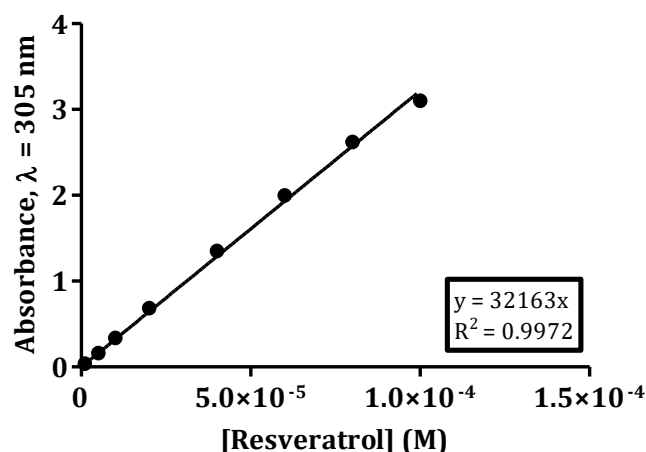


Figure 36. Resveratrol calibration curve in acetate buffer (pH = 5.0) at maximum wavelength of 305 nm.

3.4. Incubation is the most efficient method to encapsulate resveratrol

In order to quantify the amount of resveratrol that was successfully encapsulated into the DODAB:MO (1:2) liposomal system, it was necessary to quantify the resveratrol present in the liposomes as well as the resveratrol that remained free in the aqueous media. As it was reported before, the liposomes disperse light, causing a spectral variation that can influence the resveratrol quantification. So, in order to eliminate this influence, the first derivative of the standard resveratrol solutions spectra was performed and it is present in figure 37.

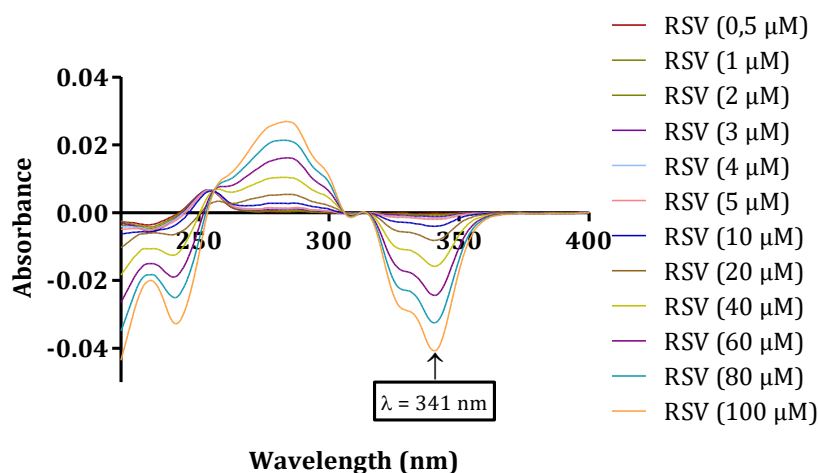


Figure 37. First derivative of the absorbance spectra of twelve resveratrol standard solutions with growing concentrations ranging from 0.5 to 100 μM solubilized in ultrapure water.

The analysis of the first derivative of the resveratrol standard solutions spectra shows that there is an intense peak at the wavelength of 341 nm. The first derivative of the absorbance of each standard solution at this wavelength was used to create a calibration curve that is present in figure 38.

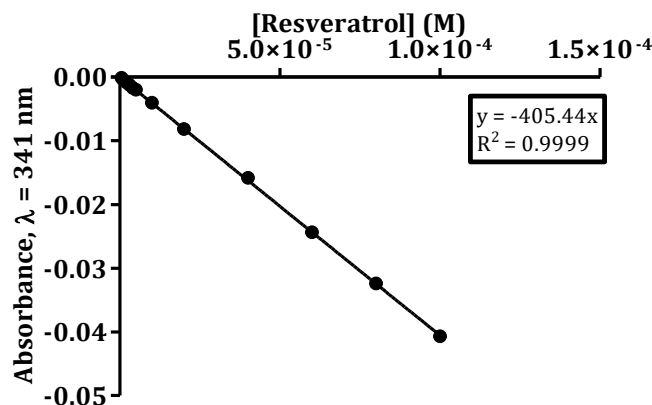


Figure 38. Resveratrol calibration curve in ultrapure water using the first derivative of the absorbance at maximum wavelength of 341 nm.

The calibration curve presented in figure 38 was used to quantify the amount of resveratrol present in the liposomes, whereas the calibration curve presented in chapter 3.3.1 was used to quantify the resveratrol that remained free in the aqueous media, since in the latter case there is no lipid present that would influence a direct quantification of resveratrol.

Figure 39 proves that, when using a calibration curve plotted from the first derivative absorbance values of the wavelength 341 nm versus resveratrol concentration, liposomes have no influence in the resveratrol quantification, since the placebo sample, containing only liposomes, nearly passes through zero at that point.

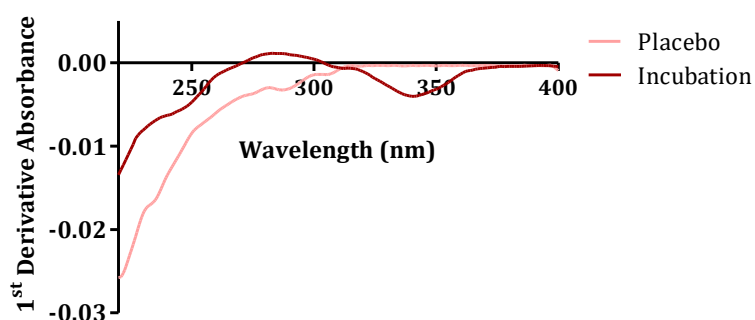


Figure 39. First derivative of the absorbance spectra of the placebo liposomes that remained in the filter after amicon ultracentrifugation (light red line) and of the resveratrol loaded liposomes produced by incubation that remained in the filter after amicon centrifugation (dark red line).

The results regarding the encapsulation efficiency of the three methods employed for a resveratrol concentration of 20 μM (2%) are presented in figure 40.

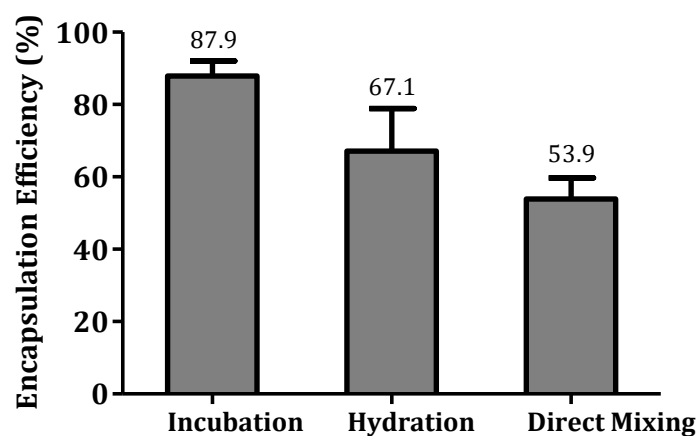


Figure 40. Graphic representation of the resveratrol (2%) encapsulation efficiency in resveratrol loaded DODAB:MO (1:2) liposomes produced by incubation, hydration and direct mixing methods.

Theoretically, and since resveratrol has a lipophilic nature, the best way to encapsulate resveratrol should be the direct mixing method, since in this method the resveratrol is directly added to the lipid mixture. However, this is not the case and according to the results obtained, resveratrol loaded liposomes produced by the incubation method of encapsulation show the highest encapsulation efficiency, with values around 88%. The fact that the incubation method is the most efficient method of encapsulation is convenient, since it has been proved before that this method has a higher shelf-stability when compared to the other encapsulation methods. Moreover, it shows more appealing characteristics, such as reduced mean liposome size and polydispersity index. Plus, the production of resveratrol loaded liposomes by this method is simple and is not very time consuming.

Since the incubation method was the one that presented higher encapsulation efficiencies, this was the method selected to test the encapsulation of different resveratrol concentrations, namely 5, 20, 40, 60, 100 and 200 μM which corresponds, respectively, to 0.5, 2, 4, 6, 10 and 20% of resveratrol to a 1 mM lipid concentration. In this case, the drug loading efficiency was assessed rather than the encapsulation efficiency since the latter only indicates the amount of drug that is encapsulated in regard to the total amount of drug added to the

system. On the other hand, the drug loading efficiency refers to the ratio of drug incorporated to the total amount of the carrier system, and so it is possible to know the amount of drug that the system is capable of accommodating. Figure 41 shows the variation of the drug loading efficiency in percentage for different resveratrol concentrations.

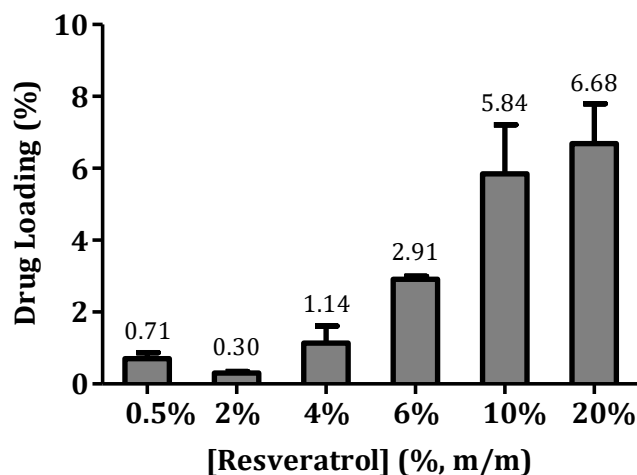


Figure 41. Drug loading efficiency of increasing concentrations of resveratrol (0.5, 2, 4, 6, 10 and 20% (m/m)) to a 1 mM lipid concentration.

As it can be seen in figure 43 the drug loading increases as the concentration of resveratrol increases, which indicates that the system is capable of incorporating high amounts of resveratrol. Since the drug loading efficiency is increasing as the resveratrol concentration increases, one might think that if the resveratrol concentration kept on increasing, the drug loading would also continue to increase. However, resveratrol is poorly soluble in water, and these solubility problems did not allow the encapsulation by incubation methods of higher amounts of the drug. However, even when 2% of resveratrol (20 μ M) was encapsulated in the liposomal system, and assuming an encapsulation efficiency of 88%, this means that the concentration of resveratrol in the formulation is 17.6 μ M which, as described, is sufficient to obtain therapeutic effects, since resveratrol can be effective at doses of 10 μ M¹³⁶.

3.5. Resveratrol promotes disorganization of the liposomal formulation and diminishes its microviscosity

As it was described in the previous chapter, in order to assess the resveratrol influence in the biophysical properties of the liposomes the DLS technique was employed. The graphic representations obtained are sigmoid profiles that show the variation of the mean count rate *versus* temperature and are presented in figure 42. The black line represents the mean count rate variation of the plain liposomes and the grey line of the resveratrol loaded liposomes. These sigmoidal profiles and its inflection points make it possible to calculate the systems' T_m and B . The purpose of this study is to reveal modifications in the values of the mean count rate before and after the phase transition and in the transition profile in the absence and presence of resveratrol. That being said, the most important information that can be acquired from these sigmoidal fittings is the system's phase transition cooperativity and the system's phase transition temperature. These parameters are required to understand the system's behavior in the absence and presence of resveratrol, and their values are presented on table 1.

The phase transition of a system results from a condition of disorder that is due to the *trans-gauche* isomerization of the lipid acyl chains. Due to the close packing of lipid molecules into a lipid bilayer, the temperature dependent increase in chain rotation is a cooperative process, which gives rise to a sharp anomaly – the phase transition¹³⁷. The transition of the system from the gel phase to the fluid phase is considered a cooperative process when it happens almost at the same time in all the points of the system. The insertion of foreign molecules in the lipid system can disturb the phase transition cooperativity as well as the phase transition temperature. Therefore, a variation in the system's phase transition cooperativity indicates that the molecule is embedded in the lipid media. If the phase transition cooperativity increases, the molecule is well distributed in the lipid media, and induces a fast lipid phase transition. On the other hand, if value of this parameter decreases, the molecule is not homogeneously distributed, disturbing the cooperative process, and the lipids will exhibit a more gradual disorder, which results in a broadening of the phase transition¹³⁷.

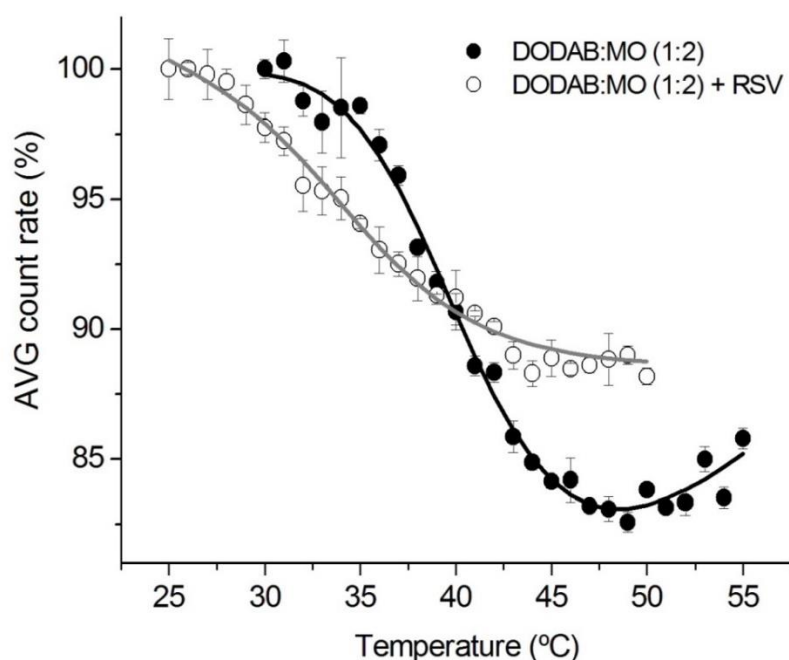


Figure 42. Representation of the mean count rate in percentage of DODAB:MO (1:2) liposomes with (white circles) and without (black circles) resveratrol versus temperature. Each point corresponds to the mean value of three measurements and the correspondent standard deviation is represented. The lines (black for plain liposomes and grey for resveratrol loaded liposomes) represent the best non-linear fitting according to the equation 12, where the refined parameters were T_m and B .

The plain DODAB:MO (1:2) system presents a high cooperativity, which means that all of the molecules of the liposome transit to a different phase practically at the same time. However, when resveratrol is encapsulated in the same system, its cooperativity is diminished. First of all, this decay in the phase transition cooperativity proves that the drug was successfully encapsulated and is, without a doubt, inserted into the formulation. This decay also indicates that the resveratrol molecules are somewhat poorly distributed in the liposomal system, since the compound is only influencing certain molecules to change their phase transition temperature – the molecules that are bond to the resveratrol. If resveratrol had an extremely good distribution in the liposome, the phase transition temperature would be altered but the cooperativity would be maintained, because the resveratrol molecule would influence all the lipid molecules in the formulation. This decrease of the phase transition cooperativity of the system containing resveratrol, by itself, cannot provide information about the location of the resveratrol molecules. However, it is possible to verify a decrease in the phase transition temperature of

the system of 5°C in the presence of resveratrol, when compared to the plain liposomal system. As it was described by Engelke *et al.*¹³⁷, when the foreign molecules are located in the headgroup regions of the lipid systems, the phase transition temperature decreases. This diminution of the system's T_m is a result of a weaker interaction of the headgroup moieties, paralleled by a lateral expansion of the interface region. This fact indicates that the resveratrol molecules are located in the most organized portion of the system, the DODAB polar headgroups. This makes sense because, despite being a lipophilic drug, resveratrol has three hydroxyl (-OH) groups, which need to be embedded in a polar zone. Therefore, resveratrol promotes a disorganization of the liposomal system by inserting itself in a rigid portion of the vesicle, which diminishes the system's microviscosity by disturbing the lipid packaging. Probably, there are also some resveratrol molecules within the non-lamellar inverted structures of MO.

Table 1. Biophysical parameters (B and T_m) of DODAB:MO (1:2) liposomes in the absence and presence of resveratrol.

	B (cooperativity)	T_m (°C)
DODAB:MO (1:2)	217 ± 58	41.7 ± 1.0
DODAB:MO (1:2) + Resveratrol	169 ± 12	36.7 ± 0.3

3.6. Resveratrol has a lipophilic character and it is encapsulated in the liposomal formulation

In figure 43 are presented the UV/Vis absorbance spectra of resveratrol loaded liposomes with increasing lipid concentrations from 50 to 2000 μM (S1 to S9) and a 43 μM concentration of resveratrol. The grey spectra correspond to the absorbance spectra of the references, with the same increasing lipid concentrations but without resveratrol. The red spectra (RSV 1, 2 and 3) represent the solutions containing only resveratrol with a 43 μM concentration, without any lipids present.

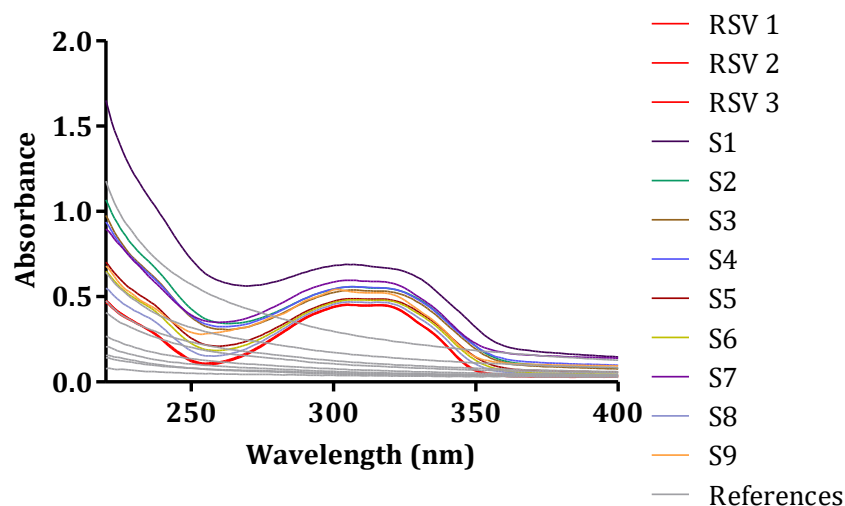


Figure 43. Absorbance spectra of three samples of resveratrol ($43 \mu\text{M}$) represented by RSV 1, RSV 2 and RSV 3, and of the samples of resveratrol loaded liposomes with increasing lipid concentrations and a fixed resveratrol concentration (S1-S9). The correspondent references prepared in the same manner as the samples but without the incorporation of the drug are presented in grey.

Although resveratrol is not present in the reference samples, it is possible to observe a spectral variation in the wavelengths of 200-300 nm that is due to the light dispersion caused by the liposomes. This spectral variation will lead to an interference in the quantification of resveratrol. In order to reduce this interference, to each spectra of resveratrol loaded liposomes was subtracted its corresponding reference. However, this subtraction is not enough to completely eliminate the interference, so it is necessary to perform the spectra derivatives. When the first derivative was performed (figure 44A), there was a visible reduction of the spectral variation that resulted from the lipid interference. This reduction was enhanced in the second (figure 44B) and third (figure 44C) derivatives, where the references spectra nearly pass through zero, which means that the interference was almost totally eliminated.

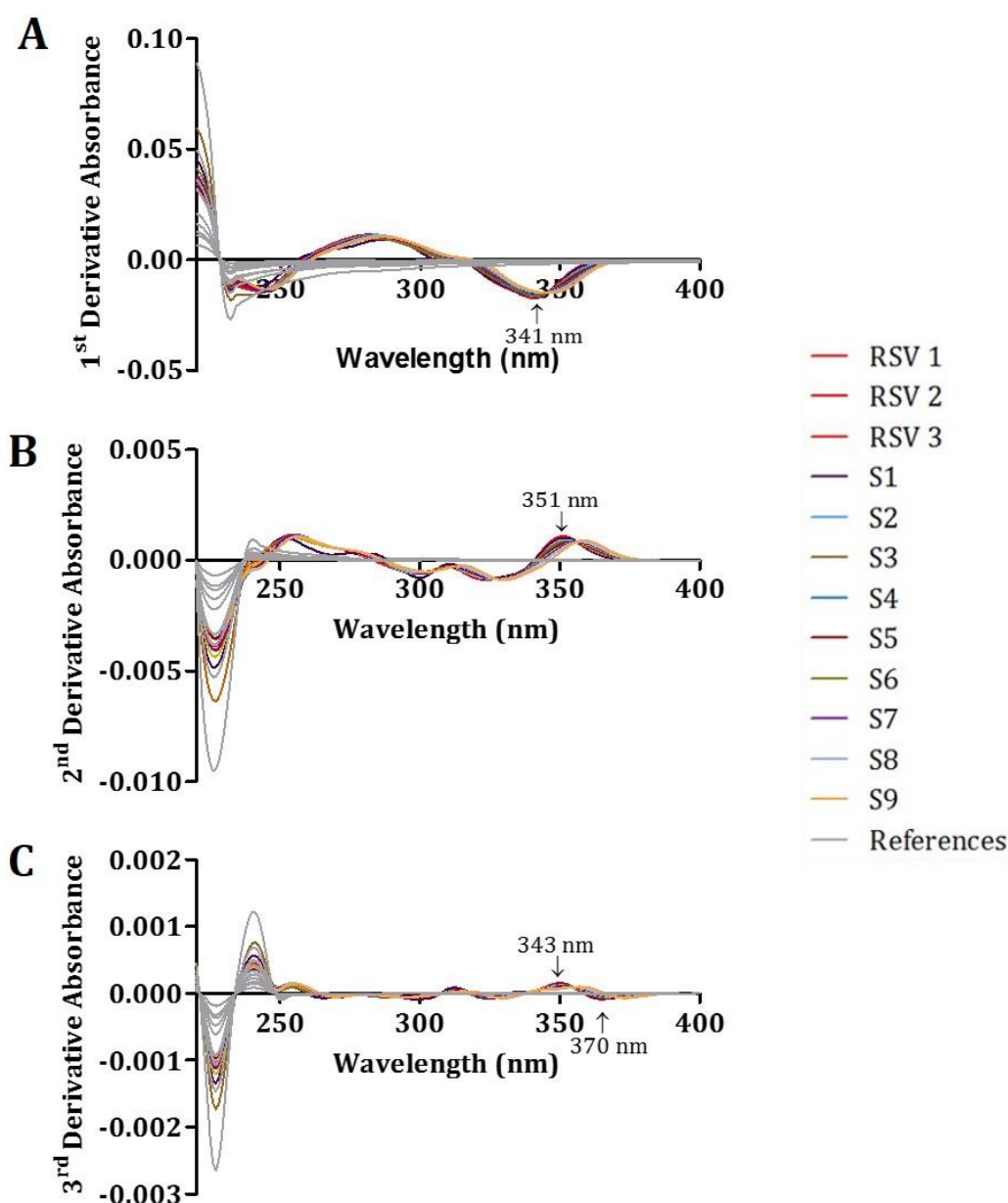


Figure 44. Representation of the first (A), second (B) and third (C) derivatives of three samples of resveratrol (43 μ M) represented by RSV 1, RSV 2 and RSV 3, of the samples of resveratrol loaded liposomes with increasing lipid concentrations and a fixed resveratrol concentration (S1-S9), and of the reference samples presented in grey. The peaks used to calculate the resveratrol Kp are identified in the spectra.

By analyzing the derivatives of the spectra, the peaks of higher or lower intensity are selected and the Kp value is calculated by a nonlinear regression (D versus $[L]$) obtained by adjusting the data to equation 14, where D corresponds to the derivative value at the selected wavelength and $[L]$ corresponds to the increasing concentrations of DODAB:MO (1:2) liposomes. The wavelength of maximum absorption (λ_{max}) chosen for the Kp calculations were for the first

derivative 341 nm, for the second derivative 351 nm and for the third derivative 343 and 359 nm. The nonlinear regressions are presented in figure 45.

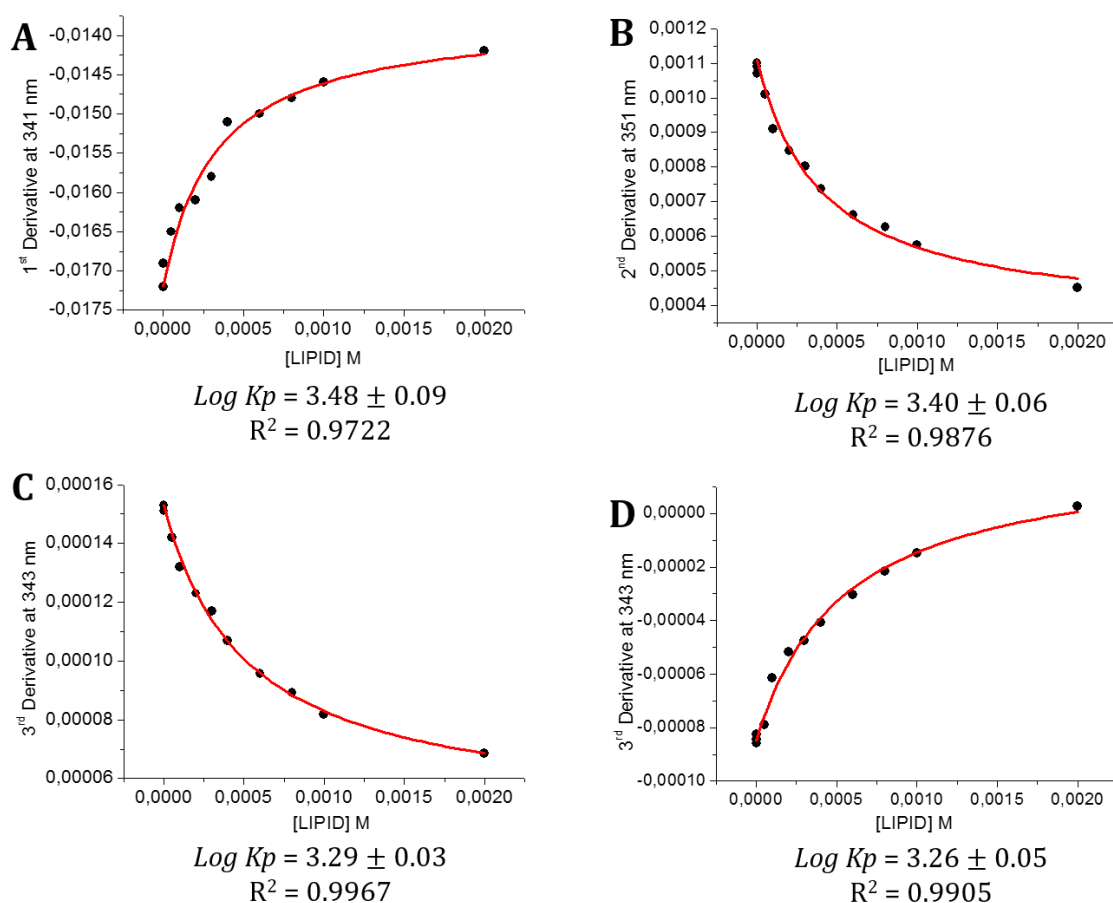


Figure 45. Representation of the absorbance values of the first derivative at $\lambda = 341$ nm (A), of the second derivative at $\lambda = 351$ nm, and of the third derivative at $\lambda = 343$ nm (C) and at $\lambda = 359$ nm (D), and respective nonlinear regressions fitted to equation 14. Below each graphic representation is presented the respective partition and correlation coefficients. The $\text{Log } Kp$ value is presented in mol.L^{-1} .

The mean value of Kp was calculated from the values obtained in each fitting and was turned to an adimensional value (by dividing the Kp value by the molar volume of the lipid in question (0.62 Lmol^{-1})) and logarithmized, resulting in a final Kp value of 3.37. In table 2 are presented the Kp values experimentally determined and the theoretical Kp values determined in a water:octanol system, in order to compare these values.

Table 2. Coefficient partition (K_p) values of resveratrol in a LUV((DODAB:MO)(1:2))/H₂O system and the respective logarithms ($\log K_p$) and coefficient partition values of resveratrol in octanol:water systems ($\log P$).

K_p (LUVs/H₂O) (molL⁻¹)	$\log K_p$ (LUVs/H₂O)^a	$\log P^b$	$\log P^c$
2329.9 ± 551.3	3.37 ± 0.10	3.10	3.40

^a $\log K_p$ value of resveratrol obtained experimentally in a LUV/H₂O system.

^b $\log P$ value of resveratrol obtained in a octanol:water system predicted by PubChem.

^c $\log P$ value of resveratrol obtained in a octanol:water system predicted by ChemAxon.

The $\log K_p$ value obtained experimentally is quite similar to the values predicted by the PubChem database and by the ChemAxon database, which corroborates the $\log K_p$ value obtained in this study. The high K_p value in this liposomal formulation proves that resveratrol has a lipophilic character and can be successfully encapsulated in the DODAB:MO (1:2) liposomal system, which validates these nanocarriers to encapsulate resveratrol. Moreover, as it is possible to observe in the figure 46, there is a pronounced bathochromic shift of about 8 nm, which is an indication that the polarity of the molecule is decreasing, which means that the drug is being displaced from a polar environment to a nonpolar environment¹¹². This once again suggests that the resveratrol molecules are being incorporated mainly in the hydrophobic portion of the liposomes and therefore are being efficiently encapsulated, indicating that the drug will be entrapped and transported within the liposomes. Additionally, the isosbestic points demonstrate that the drug is present in both phases (probably close to the headgroup region in the polar phase and inserted within the lipid chain apolar regions).

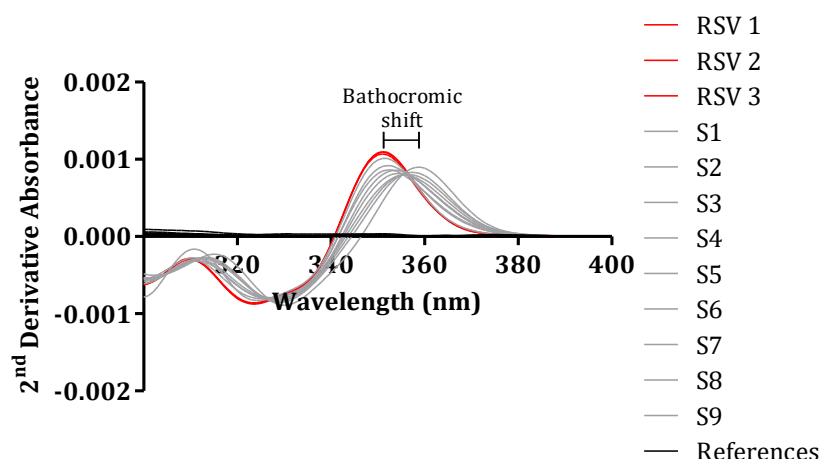


Figure 46. Representation of the second derivative of the absorbance values of three samples of resveratrol (43 μM), of the samples of resveratrol loaded liposomes with increasing lipid concentrations and a fixed resveratrol concentration, and of the reference samples. The bathochromic shift is also represented in the graphic.

Regarding the K_p determination at relevant pH values, the data processing has been made as it was described in chapter 2.8.2. For both pH values, the λ_{max} chosen were for the second derivative 352 nm and for the third derivative 311, 324, 343, 352, 359 and 367 nm. Results are summarized in table 3.

Table 3. Coefficient partition (K_p) values of resveratrol at physiological relevant pH's in a LUV((DODAB:MO)(1:2))/H₂O system and the respective logarithms ($\text{Log } K_p$).

K_p (LUVs/H ₂ O) (molL ⁻¹)		$\text{Log } K_p$ (LUVs/H ₂ O)	
pH 5	pH 7.4	pH 5	pH 7.4
1353 ± 220	1273 ± 196	3.34 ± 0.07	3.31 ± 0.03

The pH values chosen to perform the K_p determination characterize different physiological fluids and organs, for instance, in the blood stream the pH is of 7.4, and in cancer tissues the pH is of 5.

Results show that the K_p values of resveratrol in ultrapure water, at pH 5 and at pH 7.4 are 3.37 ± 0.10 , 3.34 ± 0.07 and 3.31 ± 0.03 , respectively, which are very similar values. According to López-Nicolás and García-Carmona¹³⁸, resveratrol has three acid dissociation constant (pK_a) values, namely $pK_{a1} = 8.8$, $pK_{a2} = 9.8$ and $pK_{a3} = 11.4$. These ionizations correspond to the deprotonation of the three hydroxyl

groups present in *trans*-resveratrol. The first pK_a is associated with the deprotonation of 4-*OH* because the abstraction of 4-*H* is easier than that of 3-*H* and 5-*H*. The second pK_a indicates the deprotonation of 3-*OH* or 5-*OH* (the 3- and 5-positions have the same structures since the molecule is symmetric). The third pK_a indicates the deprotonation of 5-*OH* or 3-*OH*. However, due to the high concentrations of resveratrol used to determine these values, these can be considered as apparent pK_a values. Nevertheless and taking this into account, it is not that surprising to observe such similar results. From this and the Henderson-Hasselbalch equation, it is possible to conclude that resveratrol will be 99.98% non-ionized at pH 5 and 95.5% non-ionized at pH 7.4. Since the resveratrol molecules are in the same neutral state in every condition, there will be mainly hydrophobic interactions with the membrane lipids.

3.7. Resveratrol partition in the liposomal formulation is spontaneous

In order to calculate the thermodynamic parameters associated with the partition of resveratrol in a biphasic system LUVs/H₂O, the value of K_p was determined at several temperatures and the results obtained are presented in table 4. Moreover, an example of the fittings of the third derivative values at the $\lambda_{max} = 311$ nm at different temperatures are presented in figure 47.

Table 4. Coefficient partition (K_p) values of resveratrol in a LUV((DODAB:MO)(1:2))/H₂O system and the respective logarithms ($\text{Log } K_p$) at different temperatures.

Temperature (°C)	K_p (LUVs/H ₂ O) (molL ⁻¹)	$\text{Log } K_p$ (LUVs/H ₂ O)
30	1213 ± 478	7.58 ± 0.42
37	1205 ± 626	7.57 ± 0.58
50	1573 ± 1465	7.84 ± 1.67
55	1892 ± 1868	8.02 ± 2.53
60	2651 ± 2257	8.36 ± 1.26

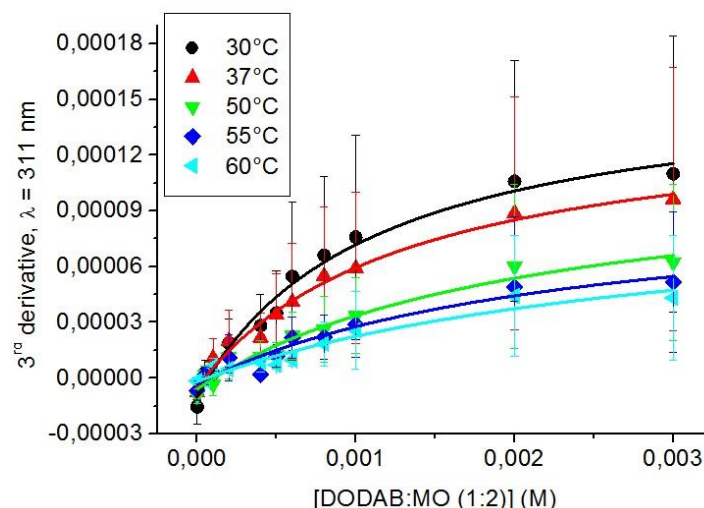


Figure 47. Fitting of the third derivative spectrophotometric data collected at $\lambda = 311$ nm for resveratrol loaded DODAB:MO (1:2) liposomes at different temperatures calculated with derivative spectroscopy at different temperatures: 30°C (black), 37°C (red), 50°C (green), 55°C (dark blue), 60°C (light blue).

The T_m of the plain liposomal system is $41.7 \pm 1.0^\circ\text{C}$, and the range of temperatures studied are above and below this temperature. This T_m will be altered in the presence of the drug. As a consequence, the liposomes will be in different phases according to the temperature. If the temperature is below the T_m , liposomes will be in a gel state (L_β), which is a more rigid state. On the other hand, if the temperature is above the T_m , liposomes will be in a liquid crystalline state (L_α), a more fluid state. Since the molecular arrangement and the lipid packing is extremely modified in the phase transition from L_β to L_α , it is possible to observe a biphasic behaviour in the Van't Hoff representation, which presents a distinct profile in the two lipid phases, as is shown in figure 48.

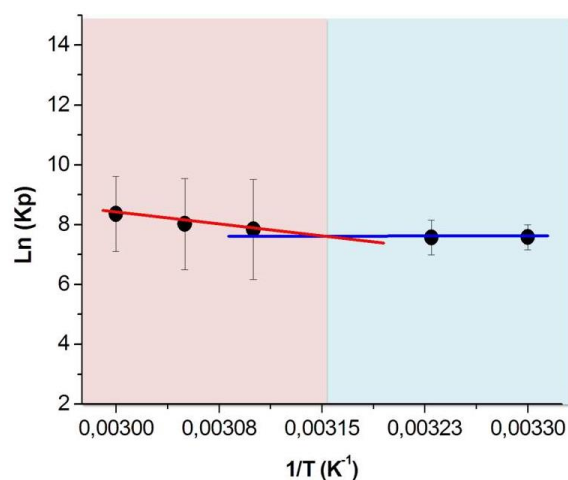


Figure 48. Van't Hoff regression for the resveratrol partition in DODAB:MO (1:2) LUVs. The pink square represents the L_α phase and the blue square represents the L_β phase.

By analyzing the graphic representation in figure 48, it is possible to extrapolate the phase transition temperature of the resveratrol loaded DODAB:MO (1:2) liposomes by determining the intersection of the two linear plots. The thermodynamic parameters obtained for the resveratrol partition coefficient were calculated based on the temperature dependence of the K_p values using the Van't Hoff equation (equation 15) and the results are presented in table 5.

Table 5. Variation of the enthalpy (ΔH) \pm SD, entropy (ΔS) \pm SD and Gibbs free energy (ΔG) obtained for the resveratrol partition between the aqueous phase and DODAB:MO (1:2) liposomes at different temperatures.

Temperature (°C)	Temperature (K)	$\Delta H_{w \rightarrow m}$ (KJ.mol ⁻¹)	$\Delta S_{w \rightarrow m}$ (KJ.mol ⁻¹ .K ⁻¹)	$\Delta G_{w \rightarrow m}$ (KJ.mol ⁻¹)
30	303	6.00 ± 0.68	0.20 ± 0.005	-17.06
37	310			-18.46
50	323	43.8 ± 5.05	0.083 ± 0.0022	-20.71
55	328			-21.12
60	333			-21.54

The enthalpy variation (ΔH) describes the energetic requirement of the system. By examining the table 5, it is possible to observe a significant difference between the ΔH before the phase transition (6.00 ± 0.68 KJ.mol⁻¹) and after the phase transition (43.8 ± 5.05 KJ.mol⁻¹). The fact that ΔH after the phase transition is considerably higher than before the phase transition means that the intermolecular forces established in the system after the phase transition will be greater than before. This is related to the fact that resveratrol more easily penetrates the lipid media in the fluid state, and thus the intermolecular forces between the drug molecules and the lipids increase. The entropy variation (ΔS) is ordinarily understood as a measure of disorder. If ΔS is higher than zero, which happens before (0.20 ± 0.005 KJ.mol⁻¹.K⁻¹) and after (0.083 ± 0.0022 KJ.mol⁻¹.K⁻¹) the phase transition, the system is becoming more disordered through the course of the reaction. As for the Gibbs free energy (ΔG), it is a thermodynamic potential that combines enthalpy and entropy into a single value and can predict the direction of a chemical reaction. When ΔG is positive, then the reaction is nonspontaneous,

which means that it requires the input of external energy to occur, when ΔG is negative, which is the case for all temperatures at study, before and after the phase transition, then the reaction is spontaneous and it does not require external energy input.

When the drug is added to the system, initially it is located only in the aqueous phase. For the drug to be able to enter the liposomal system, the bilayers must rearrange to create space to accommodate the drug. Once resveratrol is encapsulated in the liposomes, it will interact with the lipid molecules, releasing energy. Due to the disorder created by the entry of the resveratrol molecules into the liposomes, there will be an increase in entropy. After the encapsulation, the resveratrol molecules partially disappear from the aqueous phase and so, the space that these molecules were occupying is now filled with water molecules. This will create new water-water interactions and thereby release energy. However, it is likely that the resveratrol molecules that initially were located in the aqueous phase also interacted with the water molecules, especially because resveratrol has hydrophilic hydroxyl groups that can establish hydrogen bonds with water. Within the range of temperatures at study, the values of the thermodynamic parameters vary greatly. This is due to the fact that at lower temperatures the liposomes are in a more rigid state, whereas at higher temperatures they are in a more fluid state. Therefore, the more rigid the liposomes are, the more energy will be required to separate the bilayers and accommodate the resveratrol into the liposomes. This is why the resveratrol encapsulation is made above the phase transition temperature.

3.8. Resveratrol is released from liposomes in water

In figure 49 and 50 the resveratrol release profiles from the liposomal system at study are presented. Figure 49 compares the release profile in storage conditions, i.e. in ultrapure water with an approximate pH of 5.5, with the release profile in acetate buffer with a pH of 5, which aims to simulate the physiological conditions of some cancer tissues. As it is possible to observe, and although the pH of the two conditions are very similar, the release of the drug has completely distinct profiles, wherein in storage conditions the drug release is about five times higher than the release at pH 5. This may be due to the fact that, in storage conditions, the ultrapure

water doesn't have any dissolved salts or molecules, which leads to a smaller solvation shell. Moreover, the presence of salts and counter ions in the buffer cause the lipid particles to be more stable in terms of osmotic pressure, which probably maintains the drug encapsulated for a longer period of time. When the particles are suspended in ultrapure water, where there are no counter ions or salts actuating, the osmotic pressure will lead to equilibrium between the concentration of resveratrol in the media and in the liposomes, which will probably lead to the release of the resveratrol molecules to the surrounding media. Therefore, the approach used to storage these resveratrol loaded liposomes is probably not the best one since the drug content is being released and so, maybe these liposomes should be stored in buffer.

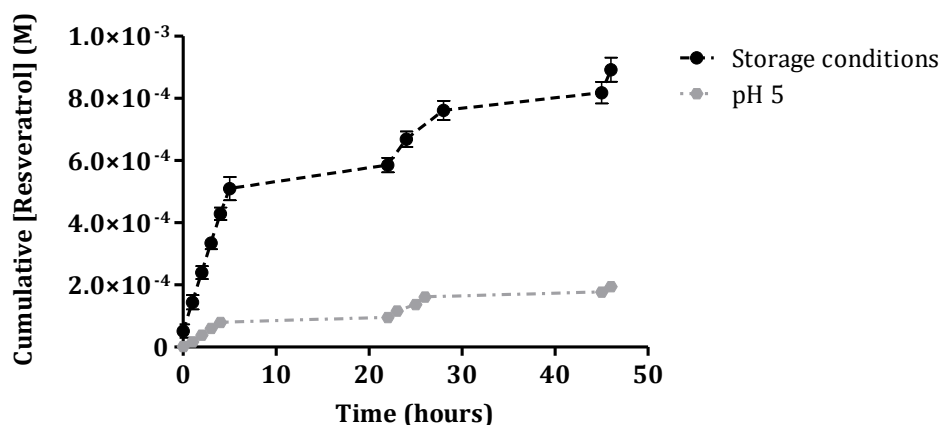


Figure 49. Cumulative resveratrol release from DODAB:MO (1:2) liposomes in storage conditions (ultrapure water, pH \approx 5.5) and in acetate buffer (pH = 5).

Regarding figure 50, it is possible to observe the release profiles that simulate two physiological conditions, namely the bloodstream (pH = 7.4) and the cancer tissue (pH = 5). In this case, the drug is released in higher amounts in pH = 7.4 during the first 24 hours, but it is released in higher amounts in pH = 5 during the 24 hours following the first ones. However, the release profiles are very similar in both cases, which makes sense since the ionization of the resveratrol molecules is not significantly different at the two pHs in study, as it was proven before by the partition coefficient assay ($\text{Log } K_p$ (pH 5) = 3.34 ± 0.07 ; $\text{Log } K_p$ (pH = 7.4) = 3.31 ± 0.03).

The protocol used in this experiment does not assume a constant agitation, being the agitation confined to the moments of aliquotation. This leads to the appearance of plateaus in the graphic representation, which represent the hours in

which no sample was taken and, therefore, no agitation was made. At these points of rest, the resveratrol molecules seem to encapsulate back into the liposomes, probably due to the fact that the resveratrol partition in the system is high, which means that the molecules have a lipophilic character and are more comfortable in the lipid vesicles than in the aqueous media.

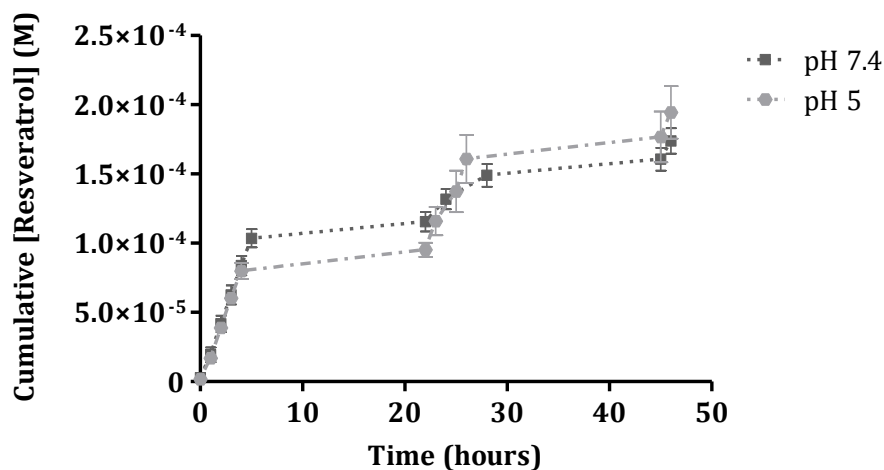


Figure 50. Cumulative resveratrol release from DODAB:MO (1:2) liposomes in HEPES buffer (pH = 7.4) and in acetate buffer (pH = 5).

The drug release can be influenced by some physicochemical properties of the liposomal carrier, such as membrane composition of the liposomes, nature of the drug entrapped into the liposomes, dosing schedule, route of administration and by the drug to lipid ratio¹³⁹. However, there are some environmental triggers that have gained attention in the recent past, namely low pH, presence of particular enzymes, heat, ultrasound, among others¹⁴⁰. In the future, this formulation in particular, should be adapted with a triggering system, probably to force the drug release at pH = 5, so that the liposomes can be able to release their content into the cytoplasm of the targeted cells¹⁴⁰. However, as resveratrol has shown to be non-toxic and to be metabolized extensively at the enterocytes level (previous to absorption), the results obtained with this formulation are still very interesting. Indeed, even with the release of resveratrol at the blood circulation, that would not constitute a problem, since resveratrol will not be metabolized at this point, and no negative effects of free resveratrol can be found.

3.9. Resveratrol loaded liposomes need PEGylation to avoid binding to HSA

Results regarding the size and ζ -potential changes of HSA molecules upon binding to free resveratrol in aqueous media are presented in figure 51.

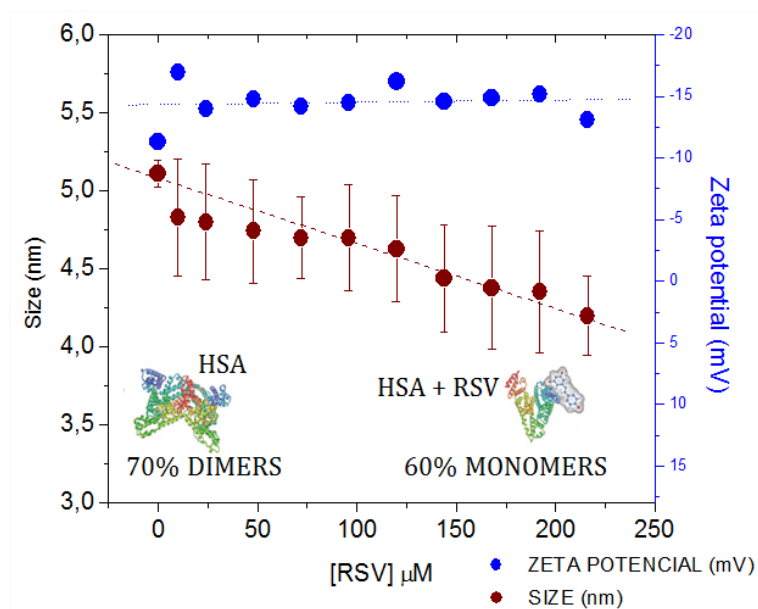


Figure 51. Size and ζ -potential changes upon binding to HSA of increasing concentrations of resveratrol in aqueous media.

From analyzing figure 51 it is possible to observe that the HSA superficial charge (≈ -15 mV) was not altered upon binding to resveratrol molecules, which makes sense since the resveratrol molecules are neutral. It is also possible to observe that when there was no resveratrol present, the mean particle size was of approximately 5.3 nm, which is consistent with the presence of dimeric forms of this protein since the reported size for HSA dimers is approximately 6nm. However, when resveratrol was added, and as the concentration of this drug increased, the HSA size was diminished, until it reached a mean value of approximately 4.2 nm. Since HSA monomers have sizes of nearly 2.68 nm, and the size of the HSA molecules is decreasing with the increase of the resveratrol concentration, it is safe to say that the resveratrol is promoting the HSA dimer dissociation upon its binding to the HSA molecules.

Results regarding the binding of resveratrol loaded liposomes to the HSA molecules are presented in figure 52.

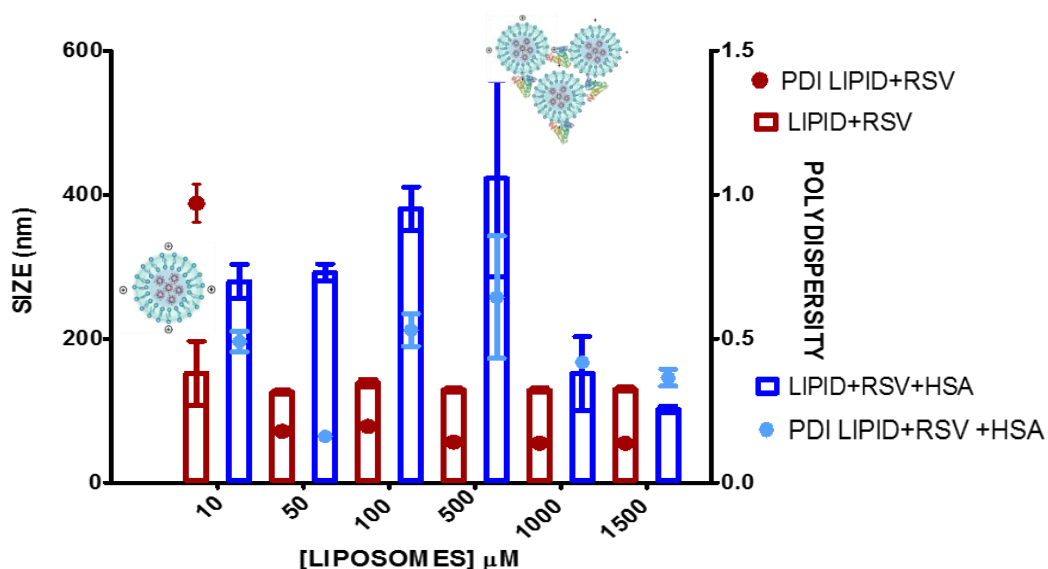


Figure 52. Mean sizes (columns) and PDI (dots) of resveratrol loaded liposomes in the presence (blue) and in the absence (red) of HSA, when the lipid concentration is increasing.

First of all, by analyzing figure 52 it is possible to observe that in the absence of HSA, and although the lipid concentration is increasing, the mean size and PDI values remain constant. This means that the lipid concentration is not affecting the size and homogeneity of the samples. However, when HSA molecules are present, the sizes of the measured particles increase considerably with the increase of lipid concentration until concentrations of 500 μM . This indicates that the HSA is promoting liposomal aggregation, because it is negatively charged and can bind to the positively charged lipid vesicles. On the other hand, when the lipid concentration is high enough (in this case above 500 μM), the size of the liposomes returns to values similar to the values obtained in the absence of HSA. This happens because, in this case, the high amount of lipid is enough to solubilize the HSA molecules available and conceal their negatively charged residues. Nonetheless, liposomes should be PEGylated to avoid the liposomal aggregation promoted by the binding of HSA.

PEGylated liposomes are polyethylene glycol (PEG)-coated liposomes and this surface modification increases particle stability by reducing its interaction with biological macromolecules¹⁴¹, such as HSA. Moreover, coating of liposomes with PEG further ensures a prolonged circulation of the carrier, allowing prolonged dosing intervals¹⁴², and induces accumulation in pathological foci, such as tumors¹⁴¹.

Figure 53 shows the variation of the ζ -potential of the lipid particles with and without resveratrol in the presence of HSA.

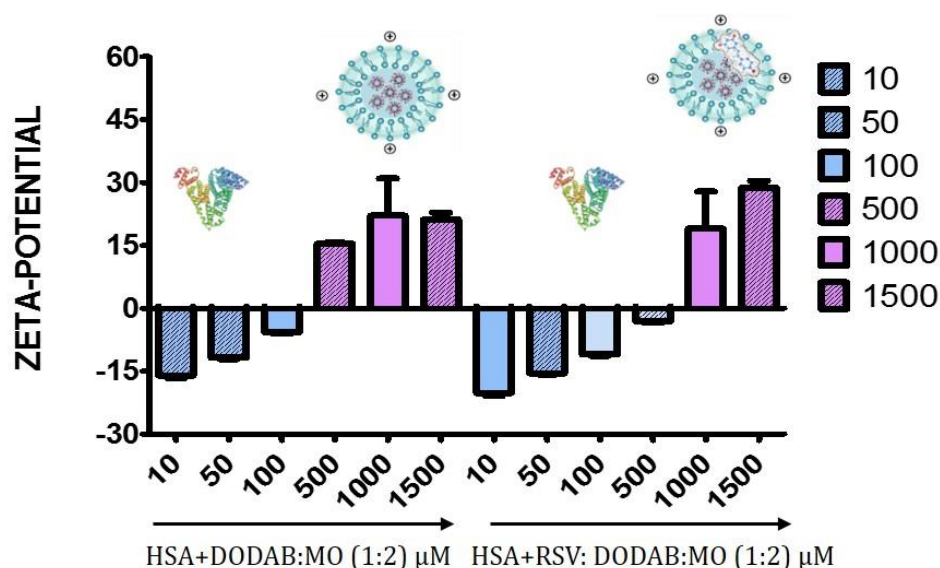


Figure 53. ζ -potential variation of plain and resveratrol loaded liposomes with increasing lipid concentrations in the presence of HSA.

As it can be seen in the graphic representation presented in figure 53, both plain liposomes and resveratrol loaded liposomes suffer an inversion of its ζ -potential. This happens because the HSA is an anionic molecule, and the liposomes are cationic. When HSA is present in surplus, the ζ -potential is negative because there are less lipid vesicles. However, as the concentration of liposomes increases, so does the ζ -potential, because their positive charges override the negative charges of HSA. Interestingly, liposomes containing resveratrol present a different binding kinetic profile than plain liposomes, which is evidenced by the slower inversion of the ζ -potential. This delay in the charge inversion of resveratrol loaded liposomes is probably due to the fact that the $-OH$ groups of the resveratrol molecules located in the more superficial part of the liposomes are hindering the binding of the HSA molecules.

Once again, it is possible to conclude that PEGylation of both plain and resveratrol loaded liposomes would be a good mechanism to avoid the aggregation of liposomes due to HSA binding.

3.10. Resveratrol does not affect the growth of yeast cells

The following experiments were designed to evaluate the effect of resveratrol in yeast cell growth. The influence of resveratrol on the growth of the yeast strain *S. cerevisiae* W303-1A was evaluated under fermentative and respiratory conditions. Results are shown in figure 54A and B, respectively.

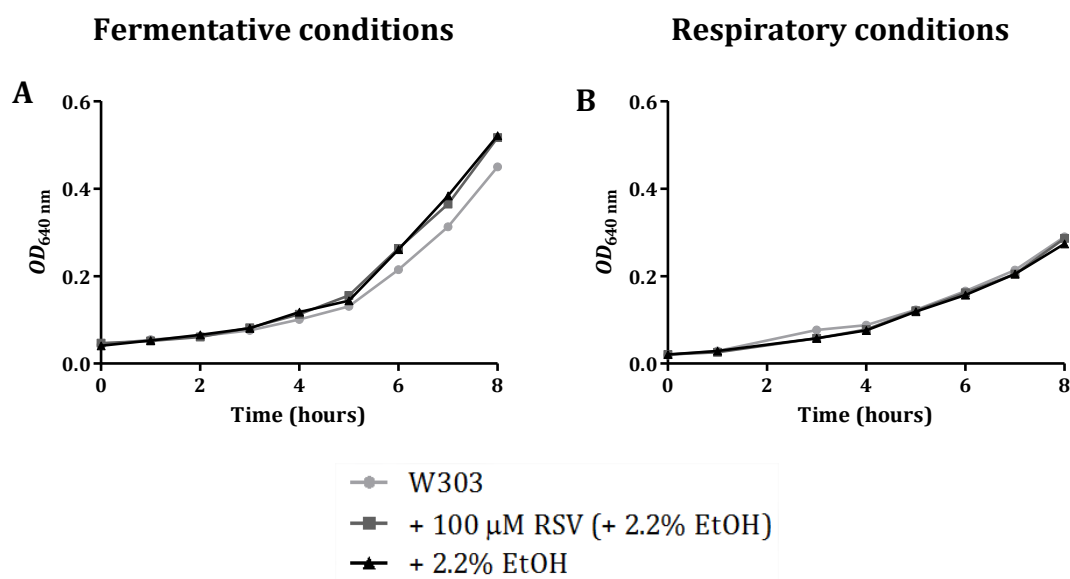


Figure 54. Growth of *S. cerevisiae* W303 in YPD medium (fermentative conditions) (A) and in lactate/ethanol medium (respiratory conditions) (B) in the presence and absence of 100 μM resveratrol. Resveratrol was prepared in ethanol 100% (v/v) before addition to the culture medium, so the final concentration of ethanol in the growth experiment was 2.2% (v/v). Control experiments with ethanol alone (final concentration: 2.2% (v/v)) and neither resveratrol nor ethanol are also shown.

As expected, the growth rate of yeast cells in respiratory conditions ($\mu_{max} = 0.2939 \text{ h}^{-1}$) was lower than in the fermentative conditions ($\mu_{max} = 0.3652 \text{ h}^{-1}$), as is reported in table 6. In yeast cell cultures growing in fermentative conditions, the elicitation with 100 μM resveratrol induced a slight increase in the specific growth rate. However, this stimulatory effect seems to be caused by the ethanol used to dissolve the resveratrol, since in yeast cell cultures with ethanol alone the same increase was observed. Under respiratory conditions, the increase in the growth rate caused by ethanol is less accentuated, since the medium already contains ethanol.

Table 6. Maximum specific growth rate (μ_{max}) of *S. cerevisiae* W303 liquid cultures.

	μ_{max} (h ⁻¹)	
	Fermentative conditions	Respiratory conditions
W303	0.3652	0.2939
+ EtOH 2.2% (v/v)	0.3785	0.3126
+ 100 μ M RSV (+ EtOH 2.2% (v/v))	0.3840	0.3109

As a whole, results show that 100 μ M resveratrol did not impair or boost the growth of *S. cerevisiae* yeast cells in both fermentative and respiratory conditions. However, this observation has to be confirmed in future research by testing increasing resveratrol concentrations, although the ones used in the present study are in the range reported in the literature to study either the effect of resveratrol in mammal cells, including cancer cells¹⁴³ or in microorganisms.

In a recent report, it was studied the effect of 109.5, 219 and 438 μ M resveratrol in the growth of *Propionibacterium acnes*. Results showed that resveratrol demonstrates a sustained antibacterial activity against *P. acnes*, whereas benzoyl peroxide, a commonly used antibacterial treatment for acne, demonstrated a short-term bactericidal response. Moreover, a combination of resveratrol and benzoyl peroxide showed high initial antibacterial activity and sustained bacterial growth inhibition, meaning that these two compounds had a synergistic effect and are a potentially novel therapeutic option in the treatment of acne vulgaris¹⁴⁴.

One might think that resveratrol has no effect in yeast cell growth because the drug is not entering yeast cells. However, according to Neves *et al.* review⁵¹, the resveratrol entrance in these cells is expected to happen since the structure of the yeast cell wall is permeable to both small polar and nonpolar molecules with a molecular weight of 620 Da, and resveratrol has a molecular weight of 228 Da. Moreover, Bishop and his coworkers¹⁴⁵ found that the loading process of resveratrol into yeast cells happens by passive diffusion driven by the concentration difference between the external medium and the internal yeast cellular medium. This loading process is additionally boosted by the hydrophobic interactions and hydrogen bonds established between the $-OH$ groups of the resveratrol molecules and the $-NH_2$, $-OH$ and $-COOH$ groups from the polar headgroups of the phospholipids in the yeast membrane.

3.11. Hydrogen peroxide inhibits yeast growth in a dose-dependent manner and resveratrol slightly counteracts this effect

H₂O₂ generates ROS that are responsible for oxidative damage, inhibiting cells metabolism and growth¹⁴⁶. In the present study, H₂O₂ was added to the yeast cell culture when the cells reached mid-exponential growth phase at increasing concentrations. As shown in figure 55, H₂O₂ promoted a dose-dependent inhibition of cell growth. At the final H₂O₂ concentration of 2 mM, yeast growth was completely inhibited.

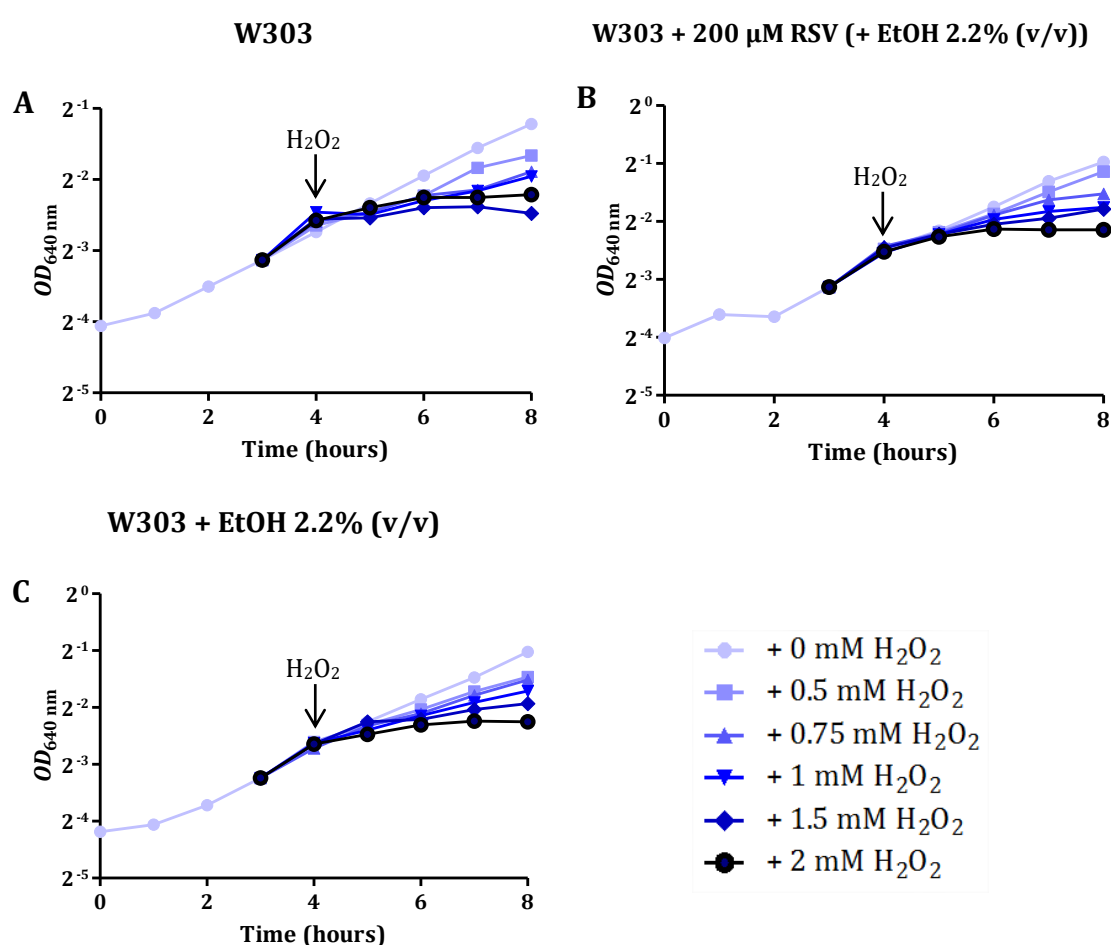


Figure 55. Growth of *S. cerevisiae* W303 in lactate/ethanol medium (respiratory conditions) in the absence (A) and in the presence of 200 μM resveratrol (+ EtOH 2.2% (v/v)) (B) and with ethanol 2.2% (v/v) (C) before and after the addition of H₂O₂ with growing concentrations (0, 0.5, 0.75, 1, 1.5 and 2 mM) to the culture media.

Resveratrol has been described in the literature as a potent agent against ROS¹⁴⁷ and so, in this study, one of the objectives was to explore the utility of the yeast model to study the protective effect of resveratrol in cells under oxidative

stress. Results regarding the effect of 200 μM resveratrol are presented in figure 55B in cells incubated with up to 2 mM H_2O_2 . As can be seen, a protective effect of resveratrol was evident when cells were treated with 0.5 mM H_2O_2 (figure 56).

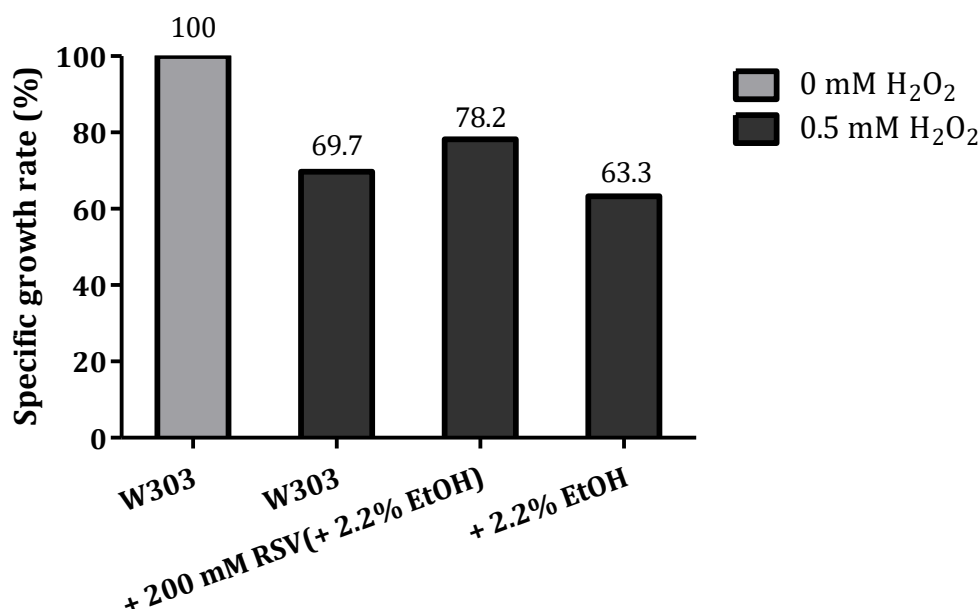


Figure 56. Protective effect of resveratrol on the inhibition of yeast cell growth mediated by 0.5 mM H_2O_2 . Growth of *S. cerevisiae* W303 occurred in lactate/ethanol medium (respiratory conditions) and 0.5 mM H_2O_2 in the absence and in the presence of 200 μM resveratrol (+ EtOH 2.2% (v/v)) or ethanol alone.

The inhibition of yeast cell growth induced by 0.5 mM H_2O_2 was as follows: 30.3% in control cells, 36.4% in the presence of ethanol 2.2% (v/v) and 21.8% in the presence of 200 μM resveratrol (+ EtOH 2.2% (v/v)), suggesting a clear protective effect of resveratrol. At higher concentrations of H_2O_2 , the role of resveratrol was not so evident, but these concentrations are probably extremely toxic.

The effect of 0.5-2 mM H_2O_2 on the specific growth rate of the cultures in the presence and absence of 200 μM resveratrol or ethanol alone are depicted in figure 57. As can be seen, the presence of H_2O_2 in the medium decreased the specific growth rate, and the inhibition kinetics obeyed an exponential relationship at H_2O_2 levels above the minimum inhibitory concentration (X_{min}). The exponential inhibition constant (k_i) and the X_{min} allowed to get an insight regarding H_2O_2 toxicity, as well as the resveratrol protective effect for the yeast strain at study (table 7).

The exposure of cells to oxidative stress leads to a stress-activated response induced by Yap1p¹⁴⁸. The presence of H₂O₂ activates the expression of the Yap1p transcription factor, which is required for oxidative stress tolerance. This activation is achieved through the multistep formation of disulfide bonds and transits from the cytoplasm to the nucleus. Yap1p is degraded in the nucleus after the oxidative stress has passed^{149,150}. Studies have been conducted regarding the induction of antioxidant defense via transcription factor Yap1p by resveratrol¹⁵¹.

These results deserve future investigations to study if during the time-scale of the experiment (4 h) resveratrol modified the expression of genes associated with the remodeling of the cell membrane or with the synthesis of anti-oxidant enzymes, including activation of the Yap1p transcription factor. Alternatively, resveratrol may act directly as a free radical scavenger.

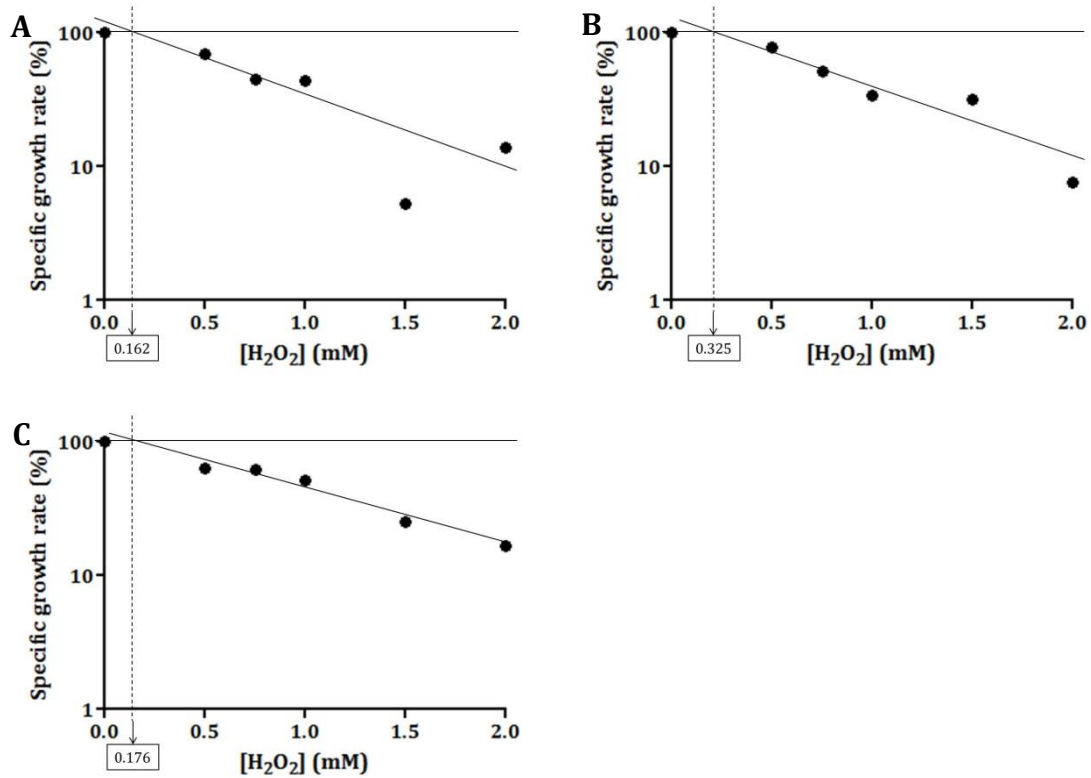


Figure 57. Dependence of the specific growth rates of *S. cerevisiae* W303 grown in lactate/ethanol medium (respiratory conditions) on the extracellular H₂O₂ concentration in the absence (A) and in the presence of 200 μ M resveratrol (+ EtOH 2.2% (v/v)) (B) or ethanol alone (C), and the respective X_{min} .

The exponential inhibition constant (k_i) was lower in the presence of 200 μ M resveratrol which is consistent with the minimum inhibitory concentration (X_{min}),

that is defined as the lowest concentration of a drug that will inhibit the visible growth of an organism³², being lower in the same conditions. This suggests a protective role of resveratrol at low H₂O₂ concentrations. As these experiments were only performed once, additional studies are necessary, eventually associated with gene expression studies, as suggested to above.

Table 7. Effect of H₂O₂ on the growth of *S. cerevisiae*. Cells were cultivated in lactate/ethanol medium (respiratory conditions) in the absence and in the presence of 200 μ M resveratrol (+ EtOH 2.2% (v/v)) and with ethanol alone, in the presence of different H₂O₂ concentrations.

	Growth parameters ^a	
	X_{min} (mM)	k_i (mM ⁻¹)
W303	0.162	1.40
+ EtOH 2.2% (v/v)	0.176	1.38
+ 200 μ M RSV (+ EtOH 2.2% (v/v))	0.325	0.98

^a X_{min} : minimum inhibitory concentration; k_i : exponential inhibition constant.

The study of the effect of H₂O₂ on yeast cell death was optimized in order to further evaluate the protective role of resveratrol. H₂O₂ was added to the yeast cell culture when the cells reached mid-exponential growth phase at increasing concentrations (0, 0.5, 1, 2 and 5 mM). As shown in figure 58, H₂O₂ induced cell death in a dose- and time-dependent manner.

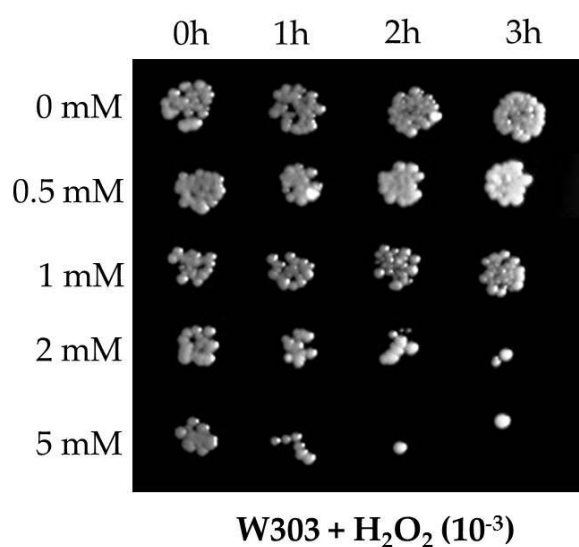


Figure 58. Spot test analysis representing the growth of *S. cerevisiae* on YPD agar medium when cells were incubated with up to 5 mM H₂O₂.

As can be seen, at 5 mM H₂O₂ the viability of the yeast cells was severely affected at incubation times > 1 h. It is well known that H₂O₂ causes oxidative damage to the cells, impairing their capacity to grow and replicate¹⁴⁶. Future experiments will be designed to evaluate the potential protective effect of resveratrol on yeast cell death induced by H₂O₂.

3.12. Resveratrol loaded liposomes are efficiently internalized by yeast cells

Due to its low water solubility, the delivery of free resveratrol is a challenging approach. To evaluate if yeast cells are capable of incorporating resveratrol loaded liposomes, these were labeled with the probe DPH and cells were observed under the fluorescence microscope 4 h after incubation. A control experiment with DPH alone was also performed. Results are shown in figure 59. When cells were incubated with resveratrol loaded liposomes labeled with DPH (figure 59.2) the blue fluorescence was located in the periphery of the cell nuclei, eventually in the lipid droplets that surround the endoplasmic reticulum. As referred before, DPH is an hydrophobic probe that exhibits weak fluorescence in aqueous media, but shines brightly when incorporated in the liposomes membrane¹²⁷. Therefore, the presence of fluorescence inside the cells suggests that resveratrol loaded liposomes are capable to cross the cell boundary.

Even though the number of studies regarding the interaction of liposomes and yeast cells is very reduced, some authors have reported the transfection of *S. cerevisiae* protoplasts with liposome-encapsulated plasmid DNA¹⁵³ and the delivery of 6-carboxyfluorescein into *S. cerevisiae* protoplasts mediated by liposomes prepared with phospholipids extracted from the same yeast cells. However, the details of these interactions remain obscure.

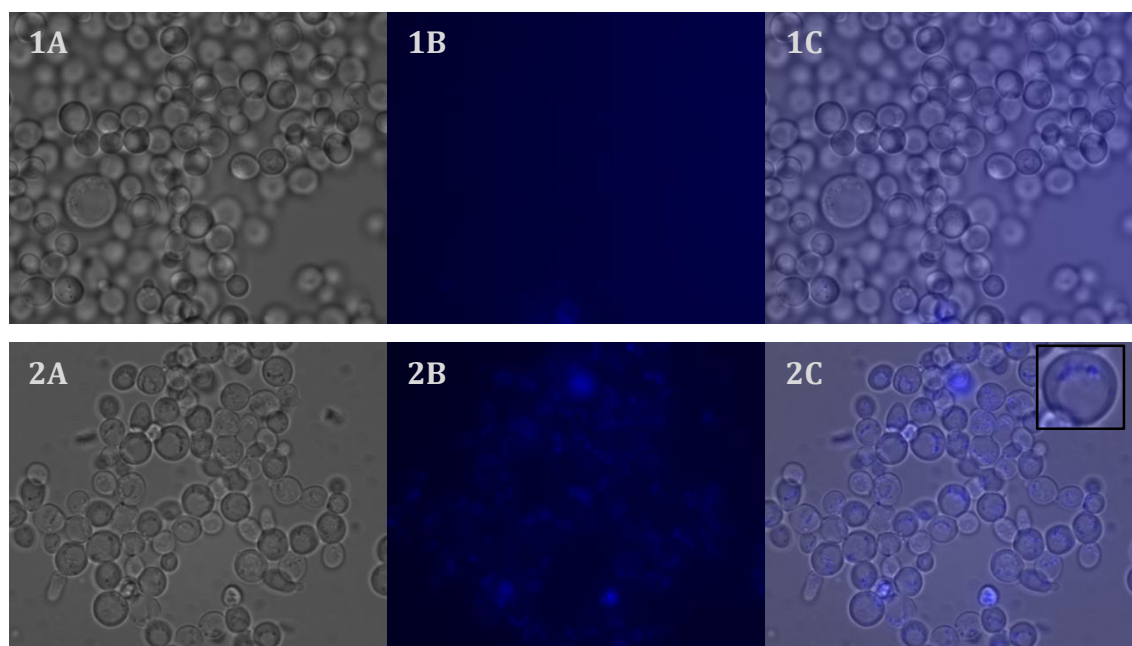


Figure 59. Bright-field (A), fluorescence (B) and overlay of both (C) micrographs of *S. cerevisiae* W303 yeast cells incubated with (1) 3 μ M DPH free fluorescent probe to study cell capacity to internalize it (control experiment) and with (2) resveratrol loaded DODAB:MO (1:2) liposomes labeled with 3 μ M DPH fluorescent probe. Scale bar = 7.5 μ m.

These findings are very relevant and open excellent perspectives for future work aimed to optimize the internalization of the compound and the formulation of a delivery system to specific cell targets. Co-localization experiments with fluorescent probes specific to the lipid droplets, such as Nile Red, may provide further evidences regarding the precise intracellular localization of resveratrol loaded liposomes.

3.13. Free and encapsulated resveratrol have no effect in cell viability

S. cerevisiae W303 cells labeled with the fluorescent probe FDA and treated either with resveratrol alone or with resveratrol loaded liposomes were analyzed by flow cytometry to study cell viability. The acquisition protocol was defined to measure forward scatter (FS), side scatter (SS) and green fluorescence (FL1) on a logarithmic scale. The graphs presented were obtained by the program *Flowing software*. Figure 60 shows a representative result.

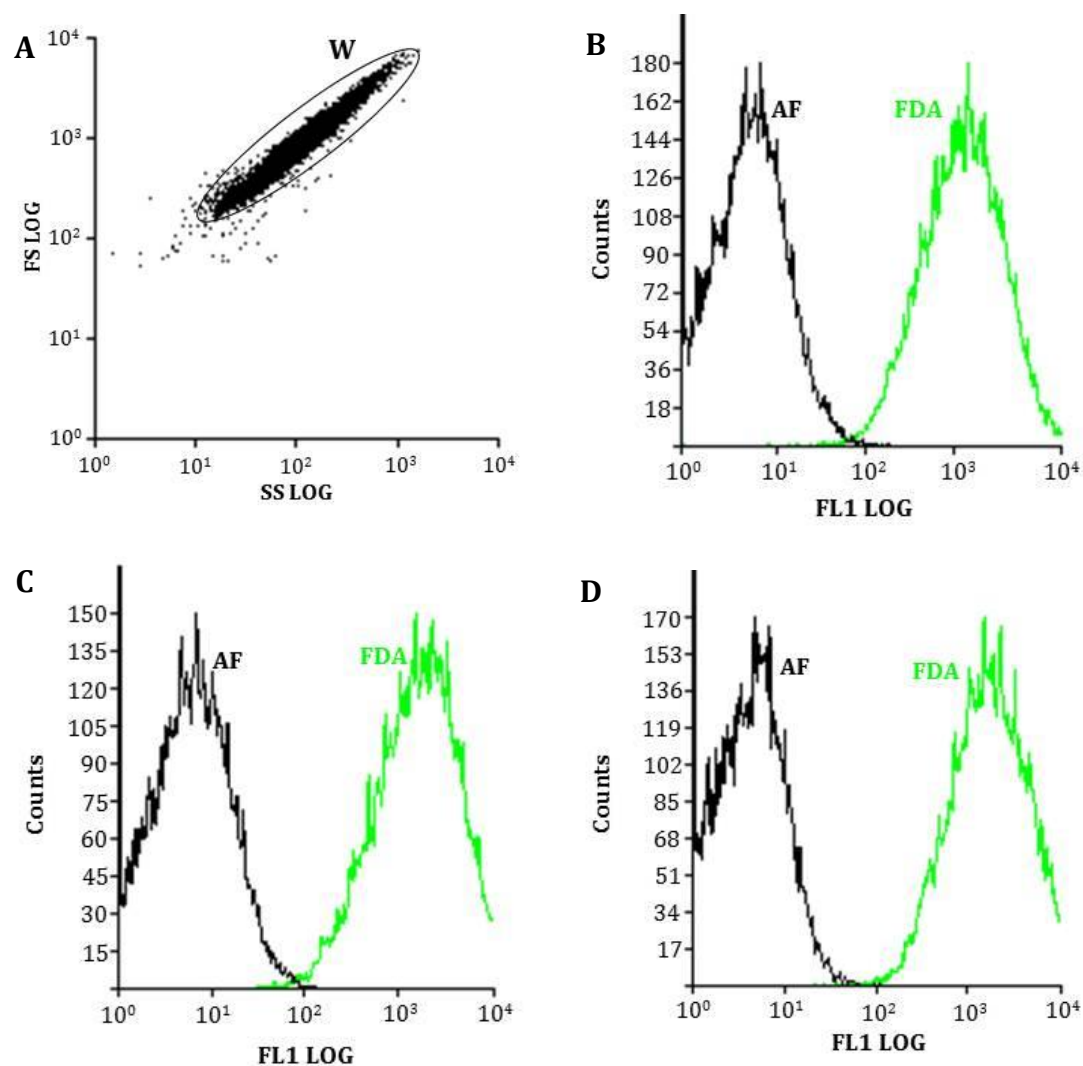


Figure 60. Flow cytometry analysis of *S. cerevisiae* W303 yeast cell populations to study cell viability with the FDA probe. Scattergram of a population of yeast cells in the absence of resveratrol (A); overlay histogram of autofluorescence (black line) and FDA induced fluorescence (green line) in the absence of resveratrol (B) and upon treatment of yeast cells with 200 μ M of free resveratrol (C) and resveratrol loaded liposomes (D).

The scattergram of figure 60A displays a well-defined population of yeast cells (gated region W). The same gate was defined for all subsequent experiments and the number of cells was set to 20000. The overlay of the histograms corresponding to the yeast cells autofluorescence and the fluorescence of yeast cells labeled with FDA (Figures 60B, 60C and 60D) shows an evident positive staining, which attests that the probe is being successfully hydrolyzed, hence yielding green fluorescence.

As can be seen in figure 61, non-treated cells and those treated with free resveratrol or with resveratrol loaded liposomes were almost 100% viable. These results suggest that neither the resveratrol nor the resveratrol loaded liposomes are

inducing cytotoxicity or cell death, as shown before in the study of resveratrol effect on yeast cell growth. Future studies will be performed in the presence of H₂O₂ to evaluate whether or not resveratrol (free or encapsulated) protects cells from H₂O₂ cytotoxic effects.

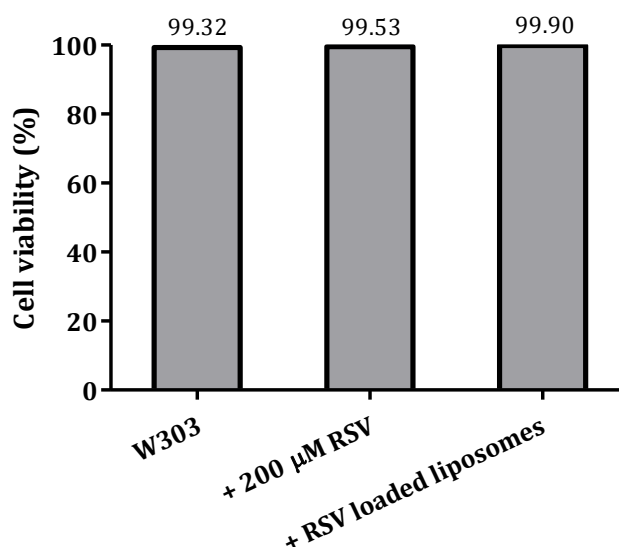


Figure 61. Effect of free and encapsulated resveratrol on cell viability in *S. cerevisiae* W303 grown in lactate/ethanol medium.

3.14. Free and encapsulated resveratrol decrease endogenous ROS levels

S. cerevisiae W303 cells were labeled with the ROS-sensitive probe DHE and treated with resveratrol alone and resveratrol loaded liposomes to study intracellular ROS by flow cytometry. The samples were analyzed by flow cytometry and an example of the collected results is presented in figure 62. The acquisition protocol was defined to measure forward scatter (FS), side scatter (SS), orange fluorescence (FL3) and red fluorescence (FL4) on a logarithmic scale. The graphs presented were obtained by the program *Flowing software*.

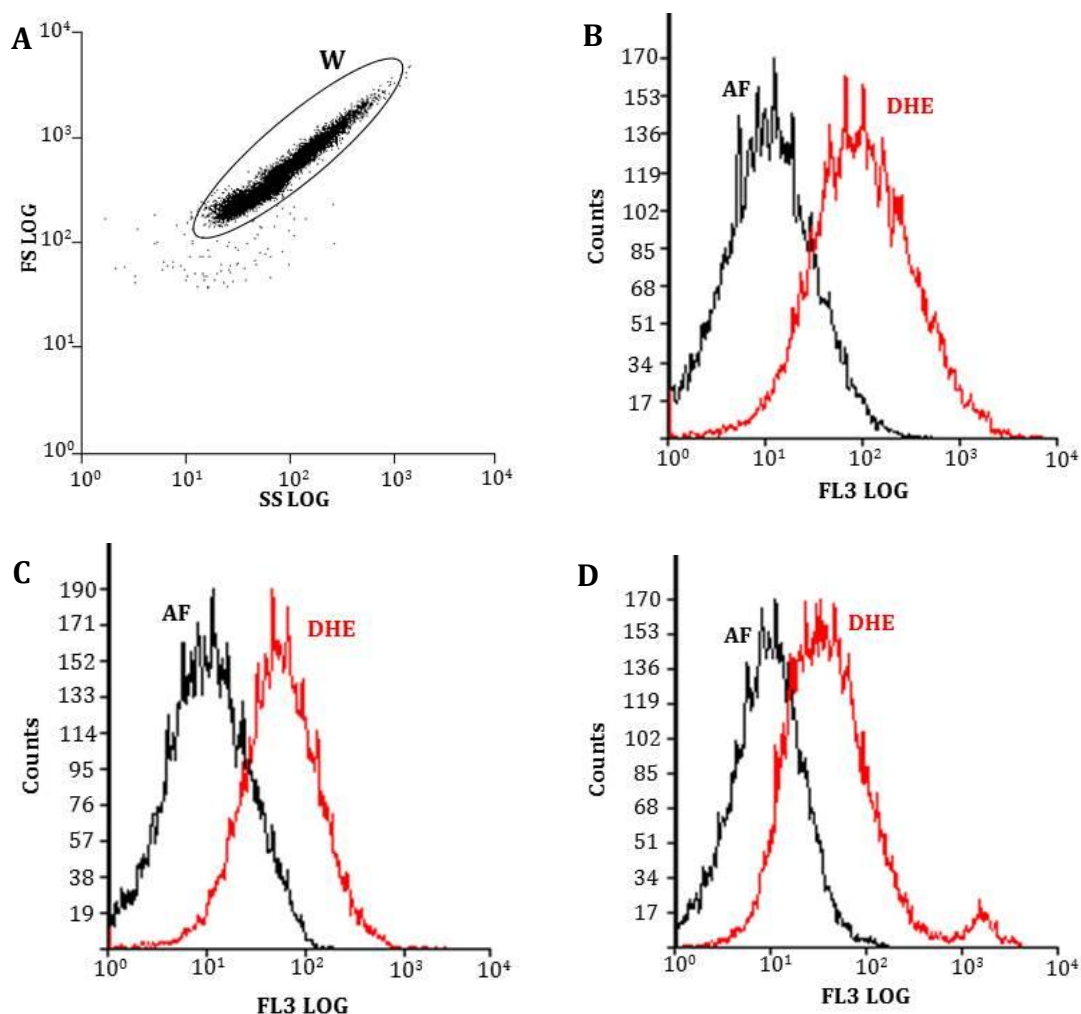


Figure 62. Flow cytometry analysis of *S. cerevisiae* W303 yeast cell populations to study the effect of resveratrol against endogenous ROS with the DHE probe. Scattergram of a population of yeast cells in the absence of resveratrol (A); overlay histogram of autofluorescence (black line) and DHE induced fluorescence (orange line) in the absence of resveratrol (B) and upon treatment of yeast cells with 200 μ M of free resveratrol (C) and resveratrol loaded liposomes (D).

The scattergram of figure 62A shows a well-defined population of yeast cells (gated region W). The same gate was defined for all subsequent experiments and the number of yeast cells was set to 20000.

The overlay of the histograms corresponding to the autofluorescence of the yeast cells and the fluorescence of yeast cells labeled with DHE clearly shows a positive staining (figure 62B), suggesting that the probe reacted with intracellular ROS. Results also show that resveratrol alone (figure 62C) or encapsulated (figure 62D) promoted a decrease of the fluorescence intensity demonstrating that resveratrol is able to quench at some extent intracellular ROS.

Figure 63 was constructed with the data of figure 62 to show the percentage of cells producing ROS-positive signals. As it can be seen, when yeast cells were treated with free resveratrol positive staining was reduced by 23% and when treated with resveratrol loaded liposomes the endogenous ROS were reduced by 49%.

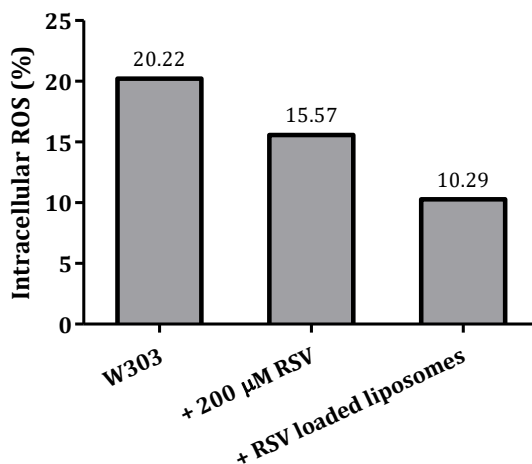


Figure 63. Effect of free and encapsulated resveratrol on the percentage of cells producing intracellular ROS in yeast cells *S. cerevisiae* W303 grown in lactate/ethanol medium.

These results suggest that resveratrol indeed played a protective role against oxidative stress in yeast, which seems to be enhanced when resveratrol was encapsulated into the liposomal formulation, which may indicate that the encapsulation allows resveratrol molecules to be more easily or rapidly incorporated into the cells.

CHAPTER 4

CONCLUSIONS AND FUTURE PERSPECTIVES

As a whole, resveratrol loaded DODAB:MO (1:2) liposomal system revealed adequate characteristics for drug delivery purposes, since particles are stable and homogeneous, are smaller than 200 nm and have a large positive superficial charge, which prevents aggregation. Incubation proved to be the best method to encapsulate resveratrol in this liposomal system, because an encapsulation efficiency of approximately 88% was achieved.

The partition coefficient of resveratrol in the liposomal system indicated that resveratrol has a lipophilic character, which suggests that it has a preferential partition into the liposome's matrix instead of remaining in the aqueous media. Also, it was observed a pronounced bathochromic shift in the derivative spectra, which is an indication that the drug is being displaced from a polar environment to a less polar environment. Moreover, results showed that resveratrol is heterogeneously distributed in the liposomal system and promotes its disorganization by inserting itself mainly in the DODAB polar headgroups, which diminishes the system's microviscosity by disturbing the lipid packaging.

Resveratrol release from liposomes was higher in water than in any of the buffers tested. Future studies will be carried out to adapt the formulation with a triggering system to force the drug release into the cytoplasm of the targeted cells. Also, resveratrol loaded liposomes tend to bind to HSA and so the formulation needs to be PEGylated to avoid this binding.

Regarding the biological activities assays, resveratrol did not affect yeast growth and attenuated the harmful effects induced by H_2O_2 . Moreover, it was found that neither free nor encapsulated resveratrol affected cell viability and that both formulations promoted a decrease of endogenous ROS. It was also observed that resveratrol loaded liposomes are successfully internalized by yeast cells.

Additional studies need to be performed in order to better understand the liposomal formulation structure, for instance with cryo-TEM studies. Also, the resveratrol release from the liposomes must be optimized and different triggering systems should be studied to induce the resveratrol release from the liposomes at the intended site. Moreover, real-time polymerase chain reaction assays to understand if resveratrol treatment is inducing the expression of antioxidant enzymes will bring additional important insights to this line of research. In what concerns liposome internalization assays in yeast cells, co-localization experiments will be performed to identify the precise intracellular localization of resveratrol loaded liposomes. In a medium-term perspective, this approach should be tested in animal cell models, including cancer cell lines.

References

1. Soleas, G. J., Diamandis, E. P., Goldberg, D. M. Resveratrol: a molecule whose time has come? And gone? *Clin. Biochem.* **30**, 91–113 (1997).
2. Frémont, L. Biological effects of resveratrol. *Life Sci.* **66**, 663–673 (2000).
3. Gescher, A. J. & Steward, W. P. Relationship between Mechanisms , Bioavailability , and Preclinical Chemopreventive Efficacy of Resveratrol : A Conundrum. *Br J Cancer* **12**, 953–957 (2003).
4. Sherman, F. in *Encyclopedia of Molecular Biology and Molecular Medicine*, vol. 6 (ed. Meyers, R. A., E.) 302–325 (VCH Pub., 1997).
5. Gershon, H. & Gershon, D. The budding yeast, *Sccharomyces cerevisiae*, as a model for ageing research: a critical review. *Mech. Ageing Dev.* **120**, 1–22 (2000).
6. Munn, A. L. Molecular requirements for the internalisation step of endocytosis: insights from yeast. *Biochim. Biophys. Acta* **1535**, 236–257 (2001).
7. Stewart, B. W. & Wild, C. P. *World Cancer Report 2014*. (2014).
8. Herceg, Z. & Hainaut, P. Genetic and epigenetic alterations as biomarkers for cancer detection, diagnosis and prognosis. *Mol Oncol* **1**, 26–41 (2007).
9. Siddiqui, I. A., Adhami, V. M., Saleem, M. & Mukhtar, H. Beneficial effects of tea and its polyphenols against prostate cancer. *Mol Nutr Food Res* **50**, 130–43 (2006).
10. IARC. Estimated cancer incidence, mortality and prevalence worldwide in 2012. (2012).
11. Hanahan, D. & Weinberg, R. A. The hallmarks of cancer. *Cell* **100**, 57–70 (2000).
12. Hanahan, D. & Weinberg, R. a. Hallmarks of cancer: the next generation. *Cell* **144**, 646–74 (2011).
13. Khan, N., Afaq, F., Saleem, M., Ahmad, N. & Mukhtar, H. Targeting multiple signaling pathways by green tea polyphenol (–)-epigallocatechin-3-gallate. *Cancer Res.* **66**, 2500–5 (2006).
14. Thakur, V. S., Gupta, K. & Gupta, S. The chemopreventive and chemotherapeutic potentials of tea polyphenols. *Curr Pharm Biotechnol* **13**, 191–199 (2012).
15. Ding, Y., Yao, H., Yao, Y., Fai, L. Y. & Zhang, Z. Protection of dietary polyphenols against oral cancer. *Nutrients* **5**, 2173–91 (2013).
16. Tsao, R. Chemistry and biochemistry of dietary polyphenols. *Nutrients* **2**, 1231–46 (2010).
17. Khoddami, A., Wilkes, M. a & Roberts, T. H. Techniques for analysis of plant phenolic compounds. *Molecules* **18**, 2328–75 (2013).
18. Signorelli, P. & Ghidoni, R. Resveratrol as an anticancer nutrient: molecular basis, open questions and promises. *J. Nutr. Biochem.* **16**, 449–66 (2005).
19. Leiro, J., Cano, E., Ubeira, F. M., Orallo, F. & Sanmartín, M. L. In Vitro Effects of Resveratrol on the Viability and Infectivity of the Microsporidian *Encephalitozoon cuniculi*. *Antimicrob. Agents Chemother.* **48**, 2497–2501 (2004).
20. Scalbert, A. & Williamson, G. Dietary Intake and Bioavailability of Polyphenols. *J. Nutr.* **130**, 2073S–2085S (2000).
21. Rice-Evans, C. A., Miller, N. J. & Paganga, G. Structure-antioxidant activity relationships of flavonoids and phenolic acids. *Free Radic Biol Med* **20**, 933–56 (1996).
22. Pietta, P. G. Flavonoids as antioxidants. *J Nat Prod* **63**, 1035–42 (2000).
23. Guo, J. J., Hsieh, H. Y. & Hu, C. H. Chain-breaking activity of carotenes in lipid peroxidation: A theoretical study. *J Phys Chem B* **113**, 15699–708 (2009).
24. Perron, N. R. & Brumaghim, J. L. A review of the antioxidant mechanisms of polyphenol compounds related to iron binding. *Cell Biochem Biophys* **53**, 75–100 (2009).

25. Halliwell, B. Are polyphenols antioxidants or pro-oxidants? What do we learn from cell culture and in vivo studies? *Arch Biochem Biophys* **476**, 107–12 (2008).
26. Yang, C. S., Maliakal, P. & Meng, X. Inhibition of carcinogenesis by tea. *Annu Rev Pharmacol Toxicol* **42**, 25–54 (2002).
27. Arts, I. C. & Hollman, P. C. Polyphenols and disease risk in epidemiologic studies. *Am J Clin Nutr* **81**, 317S–325S (2005).
28. Lambert, J. D., Hong, J., Yang, G. Y., Liao, J. & Yang, C. S. Inhibition of carcinogenesis by polyphenols: Evidence from laboratory investigation. *Am J Clin Nutr* **81**, 284S–291S (2005).
29. Franceschi, S. *et al.* Role of different types of vegetables and fruit in the prevention of cancer of the colon, rectum, and breast. *Epidemiology* **9**, 338–41 (1998).
30. La Vecchia, C. *et al.* Vegetables and fruit and human cancer: Update of an Italian study. *Int. J. Cancer* **82**, 151–152 (1999).
31. Middleton, E. J., Kandaswami, C. & Theoharides, T. C. The effects of plant flavonoids on mammalian cells: Implications for inflammation, heart disease, and cancer. *Pharmacol Rev* **52**, 673–751 (2000).
32. Duthie, S. J. & Dobson, V. L. Dietary flavonoids protect human colonocyte DNA from oxidative attack in vitro. *Eur J Nutr* **38**, 28–34 (1999).
33. Calomme, M., Pieters, L., Vlietinck, A. & Vanden Berghe, D. Inhibition of bacterial mutagenesis by Citrus flavonoids. *Planta Med* **62**, 222–6 (1996).
34. Plaumann, B., Fritsche, M., Rimpler, H., Brandner, G. & Hess, R. D. Flavonoids activate wild-type p53. *Oncogene* **13**, 1605–14 (1996).
35. Corona, G. *et al.* Inhibition of p38/CREB phosphorylation and COX-2 expression by olive oil polyphenols underlies their anti-proliferative effects. *Biochem Biophys Res Commun* **362**, 606–11 (2007).
36. Adam, L. S. & Chen, S. Phytochemicals for breast cancer prevention by targeting aromatase. *Front Biosci (Landmark Ed)* **14**, 3846–63 (2009).
37. Mantena, S. K., Baliga, M. S. & Katiyar, S. K. Grape seed proanthocyanidins induce apoptosis and inhibit metastasis of highly metastatic breast carcinoma cells. *Carcinogenesis* **27**, 1682–91 (2006).
38. Fabiani, R. *et al.* Cancer chemoprevention by hydroxytyrosol isolated from virgin olive oil through G1 cell cycle arrest and apoptosis. *Eur J Cancer Prev* **11**, 351–8 (2002).
39. Fini, L. *et al.* Chemopreventive properties of pinoretinol-rich olive oil involve a selective activation of the ATM-p53 cascade in colon cancer cell lines. *Carcinogenesis* **29**, 139–46 (2008).
40. Van Erk, M. J. *et al.* Integrated assessment by multiple gene expression analysis of quercetin bioactivity on anticancer-related mechanisms in colon cancer cells in vitro. *Eur J Nutr* **44**, 143–56 (2005).
41. Van Heist, J., Niessen, H., Hoekman, K. & Schalkwijk, C. Advanced glycation end products in human cancer tissues: Detection of Nepsilon-(carboxymethyl)lysine and argpyrimidine. *Ann N Y Acad Sci* **1043**, 725–733 (2005).
42. Bengmark, S. Advanced Glycation and Lipoxidation End Products–Amplifiers of Inflammation: The Role of Food. *JPEN J Parenter Enter. Nutr* **31**, 4300–40 (2007).
43. Kiho, T., Usui, S., Hirano, K., Aizawa, K. & Inakuma, T. Tomato paste fraction inhibiting the formation of advanced glycation end-products. *Biosci Biotechnol Biochem* **68**, 200–5 (2004).
44. Lo, C. Y. *et al.* Trapping reactions of reactive carbonyl species with tea polyphenols in simulated physiological conditions. *Mol Nutr Food Res* **50**, 1118–28 (2006).
45. Sang, S. *et al.* Tea polyphenol (–)-Epigallocatechin-3-Gallate: A new trapping agent of reactive dicarbonyl species. *Chem Res Toxicol* **20**, 1862–70 (2007).

46. Kuniyasu, H. *et al.* Expression of receptors for advanced glycation end-products (RAGE) is closely associated with the invasive and metastatic activity of gastric cancer. *J Pathol* **196**, 163–70 (2002).
47. Sparvero, L. J. *et al.* RAGE (Receptor for Advanced Glycation Endproducts), RAGE Ligands, and their role in Cancer and Inflammation. *J Transl Med* **7**, 17 (2009).
48. Takada, M., Ku, Y., Toyama, H., Suzuki, Y. & Kuroda, Y. Suppressive effects of tea polyphenol and conformational changes with receptor for advanced glycation en products (RAGE) expression in human hepatoma cells. *Hepatogastroenterology* **49**, 928–31 (2002).
49. Waterhouse, A. L. Wine and heart disease. *Chem. Ind.* 338–341 (1995).
50. Bavaresco, L. Role of viticultural factors on stilbene concentrations of grapes and wine. *Drugs Exp. Clin. Res.* **29**, 181–7 (2003).
51. Neves, A. R., Lúcio, M., Lima, J. L. C. & Reis, S. Resveratrol in Medicinal Chemistry : A Critical Review of its Pharmacokinetics , Drug-Delivery , and Membrane Interactions. *Curr Med Chem* **19**, 1663–1681 (2012).
52. Gusman, J., Malonne, H. & Atassi, G. A reappraisal of the potential chemopreventive and chemotherapeutic properties of resveratrol. *Carcinogenesis* **22**, 1111–1117 (2001).
53. Baur, J. A. & Sinclair, D. A. Therapeutic potential of resveratrol: the in vivo evidence. *Nat. Rev. Drug Discov.* **5**, 493–506 (2006).
54. Lu, Z. *et al.* Transport of a cancer chemopreventive polyphenol, resveratrol: interaction with serum albumin and hemoglobin. *J Fluoresc* **17**, 580–587 (2007).
55. Lancon, A. *et al.* Human hepatic cell uptake of resveratrol: involvement of both passive diffusion and carrier-mediated process. *Biochem Biophys Res Commun* **316**, 1132–1137 (2004).
56. Johnson, W. D. *et al.* Subchronic oral toxicity and cardiovascular safety pharmacology studies of resveratrol, a naturally occurring polyphenol with cancer preventive activity. *Food Chem Toxicol* **49**, 3319–3327 (2011).
57. Cottart, C. H., Nivet-Antoine, V., Laguillier-Morizot, C. & Beaudeux, J. Resveratrol bioavailability and toxicity in humans. *Mol Nutr Food Res* **54**, 7–16 (2010).
58. Bhat, K. P. L. & Pezzuto, J. M. Cancer Chemopreventive Activity of Resveratrol. *Ann N Y Acad Sci* **957**, 210–229 (2002).
59. Savouret, J. . & Quesne, M. Resveratrol and cancer: a review. *Biomed. Pharmacother.* **56**, 84–87 (2002).
60. Holmberg, K. *Handbook of Applied Surface and Colloid Chemistry - I.* (2002).
61. Tanford, C. *The hydrophobic effect: Formation of micelles and biological membranes.* (1980).
62. Frolov, V. A., Shnyrova, A. V & Zimmerberg, J. Lipid polymorphisms and membrane shape. *Cold Spring Harb. Perspect. Biol.* **3**, a004747 (2011).
63. Lipowsky, R. & Sackmann, E. in *Handbook of biological physics* (Elsevier B.V., 1995).
64. Tenchov, B. & Koynova, R. Cubic phases in membrane lipids. *Eur. Biophys. J.* **41**, 841–850 (2012).
65. Silva, J. P. N. Physicochemical Characterization of DNA/DODAB:MO Cationic Liposome Complexes and Study of its Potential as Nonviral Vectors. (University of Minho, 2013).
66. Balazs, D. A. & Godbey, W. T. Liposomes for use in gene delivery. *J. Drug Deliv.* (2011).
67. Antonielli, M. & Forster, S. Vesicles and liposomes: a self-assembly principle beyond lipids. *Adv. Mater.* **15**, 1323–1333 (2003).
68. Bamrungsap, S. *et al.* Nanotechnology in therapeutics: A focus on nanoparticles as a drug delivery system. *Nanomedicine* **7**, 1253–1271 (2012).

69. Akbarzadeh, A. *et al.* Liposome: classification, preparation, and applications. *Nanoscale Res. Lett.* **8**, 102 (2013).
70. Deshpande, P. P., Biswas, S. & Torchilin, V. P. Current trends in the use of liposomes for tumor targeting. *Nanomedicine (Lond)* **8**, 1–32 (2013).
71. Mayer, L. D., Hope, M. J. & Cullis, P. R. Vesicles of variable sizes produced by a rapid extrusion procedure. *Biochim. Biophys. Acta* **858**, 161–168 (1986).
72. Dua, J. S., Rana, A. C. & Bhandari, A. K. Liposome: methods of preparation and applications. *Int. J. Pharm. Stud. Res.* **3**, 14–20 (2012).
73. Sharma, A. & Sharma, U. S. Liposomes in drug delivery: progress and limitations. *Int. J. Pharm.* **154**, 123–140 (1997).
74. Cho, N. J., Hwang, L. Y., Solandt, J. J. R. & Frank, C. W. Comparison of extruded and sonicated vesicles for planar bilayer self-assembly. *Materials (Basel)*. **6**, 3294–3308 (2013).
75. Zempsky, W. T. Alternative Routes of Drug Administration-Advantages and Disadvantages (Subject Review). *Pediatrics* **100**, 143–152 (1997).
76. Coelho, J. F. *et al.* Drug delivery systems: Advanced technologies potentially applicable in personalized treatments. *EPMA J.* **1**, 164–209 (2010).
77. Rodriguez-Devora, J. I. *et al.* Physically facilitating drug-delivery systems. *Ther Deliv* **3**, 125–139 (2012).
78. Jain, K. K. Drug delivery systems—an overview. *Methods Mol Biol* **437**, 1–50 (2008).
79. Bajpai, A. K., Shukla, S. K., Bhanu, S. & Kankane, S. Responsive polymers in controlled drug delivery. *Prog. Polym. Sci.* **33**, 1088–1118 (2008).
80. Wang, C. *et al.* Combination of adsorption by porous CaCO₃ microparticles and encapsulation by polyelectrolyte multilayer films for sustained drug delivery. *Int J Pharm* **308**, 160–7 (2006).
81. Stevenson, C. L., Santini Jr., J. T. & Langer, R. Reservoir-Based Drug Delivery Systems Utilizing Microtechnology. *Adv Drug Deliv Rev* **64**, 1590–1602 (2012).
82. Tsai, C.-P., Chen, C.-Y., Hung, Y., Chang, F.-H. & Mou, C.-Y. Monoclonal antibody-functionalized mesoporous silica nanoparticles (MSN) for selective targeting breast cancer cells. *J Mater Chem* **19**, 5737–5743 (2009).
83. Allen, T. M. Liposomes. Opportunities in drug delivery. *Drugs* **54**, 8–14 (1997).
84. Yin, H. *et al.* Non-viral vectors for gene-based therapy. *Nat. Rev. Genet.* (2014). doi:10.1038/nrg3763
85. Theek, B. *et al.* Characterizing EPR-Mediated Passive Drug Targeting using Contrast-Enhanced Functional Ultrasound Imaging. *J. Control. release* 83–89 (2014). doi:10.1016/j.jconrel.2014.03.007.Characterizing
86. Torchilin, V. P. Targeted pharmaceutical nanocarriers for cancer therapy and imaging. *Am. Assoc. Pharm. Sci.* **9**, 128–147 (2007).
87. Soenen, S. J., Brisson, A. R. & Cuyper, M. Addressing the problem of cationic lipid-mediated toxicity: the magnetoliposome model. *Biomaterials* **30**, 3691–3701 (2009).
88. Huwyler, J., Drewe, J. & Krahenbuhl, S. Tumor targeting using liposomal antineoplastic drugs. *Int. J. Nanomedicine* **3**, 21–29 (2008).
89. Gao, W., Chan, J. M. & Farokhzad, O. C. pH-Responsive Nanoparticles for Drug Delivery. *Mol. Pharm.* **7**, 1913–1920 (2010).
90. Gullotti, E. & Yeo, Y. Extracellular activated nanocarriers: a new paradigm of targeted drug delivery. *Mol Pharm* **6**, 1041–1051 (2009).
91. Silva, J. P. N., Oliveira, A. C. N., Gomes, A. C. & Real Oliveira, M. E. C. D. in 1–24

92. Kunitake, T. & Okahata, Y. J. A totally synthetic bilayer membrane. *J. Am. Chem. Soc.* **99**, 3860–3861 (1977).
93. Tsuruta, L. R., Lessa, M. M. & Carmona-Ribeiro, A. M. Interactions between dioctadecyldimethylammonium chloride or bromide bilayers in water. *Langmuir* **11**, 2938–2943 (1995).
94. Benatti, C. R., Feitosa, E., Fernandez, R. M. & Lamy-Freund, M. T. Structural and thermal characterization of dioctadecyldimethylammonium bromide dispersions by spin labels. *Chemistry Phys. Lipids* **111**, 93–104 (2001).
95. Oliveira, I. M. *et al.* Aggregation behavior of aqueous dioctadecyldimethylammonium bromide/monoolein mixtures: a multitechnique investigation on the influence of composition and temperature. *J. Colloid Interface Sci.* **374**, 206–17 (2012).
96. Real Oliveira, M. E. C. D. *et al.* Use of Monoolein as a new auxiliary lipid in lipofection. 1–27 (2010).
97. Ganem-Quintanar, A., Quintanar-Guerrero, D. & Buri, P. Monoolein: a review of the pharmaceutical applications. *Drug Dev. Ind. Pharm.* **26**, 809–820 (2000).
98. Briggs, J., Chung, M. & Caffrey, M. The temperature-composition phase diagram and mesophase structure characterization of the monoolein-water system. *J. Phys. II* **6**, 723–751 (1996).
99. Rocha, M. E. B. Desenvolvimento de uma formulação lipossomal para entrega de um fármaco anticancerígeno. (University of Minho, 2014).
100. Arzensek, D. *Dynamic light scattering and application to proteins in solutions.* (2010).
101. Malvern, I. *Zetasizer Nano Series User Manual.* Malvern Instruments Ltd: Worcestershire (2004).
102. Xu, R. *Particle Characterization - Light Scattering Methods.* (2002).
103. Frkjaer, S., Hjorth, E. L. & Wrrts, O. in *Optimization of drug delivery* (eds. Bundgaard, H., Bagger Hansen, A. & Kofod, H.) 384 (1982).
104. Grit, M., de Smidt, J. H., Struijke, A. & Crommelin, D. J. A. Hydrolysis of phosphatidylcholine in aqueous liposome dispersions. *Int J Pharm* **50**, (1989).
105. Skoog, D. A., Holler, F. J. & Crouch, S. R. *Principles of Instrumental Analysis.* (Cengage Learning, 2006).
106. Sobarwiki. Schematic of UV-visible spectrophotometer. (2013). at <http://en.wikipedia.org/wiki/Ultraviolet-visible_spectroscopy#/media/File:Schematic_of_UV-visible_spectrophotometer.png>
107. Papahadjopoulos, D., Jacobson, K., Nir, S. & Isaac, T. Phase transitions in phospholipid vesicles fluorescence polarization and permeability measurements concerning the effect of temperature and cholesterol. *Biochim. Biophys. Acta* **311**, 330–348 (1973).
108. Michel, N., Fabiano, A., Polidori, A., Jack, R. & Pucci, B. Determination of phase transition temperatures of lipids by light scattering. **139**, 11–19 (2006).
109. Chien, J. Y., Friedrich, S., Heathman, M. A., de Alwis, D. P. & Sinha, V. Pharmacokinetics/Pharmacodynamics and the stages of drug development: role of modeling and simulation. *AAPS J.* **7**, 544–59 (2005).
110. Chaikin, P., Rhodes, G. R., Bruno, R., Rohatagi, S. & Natarajan, C. Pharmacokinetics/Pharmacodynamics in Drug Development: An Industrial Perspective. *J. Clin. Pharmacol.* **40**, 1428–1438 (2000).
111. Pola, A., Michalak, K., Burliga, A., Motohashi, N. & Kawase, M. Determination of lipid bilayer/water partition coefficient of new phenothiazines using the second derivative of absorption spectra method. *Eur. J. Pharmacol. Sci.* **21**, 421–427 (2004).
112. Magalhães, L. M. *et al.* High-throughput microplate assay for the determination of drug partition coefficients. *Nat. Protoc.* **5**, 1823–30 (2010).

113. Modi, S. & Anderson, B. D. Determination of drug release kinetics from nanoparticles: overcoming pitfalls of the dynamic dialysis method. *Mol. Pharm.* **10**, 3076–89 (2013).
114. Loew, S., Fahr, A. & May, S. Modeling the Release Kinetics of Poorly Water-Soluble Drug Molecules from Liposomal Nanocarriers. *J. Drug Deliv.* **376548**, (2011).
115. Schroeder, A. *et al.* Controlling Liposomal Drug Release with Low Frequency Ultrasound: Mechanism and Feasibility. *Langmuir* **23**, 4019–4025 (2007).
116. Liu, B., Yang, C., Yan, X., Wang, J. & Lv, Y. Interaction of Avelox with Bovine Serum Albumin and Effect of the Coexistent Drugs on the Reaction. *Int. J. Anal. Chem.* **2012**, (2012).
117. Ulrich, K. H. Molecular aspects of ligand binding to serum albumin. *Pharmacol Rev* **33**, 17–53 (1981).
118. Bertucci, C. & Domenici, E. Reversible and covalent binding of drugs to human serum albumin: methodological approaches and physiological relevance. *Curr Med Chem* **9**, 1463–1481 (2002).
119. Copeland, R. A. in *Enzymes: a practical introduction to structure, mechanism, and data analysis* **7**, 76–95 (John Wiley & Sons, 2000).
120. Wijeratne, S. S. K., Cuppett, S. L. & Schlegel, V. Hydrogen Peroxide Induced Oxidative Stress Damage and Antioxidant Enzyme Response in Caco-2 Human Colon Cells. *J Agric Food Chem* **53**, 8768–8774 (2005).
121. Fang, C., Bourdette, D. & Banker, G. Oxidative stress inhibits axonal transport: implications for neurodegenerative diseases. *Mol. Neurodegener.* **7**, 29 (2012).
122. Jan, S. Fluorescence Microscopy and Fluorescent Probes, Volume 1 (Google eBook). 306 (1996).
123. Spring, K. R. & Davidson, M. W. Introduction to Fluorescence Microscopy. *Nikon Microsc. [online]* (2003). at
<<https://www.microscopyu.com/articles/fluorescence/fluorescenceintro.html>>
124. Kubitscheck, U. *Fluorescence microscopy: from basic principles to biological applications*. (2013).
125. Spring, K. R. Fluorescence Microscopy. (2003). doi:10.1081/E-EOE
126. Silva, J. P. N. *et al.* DODAB: monoolein-based lipoplexes as non-viral vectors for transfection of mammalian cells. *Biochim. Biophys. Acta* **1808**, 2440–9 (2011).
127. Plášek, J. & Jarolím, P. Interaction of the Fluorescent Probe 1,6-Diphenyl-1,3,5-Hexatriene with Biomembranes. *Gen Physiol Biophys* **6**, 425–437 (1987).
128. FluoProbes®. DPH: product information. **19**,
129. BD Biosciences. *Introduction to Flow Cytometry: A Learning Guide*. (2000).
130. Ingham, E. R. & Klein, D. A. Relationship between fluorescein diacetate-stained hyphae and oxygen utilization, glucose utilization, and biomass of submerged fungal batch cultures. *Appl Env. Microbiol* **44**, 363–370 (1982).
131. Owusu-Ansah, E., Yavari, A. & Banerjee, U. A protocol for in vivo detection of reactive oxygen species. *Nat. Protoc.* (2008). doi:10.1038/nprot.2008.23
132. Wojtala, A. *et al.* Methods to Monitor ROS Production by Fluorescence Microscopy and Fluorometry. *Methods in Enzymology* **542**, (Elsevier, 2014).
133. Kobayashi, H., Watanabe, R. & Choyke, P. L. Improving conventional enhanced permeability and retention (EPR) effects; what is the appropriate target? *Theranostics* **4**, 81–89 (2014).
134. Oliveira, A. C. N. *et al.* Dioctadecyldimethylammonium: Monoolein Nanocarriers for Efficient in Vitro Gene Silencing. *ACS Appl. Mater. Interfaces* **6**, 6977–6989 (2014).
135. Kedmi, R., Ben-Arie, N. & Peer, D. The systemic toxicity of positively charged lipid nanoparticles and the role of Toll-like receptor 4 in immune activation. *Biomaterials* **31**, 6867–75 (2010).

136. Bagchi, D. *Phytopharmaceuticals in Cancer Chemoprevention. Series in Modern Nutrition Science* (CRC Press, 2004).
137. Engelke, M., Bojarski, P., Bloß, R. & Diehl, H. Tamoxifen perturbs lipid bilayer order and permeability: comparison of DSC, fluorescence anisotropy, Laurdan generalized polarization and carboxyfluorescein leakage studies. *Biophys. Chem.* **90**, 157–173 (2001).
138. López-Nicolás, J. M. & García-Carmona, F. Aggregation State and pKa Values of (E)-Resveratrol As Determined by Fluorescence Spectroscopy and UV-Visible Absorption. *J Agric Food Chem* **56**, 7600–7605 (2008).
139. Liang, Y. Drug Release and Pharmacokinetic Properties of Liposomal DB-67. (University of Kentucky Master's Theses. Paper 17, 2010).
140. Chen, W. C. & Huang, L. Non-viral vector as vaccine carrier. *Adv Genet* **54**, 15–37 (2005).
141. Meyer, O. *et al.* Cationic liposomes coated with polyethylene glycol as carriers for oligonucleotides. *J. Biol. Chem.* **273**, 15621–15627 (1998).
142. Rip, J. *et al.* Glutathione PEGylated liposomes: pharmacokinetics and delivery of cargo across the blood-brain barrier in rats. *J. Drug Target.* **22**, 460–7 (2014).
143. Carter, L. G., D'Orazio, J. A. & Pearson, K. J. Resveratrol and cancer: focus on in vivo evidence. *Endocr Relat Cancer* **21**, 209–25 (2014).
144. Taylor, E. J. M., Yu, Y., Champer, J. & Kim, J. Resveratrol demonstrates antimicrobial effects against *Propionibacterium acnes* in vitro. *Dermatol Ther* **4**, 249–257 (2014).
145. Bishop, J. R. P., Nelson, G. & Lamb, J. Microencapsulation in yeast cells. *J Microencapsul.* **15**, 761–773 (1998).
146. Dhar, R., Sägesser, R., Weikert, C. & Wagner, A. Yeast adapts to a changing stressful environment by evolving cross-protection and anticipatory gene regulation. *Mol Biol Evol* **30**, 573–588 (2013).
147. Gülçin, I. Antioxidant properties of resveratrol: A structure-activity insight. *Innov Food Sci Emerg Technol* **11**, 210–218 (2010).
148. Delaunay, A., Isnard, A. D. & Toledano, M. B. H₂O₂ sensing through oxidation of the Yap1 transcription factor. *EMBO J* **19**, 5157–5166 (2000).
149. Schnell, N., Krems, B. & Entian, K. D. The PAR1 (YAP1/SNQ3) gene of *Saccharomyces cerevisiae*, a c-jun homologue, is involved in oxygen metabolism. *Curr Genet* **21**, 269–73 (1992).
150. Fernandes, L., Rodrigues-Pousada, C. & Struhl, K. Yap, a novel family of eight bZIP proteins in *Saccharomyces cerevisiae* with distinct biological functions. *Mol Cell Biol* **17**, 6982–93 (1997).
151. Escoté, X. *et al.* Resveratrol induces antioxidant defence via transcription factor Yap1p. *Yeast* **29**, 251–263 (2012).
152. Andrews, J. M. Determination of minimum inhibitory concentrations. *J. Antimicrob. Chemother.* **48**, 5–16 (2001).
153. Nagataand, T. & Toe, A. Japan Patent 107183. (1983).